**The University of Melbourne**

**School of Chemical and Biomedical Engineering**

**Department of Chemical Engineering**

# Application of pulsed membrane contactor for $CO_2$ capturing from flue gas

**Elaheh Hosseini**

**Submitted in Total Fulfilment of the Requirements of the Degree of Doctor of Philosophy**

**March 2021**

# ABSTRACT

Climate change resulting from the emission of greenhouse gases, in particular $CO_2$ into the atmosphere has become a global challenge in recent years. Post-combustion $CO_2$ capture is an effective way to mitigate $CO_2$ emissions from power plants. Gas-solvent hollow fibre membrane contactors have been introduced as a promising technology for post-combustion $CO_2$ capture, as contactors combine the benefits of membrane technology with chemical absorption. Although the membrane acts as a permeable barrier adding further mass transfer resistance approximately by 40% to the contactor system, the membrane module provides 10-fold reduction in equipment size and 30 times higher interfacial area than that of gas absorbers. Therefore, there are three main resistances to mass transfer in gas-solvent membrane contactor systems; namely the membrane (porous and non-porous layers), solvent phase boundary layer and gas phase boundary layer. To reduce the membrane mass transfer resistance, ultra-thin film hollow fibre membranes have been utilised. However, the solvent phase boundary layer and gas phase boundary layer resistances remain considerable, and therefore techniques are required that will reduce these resistances and enhance membrane contactor performance.

In this thesis, solutions to overcome the mass transfer challenges of gas-solvent membrane contactor systems for $CO_2$ capture from simulated flue gas have been investigated. Inducing additional mixing to the solvent and gas phase boundary layers is one of the most effective methods for improving mass transfer. To generate mixing and changing the hydrodynamics of the solvent and gas flow, oscillating and vibrating conditions have been designed and integrated into gas-solvent membrane contactor systems. Oscillating the flow of either the solvent or gas phases induces additional mixing within the respective boundary layers, while applying vibration to the membrane module induces mixing across all stages of mass transfer. The effect of these new techniques on the solvent and gas phase mass transfer coefficients have been investigated and reported here. The solvent side mass transfer coefficient increased by up to 50% and 13% under oscillating and vibrating conditions, respectively. The reason for these enhancements was due to disruption to the solvent phase's boundary layer, resulting in additional mixing that produced a higher $CO_2$ flux through the solvent phase. Moreover, the gas phase mass transfer coefficient increased by 28% on average under oscillating flow due to an increase in gas phase mixing within the lumen side of the membrane fibres. Vibrational conditions had a stronger impact, enhancing the gas phase mass transfer coefficient by a factor of two.

The frequency and amplitude have been presented as the key adjustable parameters of the oscillating operating modes. For the vibrating unit, oscillating and displacement amplitude have been contributed to the definition of operating conditions. The mass transfer performance on the gas and solvent phases of membrane contactor systems has been investigated for variable oscillating/vibrating frequencies and amplitudes. Oscillating solvent flow frequency has been investigated between 0.83 and 2.03Hz, while the vibrating unit worked within the range of 0.5 to 2.3Hz. The solvent boundary layer thickness has been found to reduce with increasing oscillating/vibrating solvent flow frequency. The enhancement in the gas phase was strongly linked with oscillating/displacement amplitude, associated with the magnitude of pressure wave propagating through the gas phase.

The present thesis has introduced novel experimental apparatuses and mass transfer analysis methods that add to our understanding of mass transfer phenomena in gas-solvent membrane contactors. Empirical correlation models, in terms of the dimensionless Sherwood number, have been proposed for the first time to predict the mass transfer performance of gas-solvent membrane contactor systems under both oscillating and vibrating conditions. To indicate the effect of oscillating parameters on the Sherwood number correlations, the frequency and amplitude have been incorporated into the definition of root mean squared velocity of oscillating solvent/gas flow resulting in oscillating Reynolds number. The effect of vibrational parameters has been presented in the form of dimensionless vibration number incorporated within the new vibrating Sherwood number correlation of the gas-solvent membrane contactor system. The novel Sherwood number correlations have enabled the influence of oscillation and vibration on the solvent and gas boundary layers (e.g. the boundary layer thickness) to be quantified.

Overall, the aim of this thesis was to improve the mass transfer performance of gas-solvent membrane contactors for $CO_2$ capture. This thesis demonstrated that the application of oscillating solvent flow, oscillating gas flow and vibrating solvent/gas flow are three novel approaches that achieve higher $CO_2$ flux and mass transfer within membrane contactors than possible under conventional flow regimes. Furthermore, the application of oscillating and vibrational conditions to larger scale membrane modules is readily achievable, therefore the methods developed here show great potential for being used on industrial scales.

# PREFACE

The two result chapters including **chapters 4** and **5** of this thesis have been published as below.

- **E. Hosseini**, G.W. Stevens, C.A. Scholes, Membrane gas-solvent contactors undergoing oscillating solvent flow for enhanced carbon dioxide capture, **Separation and Purification Technology**. 227 (2019) 115653.
- **E. Hosseini**, E. Soroodan Miandoab, G.W. Stevens, C.A. Scholes, Absorption of $CO_2$ from flue gas under oscillating gas flow conditions in gas-solvent hollow fibre Membrane Contactors, **Separation and Purification Technology**. 249 (2020) 117151.

# ACKNOWLEDGEMENTS

I would like to express my gratitude to my primary supervisor, Dr. Colin Scholes, for giving me the opportunity to be a part of his research team in chemical engineering department at The University of Melbourne. Many thanks for your support and untiring guidance during my PhD journey. I am so grateful for the time you allocated for reading and editing my manuscripts and presentations. Thank you for all weekly face to face and online meetings during COVID-19 which helped me a lot to narrow down the research challenges.

I would like to thank my co-supervisor, Prof. Geoff Stevens, for his technical input, valuable advice and supports along my PhD candidature. Many thanks for your constructive comments on my manuscripts. I deeply appreciate your approach to encourage me to think about different aspects of new proposed methods. Thank you for all weekly meetings that helped me to overcome challenges I faced in experimental and modelling works.

I would like to sincerely thank Prof. Sandra Kentish for giving me the opportunity to attend the membrane group meetings. Thank you for your valuable comments on my experimental results. I deeply appreciate your support to attend a summer school at University of Bologna in Italy. Many thanks for involving me in scientific discussions in conferences.

I would like to thank my committee chair, Prof. Amanda Ellis, for her advice and mentorship during my PhD period.

I would like to thank The University of Melbourne for Melbourne Research Scholarship (MRS). I would like to acknowledge the Particulate Fluid Processing Centre at The University of Melbourne, Clive Pratt and University of Bologna for awarding me travel grants.

I would like to thank Dr. Mohamed Hussein Ali Abdellah for his help and brilliant ideas in setting up the experimental rig.

I am thankful to all the past and present membrane group and capture lab members (Nouman, Armineh, Liang, George, Sahar, Thomas, Shirley, Lily, Masih, Yidi and Moataz) for their help and generous advice. I am also thankful to all my friends for cheering me up during stressful times.

I would like to thank my beloved fiancé, Ehsan, for his support, love and understanding. Your infinite help in every step of my PhD journey made it easier for me.

Finally, I would like to thank my parents and sister for their endless and unconditional support and kindness. I deeply appreciate your patience and encouragement during stressful and difficult times of my PhD.

# DECLARATION

This is to certify that:

- The thesis comprises only my original work towards the PhD except where indicated in the acknowledgements.
- Due acknowledgement has been made in the text to all other materials used.
- This thesis is less than 100,000 words in length, exclusive of the tables, figures, maps, bibliography and appendices.

Elaheh Hosseini

March 2021

# CONTENTS

# LIST OF FIGURES

# LIST OF TABLES

# CHAPTER 1: INTRODUCTION

Anthropogenic $CO_2$ emissions from fossil fuel power plants and industrial processes are growing at an alarming rate. The Intergovernmental Panel on Climate Change (IPCC) expects a long-term temperature increase of 2°C by 2050, if $CO_2$ emissions remain on current projections [1,2]. Therefore, $CO_2$ emissions and the resulting change in climate have become a critical environmental issue [3]. The challenges arising from climate change include rising sea levels, increasing storm power, loss in biodiversity, loss in predictable weather patterns, loss in water security, loss in food security and soil change [4]. Carbon capture and storage (CCS) has been suggested as a practical way to mitigate greenhouse gas emissions from large point sources, such as power stations and industrial processes [5]. CCS refers to three main scenarios including:

- Pre-combustion carbon capture: In this scenario, $CO_2$ is separated from hydrogen/syngas prior to combustion [6].
- Oxy-fuel combustion carbon capture: This scenario includes $CO_2$ capture from flue gases released from fossil fuels combusted under pure oxygen conditions [7].
- Post-combustion carbon capture: This scenario enables $CO_2$ separation from flue gases released from the combustion of fossil fuels [8].

These capture scenarios in power generation plants are shown in Figure 1.1 [9].

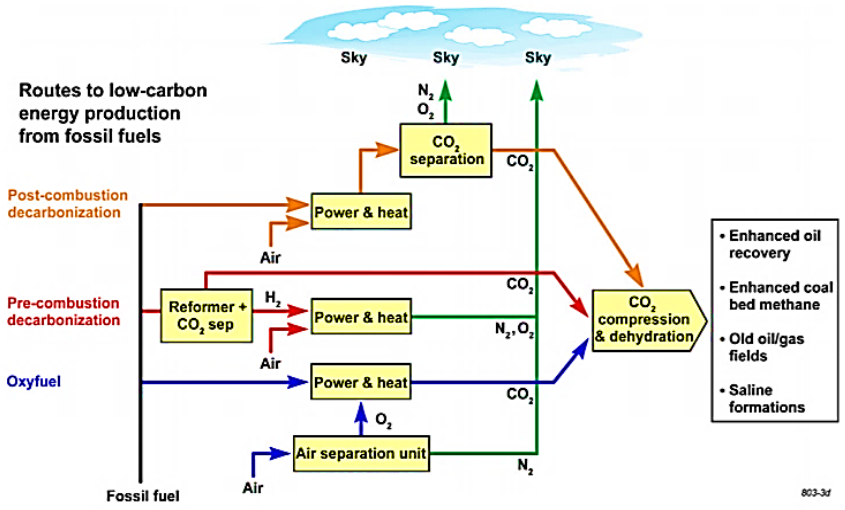


Fig. 1.1. CCS scenarios in power generation plant [9]

Post-combustion carbon capture is designed to separate $CO_2$ from flue gases which are released after combustion fossil fuels, primarily coal, in power generation plants. The composition of the flue gas varies depending upon the fuel used [10]. Table 1.1 shows the post-combustion flue gas composition for different large scale point sources [11].

Table 1.1. Volumetric percentage of industrial flue gas

| Plant | Stream | $CO_2$ | $N_2$ | $O_2$ | $H_2O$ | CO | $H_2$ | Others |
|---|---|---|---|---|---|---|---|---|
| Gas Turbine | post-combustion exhaust | 3.4-3.8 | 74.4-75.7 | 12.6-13.8 | 6.9-8.3 | - | - | 0.0.9 |
| NG-fired Power Plant | post-combustion flue gas | 8.6-9 | 70.9-71 | 2.4-13 | 7.8-17.3 | - | - | 0-0.9 |
| Coal-fired Power Plant | post-combustion flue gas | 12.6-14 | 71.4-74 | 3-4.3 | 8-10.8 | - | - | 0.9-1 |

Different technologies have been proposed for post-combustion carbon capture, including chemical and physical absorption, adsorption, cryogenic liquefication and membrane gas separation [12]. Among the post-combustion carbon capture technologies, solvent-based carbon capture, i.e. chemical absorption, is the conventional technology [13]. A simple schematic of chemical absorption using packed bed columns is shown in Figure 1.2 [14]. In this process, $CO_2$ reacts with the solvent at the gas-solvent interface, following which the $CO_2$-solvent complex transfers into the bulk flow of the solvent. the exiting solvent is preheated in a heat exchanger and transferred to a desorption unit where the regeneration of the $CO_2$-rich solvent takes place under high temperature conditions and $CO_2$ is released. The $CO_2$-lean solvent is recovered from the desorption unit which is cooled down and returned to the absorption unit, beginning the process again [12].

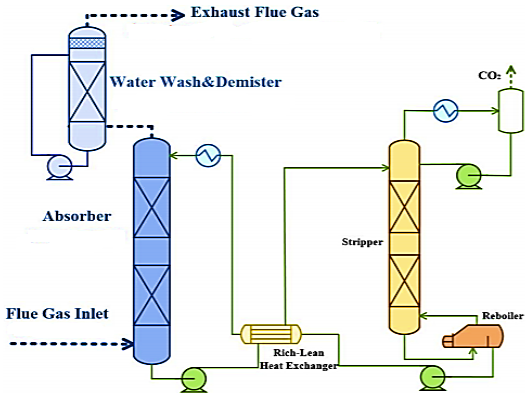


Fig. 1.2. Schematic diagram of chemical absorption system [14]

The chemical absorption process not only experiences operational difficulties and challenges such as solvent loss, equipment corrosion, flooding, foaming, channelling and entrainment but is an energy-intensive technology [13]. To overcome these challenges, energy-efficient gas-solvent membrane contactors have been suggested as a hybrid technology that is easier to scale-up and combines the benefits of membranes and solvent absorption [15,16]. In gas-solvent membrane contactors, $CO_2$ from the bulk flue gas diffuses across the membrane and is absorbed into a $CO_2$ selective solvent phase (Figure 1.3) [17].

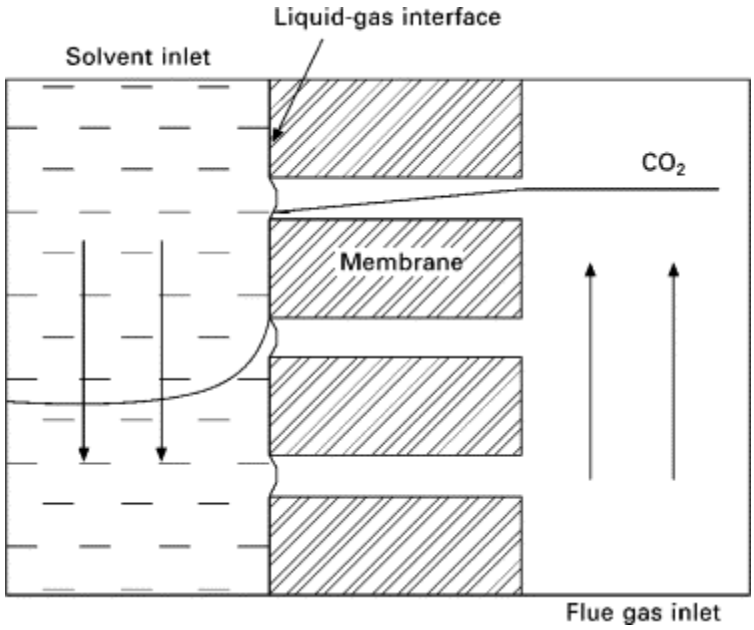


Fig. 1.3. Membrane contactor principles for selective chemical separation of a gas into a chemical solvent [15]

Although gas-solvent membrane contactor holds a great promise in $CO_2$ capture [8], the technology faces challenges in terms of membrane resistance and mass transfer resistances in solvent and gas phase boundary layers. The use of ultra-thin composite membranes minimizes the membrane resistance [8] but the mass transfer resistances in the gas and solvent boundary layers remain significant challenges as they are limiting the mass transfer performance by 50-88% at some circumstances [18]. Therefore, novel approaches are required to lower the mass transfer resistance of gas-solvent membrane contactors.

This thesis focused on reducing the gas and solvent boundary layer resistances to improve the efficiency of the gas-solvent membrane contactor technology and therefore make it more competitive with commercial technologies for post-combustion carbon capture. Primarily, this thesis focuses on inducing additional mixing within the respective phases and membrane to enhance mass transfer and improve the performance of membrane contactors. The rigid

structure of the membrane module prevents conventional mixing techniques used on solvent absorption columns from being applied to a contactor system. Therefore, approaches using pulsation conditions (oscillating flow and contactor vibration) are applied and the resulting improvements in performance the focus of this thesis.

In Chapter 2 mass transfer operation in gas-solvent membrane contactors is explained and criteria for selecting membrane materials and solvents are presented. A comprehensive review of the gas-solvent membrane contactors used for different applications in the academic literature is presented and the design of hollow fibre membrane contactors is briefly provided. Moreover, a through discussion on the theory of gas-solvent membrane contactors is given, highlighting an approach to model mass transfer phenomenon in gas-solvent membrane contactors based on dimensionless numbers. Mass transfer resistances in the solvent and gas boundary layers are examined as challenges adversely impacting the separation performance of membrane contactors. Finally, methods for overcoming these challenges are presented and reviewed.

In Chapter 3 the preparation of hollow fibre membrane contactors is described in detail and the operation of experimental rigs for hollow fibre membrane contactors is explained. Then, the design of oscillating and vibrating units applied for generating additional mixing within membrane contactors is presented. Moreover, the method of analysis of $CO_2$ content in the solvent is discussed.

Chapter 4 studies the effect of oscillating solvent flow on the overall mass transfer coefficient of gas-solvent hollow fibre membrane contactors using pure $CO_2$. Results are compared to non-oscillating solvent flow conditions. Moreover, the influence of oscillating amplitude and frequency on the overall mass transfer coefficient is provided and a Sherwood number correlation is proposed to hollow fibre membrane contactors under oscillating solvent flow.

In Chapter 5 a mixture of 10% $CO_2$ in $N_2$ (balance) is used as the feed gas which is forced to oscillate at different amplitudes and frequencies, while keeping the solvent flow at non-oscillating conditions. The overall mass transfer coefficient based on the gas side is calculated and compared to that of non-oscillating gas condition. Also, the effect of oscillating amplitude and frequency on the overall gas-based mass transfer coefficient is investigated. A Sherwood number correlation is suggested for this system, accounting for both oscillating and non-oscillating conditions.

Chapter 6 studies the effect of generating disturbances in both solvent and gas phase boundary layers on the mass transfer performance of hollow fibre membrane contactors. A novel vibrating system is designed and used for this purpose. Under vibrating conditions, the overall mass transfer coefficients based on the solvent and gas sides are calculated and compared to non-vibrating conditions. The new system design allows amplitude and frequency of vibration to change. As a result, the impact of vibrating parameters on the overall mass transfer coefficients is investigated. Finally, mass transfer in vibrating membrane contactors is quantified as a function of a new dimensionless vibration number.

Chapter 7 concludes the main outcomes of the present thesis and suggests future works.

# CHAPTER 2: LITERATURE REVIEW

## 2.1. Introduction

This chapter provides an overview of hollow fibre membrane contactor technology. First, the concept of separation using hollow fibre membrane contactors is described and a review of the early and recent membrane contactors used in different chemical engineering processes is presented. Moreover, the potential compositions for membranes and $CO_2$-selective solvents used in gas-solvent membrane contactor systems are explained in detail. To model the separation performance of membrane contactors, a comprehensive review on mass transfer correlations is provided. Additionally, the mass transfer resistances in the solvent and gas phases, as well as in the membrane are described in detail and the importance of membrane material type is highlighted. Most importantly, the mass transfer resistances in the gas and solvent phase boundary layers are introduced as the main challenges of gas-solvent membrane contactor technology. Then, different methodologies for reducing these resistances are described providing potential ideas to improve the performance of gas-solvent membrane contactors. Finally, the scope of this thesis is outlined.

## 2.2. Gas-solvent membrane contactors

The membrane contactor technology has potential for being employed in the chemical, petrochemical, pharmaceutical, and metallurgical industries for water and gas treatments. For example, membrane contactors have been successfully used in aromatic pollutants recovery from water, selective removal of heavy metals from a galvanic process bath and ammonia product recovery from an off-gas stream [19]. There are other applications that the membrane contactor technology hold promise including $CO_2$ capture from post-combustion flue gases released from power generation plants, as well as desulfurization of these flue gases, indoor air conditioning, acid gas removal from natural gas or biogas, and natural gas dehydration [19,20]. Klaassen [21] developed a membrane contactor pilot plant for desulphurization of flue gases and indicated more than 95% $SO_2$ recovery [21]. Hedayat et al. [22] successfully demonstrated the simultaneous removal of $CO_2$ and $H_2S$ from natural gas using hollow fibre membrane contactors [22].

Membrane contactors can provide a sufficient flux of $CO_2$ for absorption, while the direct contact of the gas and solvent phases is prevented which in turn eliminates the operational drawbacks of chemical absorption such as entrainment and flooding [17]. As a hybrid technology, membrane contactors integrate the advantages of membrane gas-separation and solvent absorption technologies [24]. Moreover, it shows excellent operational flexibility, as it provides independent control of gas and solvent flow to overcome flooding and channelling problems [13,25]. Additionally, the chemical absorption technology is energy-intensive, while membrane contactor systems are cost effective. In some circumstances, the cost of operation is reduced by 38-42%, as a higher surface area (i.e. interfacial area between gas and liquid phase) per unit volume is provided in a small size of equipment (~10 fold reduction in size) [8,13,24]. Feron et al. [26] showed the equipment cost decreased by 30% using gas-solvent membrane contactors.

Using hollow fibre membrane contactors for post-combustion carbon capture, $CO_2$ diffuses through the membrane and chemically reacts with the solvent (Figure 2.1) [13] and the chemical potential gradient between gas and solvent phase provides the driving force for the capture process [27]. The membrane only acts as a barrier between the gas and solvent, and it is the solvent that offers the selectivity to $CO_2$ in contrast to membrane gas separation technology in which the membrane provides the selectivity. As a result, hollow fibre membranes with high permeability to $CO_2$ and a solvent with a high $CO_2$ reaction rate (i.e. high

kinetic constant) is required to obtain high performance gas-solvent membrane contactors [8,20].

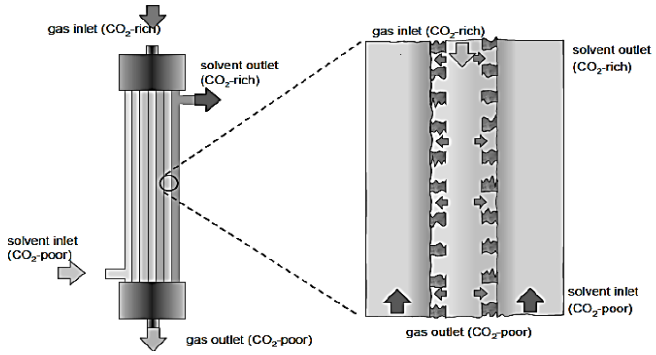


Fig. 2.1. A simple schematic of $CO_2$ capture using a gas-solvent membrane contactor [28]

### 2.2.1. Membranes used in gas-solvent membrane contactors

The membrane plays an important role in the separation performance of contactors, with the material needing specific characteristics such as high thermal resistance, chemical stability and hydrophobicity to mitigate mass transfer resistance due to the membrane [8]. In early studies of $CO_2$ capture using the membrane contactor technology, porous membranes such as poly-vinyl pyrrolidone (PVP) and polysulfone (PSf) were used. However, these polymers caused pore-wetting problems (Figure 2.2) [29] where the solvent penetrated into the pores and chemically reacted with the membrane. As a result, the separation performance was reduced by 60% [30]. There are three modes of operation for gas-solvent membrane contactors which are described below [31]:

1. Non-wetting mode in which membrane pores are completely filled with the gas phase and no solvent is present inside the pores (Figure 2.2.a).

2. Fully wetting mode in which membrane pores are completely wetted with the solvent. This mode of operation will lead to significant mass transfer resistance of the membrane (Figure 2.2.b).

3. Partially wetting mode in which microporous membrane pores are partially filled with the solvent over operating time. This operating mode also causes inadequate separation due to an extra mass transfer resistance in the membrane (Figure 2.2.c).

Various attempts have been made to overcome the wetting problem including using hydrophobic microporous membranes and composite membranes [32–34]. Hydrophobic microporous membranes such as polypropylene (PP), poly-tetra-fluoro-ethylene (PTFE), and poly-vinylidene-fluoride (PVDF) have been suggested to overcome the wetting problem, but all of them resulted in partial wetting of the pores [31]. As a case study, Mansourizadeh and Mousavian [35] studied $CO_2$ capture process using a hollow fibre gas-solvent membrane contactor with the microporous polyvinylidene fluoride (PVDF) as the membrane and diethanolamine as the solvent. Since partial wetting occurred during the operation, they observed 26% reduction in the mass transfer rate after 10 hours of operation [35]. To tackle the wetting problems, it has been suggested to use composite hollow fibres comprised of a dense polymeric film (i.e., non-porous layer) supported by a porous polymer. Using these hollow fibres causes membrane contactors to operate at the non-wetting mode [36]. The application of these composite non-wetted fibres in the membrane contactor systems had been evaluated by Kreulen et al. in 1993 [36]. They coated the microporous polypropylene with a thin layer of

silicone rubber and claimed that the absorption rate of these composite membranes is greater than that of microporous polypropylene without coating [36].

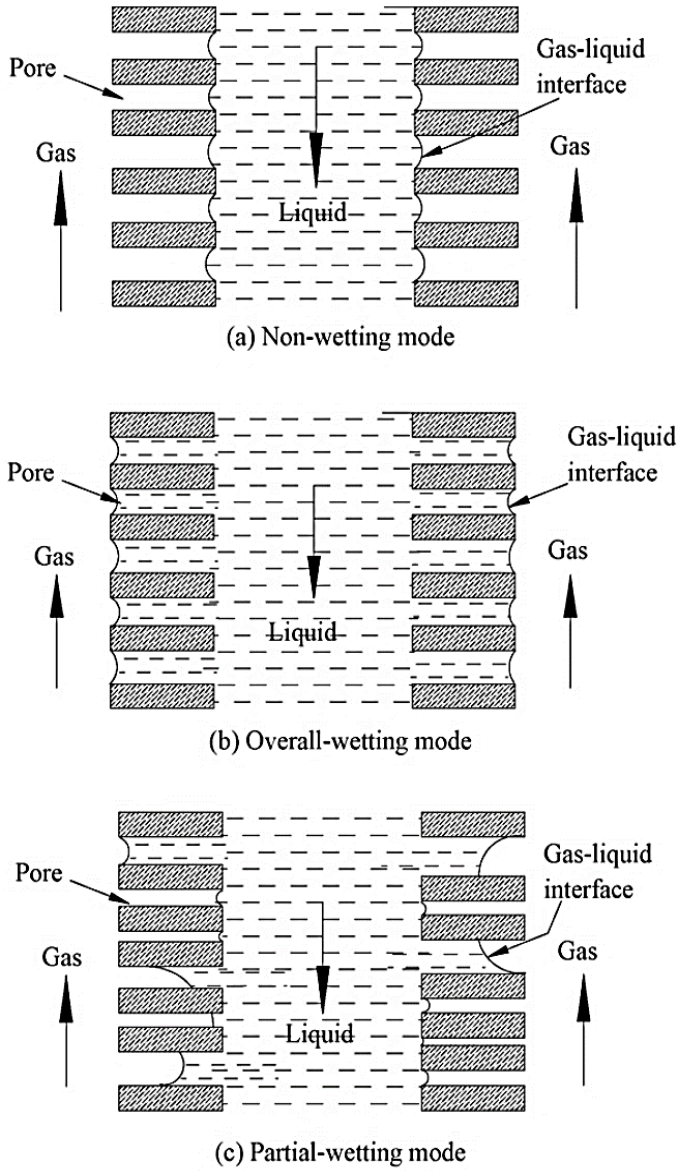


Fig. 2.2. Different wetting modes in gas-solvent hollow fibre membrane contactor systems [31]

In addition, the idea of introducing a dense polymeric layer to the structure of hollow fibres prevents the gas phase generating bubbles inside the solvent phase. This, in turn, provides the membrane contactors with an ability to work at high transmembrane pressures [6,37]. However, this dense layer adds an extra mass transfer resistance to the membrane contactor systems. As a result, the dense layer must be very thin to have negligible mass transfer resistance. Moreover, these dense polymeric layers should have high permeabilities to gases to provide sufficient mass transport across the hollow fibre membranes. Polydimethylsiloxane

(PDMS), for example, shows great potential to be used as a dense skin layer because of its high gas permeability, low chemical reactivity, high hydrophobicity, and high thermal resistance [38]. Thus, these hollow fibres have been selected in the present thesis to eliminate the wetting problems and achieve high mass transfer rates.

### 2.2.2. Solvent in gas-solvent membrane contactors

Although many potential solvents are currently used in absorption processes, the solvent selection in membrane contactors does have limitations [39]. It is important to consider that the solvent should be chemically incompatible with the hollow fibre membrane materials and possess high surface tension [8]. Moreover, a solvent with high chemical reactivity toward $CO_2$, low vapor pressure, low corrosiveness and minimum environmental footprints will improve the process efficiency.

Alkanolamines, especially mono ethanolamine (MEA), are the most common solvents in industrial absorption columns, as they have a high absorption rate in comparison to alkaline solvents. However, they have been faced with critical challenges due to a high energy requirement for the regeneration process, the ability to get oxidize and become corrosive in the pure state [40–42]. To overcome these challenges, alternative solvents such as amino acid salts have been considered [43]. These solvents also have low viscosity which helps to reduce the mass transfer resistance [44]. Among amino acid salt-based solvents, potassium glycinate is comparatively cheap and commercially available. This solvent shows high loading capacity, as it contains two amino groups reacting with the $CO_2$ [45,45,46]. Portugal et al. [43] showed the overall kinetic constant of mono-ethanol amine (MEA) at 298 °C is 5,920 $s^{-1}$, while, at the same temperature, the overall kinetic constant of potassium glycinate was 13,400 $s^{-1}$ [43]. This reflects that potassium glycinate is a fast absorbent in comparison with MEA.

The kinetic constant of aqueous amino acid salts is explained using the zwitterionic mechanism suggested by Caplow [47]. In the first step, $CO_2$ reacts with potassium glycinate to form a zwitterion [43,48]:

$$H_2N - CH_2 - COO - K^+ + CO_2 \leftrightarrow {}^{-}_{1}OOC^{+}H_2N - CH_2COO^{-}K^{+} \quad (2.1)$$

In the second step, zwitterion deprotonates by a base ($B_i$):

$${}^{-}_{1}OOC^{+}H_2N - CH_2COO^{-}K^{+} + B_i \rightarrow {}^{-}_{1}OOCHN - CH_2 - COO^{-}K^{+} + B_iH^{+} \quad (2.2)$$

in which that $H_2O$, $OH^-$ and $H_2NCH_2COO^-K^+$ act as bases in potassium glycinate solution.

The overall kinetic constant ($k_{ov}$) and absorption rate of $CO_2$ ($-r_{CO_2}$) by potassium glycinate are described by:

$$k_{ov} = 2.42 * 10^{16} \exp\left(\frac{-8544}{T}\right) \exp(0.44 C_{PG})\, C_{PG} \quad s^{-1} \tag{2.3}$$

$$-r_{CO_2} = 2.42 * 10^{16} \exp\left(\frac{-8544}{T}\right) \exp(0.44 C_{PG}) C_{PG} C_{CO_2} \tag{2.4}$$

Here, $C_{PG}$ is the molar concentration of potassium glycinate solution (mol/m$^3$) and T is the temperature of the solution (K).

## 2.3. Gas-solvent membrane contactor module design and operation

Commercially, membranes are fabricated as plate-and-frame, tubular, spiral wound and hollow fibre modules [49]. Hollow fibre membrane modules have been widely used in membrane gas separation and their application has been extended to gas-solvent membrane contactors, particularly for post-combustion carbon capture, as they provide a higher interfacial area between the gas and solvent in comparison to other modules [50]. Similar to the design of shell and tube heat exchangers, hollow fibre membranes are bundled (usually known as the lumen side) and placed inside a housing (usually known as the shell side). In the gas-solvent hollow fibre membrane contactors, as mentioned earlier, composite hollow fibres consisting of an ultra-thin and hydrophobic dense polymer on a porous support are usually preferred. This dense layer can be coated on the internal or external circumference of the hollow fibres. To avoid the pore wetting, the solvent is introduced to the membrane contactors in a way it directly contacts the dense polymeric layer. Usually, the solvent on the shell side with the dense layer coated on the external circumference of the fibres provides a better mass transfer performance. With this arrangement, the gas enters the lumen side [51].

The flow configuration in the gas-solvent hollow fibre membrane contactors plays a critical role in the mass transfer performance of these systems. Longitudinal (i.e. parallel flow module) and cross flow configurations are commonly used in the gas-solvent membrane contactors (Figure 2.3). In the longitudinal flow configuration, the gas flows parallel to the solvent on the opposite side of the hollow fibre membrane in co-current or counter-current fashion. However, in some circumstances, the counter-current flow enhances the separation performance by 20% relative to co-current flow [50]. In the cross flow configuration, the fluid in the shell side circulates perpendicular to the flow direction inside the hollow fibre [52]. Due to the ease of preparation and well-defined fluid dynamic, longitudinal flow configuration is mostly

considered by researchers [8]. Therefore, the longitudinal counter-current configuration of flow was used in this thesis.

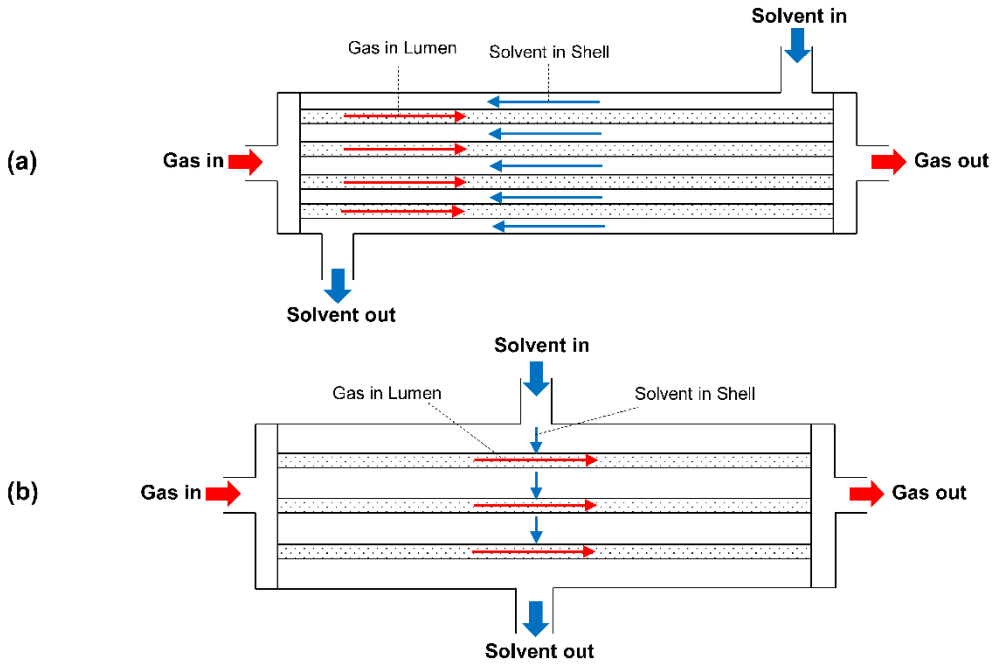


Fig. 2.3. Flow configurations in hollow fibre membrane contactors: (a) counter-current and (b) cross flow

Table 2.1 provides the specifications of gas-solvent hollow fibre membrane contactor systems used in the academic literature for $CO_2$ capture.

Table 2.1 The specifications of gas-solvent membrane contactors studied in the literature for $CO_2$ capture

| **$CO_2$ concentration in flue gas (V%)** | **Solvent type** | **Membrane composition** | **Fibre Num.** | **Fibre length (cm)** | **Fibre thickness (µm)** | **Gas flow rate (L/min)** | **Gas flow velocity (m/s)** | **Solvent flow rate (L/min)** | **Solvent velocity (m/s)** | **[Ref.]** |
|---|---|---|---|---|---|---|---|---|---|---|
| 14 | Potassium glycinate<br>MEA<br>MDEA | PP<br>(microporous) | 7000 | 80 | 98 | - | 0.211m/s<br>0.2-0.55<br>m/s | - | 0.02-0.11<br>m/s | [12] |
| 14 | PG | PTFE | 7000 | 15 | 98 | - | 0.211 m/s | - | 0.05 m/s | [53] |
| - | 2-<br>aminoethanesulfonicacid | Hydrophobic<br>microporous<br>PTFE | - | - | - | - | - | - | 0-0.7 m/s | [54] |
| - | MEA | Non-porous PDMS | - | 30.2 | - | 0.3<br>L/min | - | - | 0.025 m/s | [32] |
| 11.99 | PuraTreatTM<br>MEA | PP<br>PTFE<br>PDMS | 9600 | 14 | 11000 | - | - | 0-<br>0.03L/min | - | [55] |
| 10 | MEA<br>Potassium Carbonate | PP<br>PTFE | - | 14.7 | - | - | - | 0-<br>0.05L/min | - | [56] |
| 5 | PAMAM (1)<br>MEA (2) | PP<br>PMP | - | 17 | - | 0.0087<br>L/min | - | 0.0068<br>L/min | - | [57] |

| **$CO_2$ concentration in flue gas (V%)** | **Solvent type** | **Membrane composition** | **Fibre Num.** | **Fibre length (cm)** | **Fibre thickness (µm)** | **Gas flow rate (L/min)** | **Gas flow velocity (m/s)** | **Solvent flow rate (L/min)** | **Solvent velocity (m/s)** | **[Ref.]** |
|---|---|---|---|---|---|---|---|---|---|---|
| 10-15 | NaOH or Potassium carbonate | PDMS | - | - | 60 | 0.283 L/min | - | - | 0.051 m/s | [58] |
| - | Water + glycerol | PP Polysulfone | - | - | - | - | - | - | 0.0017–0.0115 m/s | [36] |
| 4 | Water or NaOH solution | Polyethersulfone | 34 | - | - | 0.18 L/min | 0-0.06 m/s | - | 0-0.03 m/s | [59] |
| 5 | PG | PDMS | - | 5-50 | - | 5 L/min | - | 0.01-0.5 L/min | - | [60] |
| 14 | MEA | PTFE | - | - | - | - | - | - | - | [24] |

## 2.4. Theory of mass transfer in gas-solvent membrane contactors

Assuming the solvent on the shell side, the molar flux ($N_L$) of an arbitrary component like $CO_2$ in the solvent boundary layer is given by [44]:

$$N_L = \frac{(C_{out} - C_{in})L}{A_{out}} = K_L C_{LM} \quad (2.5)$$

where L is the inert solvent flow rate ($m^3/s$), $A_{out}$ is the mass transfer area based on the outside diameter of the lumen side ($m^2$), $C_{in}$ and $C_{out}$ are the inlet and outlet molar concentrations of $CO_2$ in the solvent ($mol/m^3$), respectively. $C_{LM}$ represents the log mean average of the concentration driving force between the solvent and bulk gas phases, $K_L$ is the overall solvent-based mass transfer coefficient (m/s). With the gas on the lumen side, the molar flux in the gas boundary layer ($N_G$) is determined by [62]:

$$N_G = \frac{(Y_{in} - Y_{out})G}{A_{in}} = K_G C_{LM} \quad (2.6)$$

in which G is the gas molar flow rate (mol/s), $A_{in}$ is the mass transfer area based on the internal diameter of the lumen side ($m^2$), Y is the mole fraction of $CO_2$ in the gas phase and $K_G$ represents the overall gas-based mass transfer coefficient (m/s) [61,62].

In the membrane contactor systems, the overall mass transfer coefficient strongly depends on the mass transfer resistance in the gas phase boundary layer, the resistance in the solvent phase boundary layer, and the membrane resistance (Figure 2.4).

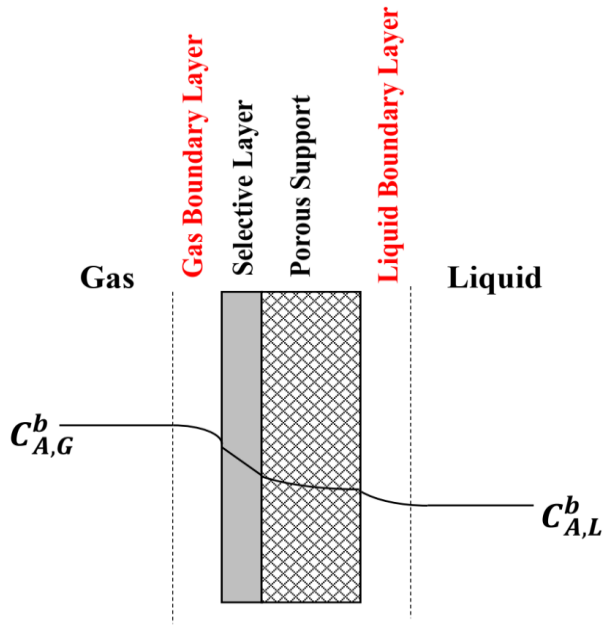


Fig. 2.4. Mass transfer resistances in gas-solvent membrane contactor systems

The overall mass transfer resistances in the solvent and gas phase boundary layers, $\frac{1}{K_L}$ and $\frac{1}{K_G}$ respectively, can be modelled using the concept of "resistances in series" [61]:

$$\frac{1}{K_L} = \frac{Hd_{out}}{k_g d_{in}} + \left(\frac{Hd_{out}}{k_m d_{ln}}\right)_{porous} + \left(\frac{Hd_{out}}{k_m d_{ln}}\right)_{non-porous} + \frac{1}{Ek_l} \quad (2.7)$$

$$\frac{1}{K_G} = \frac{1}{EHk_l} + \left(\frac{d_{out}}{k_m d_{ln}}\right)_{porous} + \left(\frac{d_{out}}{k_m d_{ln}}\right)_{non-porous} + \frac{d_{out}}{k_g d_{in}} \quad (2.8)$$

Here, $k_g$ is the mass transfer coefficient of $CO_2$ across the gas boundary layer (m/s), $k_m$ is the mass transfer coefficient of $CO_2$ through the membrane (m/s), $d_{in}$ is the inside diameter of fibre (m), $d_{out}$ is the outside diameter of fibre (m), $d_{ln}$ is the logarithmic mean diameter of the membrane (m) and $k_l$ is the mass transfer coefficient of $CO_2$ through the solvent boundary layer (m/s). H is the Henry's law constant for $CO_2$ in the solvent and E is the enhancement factor related to the reaction between $CO_2$ and potassium glycinate [6,63–65].

The enhancement factor E depends on the concentration of the reactants and reaction rates and is determined based on the regime of the reaction between the gas and the solvent. The reaction regime is identified using the dimensionless Hatta number (Ha) which is defined by [43].

$$Ha = \frac{\sqrt{k_{ov} D_{CO_2}}}{k_l} \quad (2.9)$$

where $D_{CO2}$ is the diffusion coefficient of $CO_2$ in potassium glycinate ($m^2/s$) and  is the overall kinetic constant of $CO_2$ reacting with potassium glycinate ($s^{-1}$) and is defined by Eq. (2.3).

If $3 < Ha << E_\infty$ the fast pseudo-first order (PFO) reaction regime takes place and the enhancement factor will be equal to Ha [43]. The infinite enhancement factor, $E_\infty$, corresponds to an instantaneous reaction and is described by the penetration theory of Higbie [43].

$$E_\infty = \sqrt{\frac{D_{CO_2}}{D_{PG}}} + \frac{C_s}{v_{CO_2}\frac{P_{CO_2}}{H_{CO_2}}}\sqrt{\frac{D_{PG}}{D_{CO_2}}} \quad (2.10)$$

in which $v_{CO_2}$ is the stoichiometric coefficient of $CO_2$ in reaction with potassium glycinate and $D_{PG}$ is the potassium glycinate diffusion coefficient ($m^2/s$) [43].

Another reaction regime, intermediate reaction, is a situation between PFO and instantaneous reaction regime. DeCoursey [66], Van Swaaij et al. [67] and Versteeg et al. [68] proposed an enhancement factor correlation based on the surface renewal theory [43].

$$E = -\frac{Ha^2}{2(E_\infty - 1)} + \sqrt{\frac{Ha^4}{4(E_\infty - 1)^2} + \frac{E_\infty . Ha^2}{E_\infty - 1} + 1} \quad (2.11)$$

In this thesis, all of the experiments were in the intermediate reaction regime in the shell side of the membrane contactor.

The Henry's law constant (i.e. physical solubility) of $CO_2$ in aqueous amino acid salt is calculated using the salting out effect theory. At high amino acid salt concentrations, salting out effect is explained in the form of Sechenov correlation [69,70]:

$$\log\left(\frac{C_{G,w}}{C_G}\right) = KC_{PG} \quad (2.12)$$

In Eq. (2.12), $C_{G,W}$ and $C_G$ are the physical solubilities of carbon dioxide in pure water and amino acid salt solution and K is Sechenov constant ($m^3$. $kmol^{-1}$). K is determined based on the Schumpe model:

$$K = \sum(h_i + h_G)n_i \quad (2.13)$$

$$h_G = h_{G,o} + h_T(T - 298.15K) \quad (2.14)$$

where $n_i$ represents the index of the ion i in the formula of the amino acid salt, $h_i$ and $h_{G,o}$ are the ion and gas specific constants ($m^3$.$kmol^{-1}$), respectively. $h_T$ is the gas specific parameter for the temperature effect ($m^3$. $kmol^{-1}$. $K^{-1}$) [69].

The mass transfer resistance is divided into porous ($(1/k_m)_{porous}$) and non-porous layer mass transfer resistances ($(1/k_m)_{non\text{-}porous}$) [71].

$$\left(\frac{1}{k_m}\right)_{porous} = \frac{\delta_p \tau}{D_{CO_2}\varepsilon} \quad (2.15)$$

$$\left(\frac{1}{k_m}\right)_{non-porous} = \frac{\delta_{np} \nu_m}{PRT} \quad (2.16)$$

where $\delta_p$ is the porous support thickness (m), $\tau$ is the pore tortuosity, $\varepsilon$ is the porosity, $D_{CO_2}$ is the gas diffusivity into the pores ($m^2/s$), $\delta_{np}$ is the non-porous layer thickness (m), $\nu_m$ is the molar volume of gas ($m^3$/mol) and P is the permeability through the non-porous layer ($m^2$.$mol^{-1}$.$pa^{-1}$.$s^{-1}$) [71].

If pure $CO_2$ is introduced into the lumen side, the non-porous layer mass transfer resistance as a constant value could be defined by the Wilson plot method (Eq. (2.17)). This method employs

the solvent phase overall mass transfer coefficient and solvent phase velocity to calculate the membrane mass transfer coefficient.

$$\frac{1}{K_L} = C_1 \overline{u_0}^{-\theta} + \frac{Hd_{out}}{k_m d_{ln}} \tag{2.17}$$

Here, $\overline{u_0}$ is the average solvent velocity (m/s) and θ is a fitting parameter providing the best linear relationship. Therefore, the $1/k_m$ can be determined by a linear fitting of $\frac{1}{K_L}$ versus $u^{-\theta}$ [63].

To model the mass transfer through the solvent boundary layer on the shell side of the gas-solvent membrane contactor, the shell side Sherwood number ($Sh_s$) correlation is introduced. $Sh_s$ is modelled as a function of Reynolds number ($Re_s$), Schmitt number ($Sc_s$), and module parameters of the specific study. The general form of $Sh_s$ is defined by [72]:

$$Sh_s = \frac{k_l d_h}{D_{CO_2}} = f(\Phi)\left(\frac{d_h}{l}\right)^{\vartheta} Re_s^{\alpha} Sc_s^{\beta} \tag{2.18}$$

where, ϑ, α, and β are constants, Φ is packing density, $d_h$ is the hydraulic diameter of shell (m) and l is module length (m). The general correlations of $Re_s$, $Sc_s$, and $d_h$ are described as:

$$Re_s = \frac{\rho_L \overline{u_{0,L}} d_h}{\mu_L} = \frac{4\rho_L L}{n\pi d_{out}\mu_L} \tag{2.19}$$

$$d_h = \frac{d_{cin}^2 - n d_{out}^2}{n d_{out}} \tag{2.20}$$

$$Sc_s = \frac{\mu_L}{\rho_L D_{CO_2}} \tag{2.21}$$

where $\overline{u_{0,L}}$ is the average solvent velocity (m/s), n is the number of hollow fibres and $d_{cin}$ is the contactor inner diameter (m) [72]. Some of the empirical correlation for $Sh_s$ in randomly-packed hollow fibre membrane contactor is reported in Table 2.2.

The lumen side mass transfer is expressed by the lumen side Sherwood number ($Sh_t$). Table 2.3 shows some of the empirical correlations for the lumen side Sherwood number in hollow fibre membrane contactors. $Sh_t$ is defined as a function of $d_h$, l, the lumen side Reynolds ($Re_t$) and Schmitt ($Sc_t$) numbers [73].

$$Sh_t = \frac{k_g d_h}{D_{CO_2,g}} = e\left(\frac{d_h}{l}\right)^{c} Re_t^{r} Sc_t^{d} \tag{2.22}$$

$$Re_t = \frac{\rho_g \overline{u_g} d_{in}}{\mu_g} \tag{2.23}$$

$$Sc_t = \frac{\mu_g}{\rho_g D_{CO_2,g}} \tag{2.24}$$

where $D_{CO_2,g}$ is the diffusivity of $CO_2$ in the gas phase ($m^2/s$) and $\overline{u_g}$ is the average gas velocity (m/s) [71].

For the laminar flow, the $Sh_t$ is obtained from the Graetz- Lévêque correlations [62,73]:

$$Sh_t = 1.62 Gz_t^{\frac{1}{3}} \qquad Gz_t > 6 \tag{2.25}$$

$$Sh_t = 0.5 Gz_t \qquad Gz_t < 6 \tag{2.26}$$

where the Graetz number (Gz) is given by [62]:

$$Gz_t = Re_t Sc_t \left(\frac{d_{in}}{l}\right) \tag{2.27}$$

The Graetz- Lévêque analysis assumes that the concentration of components remains constant in the centre of fibres [74]. As a result, in one investigation, Wickramasinghe et al. [74] has shown that the Graetz-Lévêque correlation overestimates the Sherwood number at low flow conditions, i.e. $Gz < 6$. In this thesis, a generic form was used to express $Sh_t$ given by [74]:

$$Sh_t = \gamma Gz_t^{\eta} \tag{2.28}$$

for which $\gamma$ and $\eta$ are two adjustable parameters determined from fitting Eq. (2.28) to the experimental data.

Table 2.2. Empirical correlation for $Sh_s$ in randomly- packed hollow fibre membrane contactor [72]

| Correlations | Conditions | Notes | Reference |
|---|---|---|---|
| $\mathbf{Sh_s = 0.055 Re^{0.72} Sc^{0.33}}$ | $0.1 < Re < 250$ ; $0.32 < \Phi < 0.45$ | Gas-solvent systems; Handmade and commercial modules | [72] |
| $\mathbf{Sh_s = (0.52 - 0.64\Phi) Re^{(0.36+0.3\Phi)} Sc^{0.33}}$ | $0 < Re < 100$; $0.3 < \Phi < 0.7$ | Gas-solvent systems; Handmade modules OD/ID = 500/300 μm | [75] |
| $\mathbf{Sh_s = 0.1789\Phi^{0.86} Re^{0.34} Sc^{0.33}}$ <br> $\mathbf{Sh_s = (0.167 - 0.798\Phi + 1.738\Phi^2 - 1.37\Phi^3) Re^{0.7} Sc^{0.33}}$ | $Re < 400$; $400 < Re$; $0.029 < \Phi < 0.53$ | Gas-solvent systems; Handmade modules Sealed end contactors OD/ID = 650/390 μm | [76] |
| $\mathbf{Sh_s = \frac{1}{0.86 - 0.3\Phi} Gz^{(0.14+0.3\Phi)}}$ | $60 < Re < 1200$; $0.2 < \Phi < 0.5$ | Gas-solvent systems; Handmade modules | [77] |
| $\mathbf{Sh_s = (0.163 + 0.27\Phi) Gz^{0.6}}$ | $178 < Re < 1194$ ; $0.2 < \Phi < 0.5$ | Gas-solvent systems; Handmade modules OD/ID = 420/340 μm | [78] |
| $\mathbf{Sh_s = (0.3045\Phi^2 - 0.3421\Phi + 0.15) Re^{0.9} Sc^{0.33}}$ | $32 < Re < 1290$ ; $0.08 < \Phi < 0.7$ | Gas-solvent systems; Handmade modules OD/ID = 1000/600 μm | [79] |
| $\mathbf{Sh_s = 0.24 (Re \frac{d_h}{l})^{0.59} Sc^{0.33}}$ | - | Gas-solvent systems; Handmade modules Sealed end contactors | [80] |

| Correlations | Conditions | Notes | Reference |
|---|---|---|---|
| $\mathbf{Sh_s} = (\mathbf{0.53} - \mathbf{0.58\Phi})\mathbf{Re}^{\mathbf{0.53}}\mathbf{Sc}^{\mathbf{0.33}}$ | $21 < \mathrm{Re} < 324$ ; $0.32 < \Phi < 0.76$ | Gas-solvent systems; Handmade modules OD/ID = 670/300 μm | [81] |
| $\mathbf{Sh_s} = \mathbf{1.25}(\mathbf{Re}\frac{\mathbf{d_h}}{\mathbf{l}})^{\mathbf{0.93}}\mathbf{Sc}^{\mathbf{0.33}}$ | $0.5 < \mathrm{Re} < 500$ ; $0.02 < \Phi < 0.33$ | Gas-solvent Handmade modules OD/ID =466/413 μm | [82] |

Table 2.3. Tube side mass transfer analysis through lumen side of hollow fibre membrane contactor

| Validity range | Sc | $d_h/l$ | $Sh_t$ | Reference |
|---|---|---|---|---|
| $\mathbf{Gz > 10}$ | 671 | $1.95 \times 10^{-3}$ | $1.61Gz^{1/3}$ | [83] |
| $\mathbf{Re > 5}$ | 507 | $4.2 \times 10^{-4}$ | $1.61Gz^{1/3}$ | [84] |
| - | - | - | $1.5Gz^{1/3}$ | [85] |
| $\mathbf{Gz > 4}$ | 476 | $0.71 - 2.4 \times 10^{-3}$ | $1.61Gz^{1/3}$ | [74] |

## 2.5. Challenges ahead of gas-solvent hollow fibre membrane contactors

Although the gas-solvent hollow fibre membrane contactors improve the performance of $CO_2$ capture process in comparison to the conventional absorption columns, it imposes some limitations in terms of mass transfer resistances. Using thin-film non-porous hollow fibre membranes, the solvent phase boundary layer dominates the overall mass transfer resistance in the gas-solvent membrane contactors [29,38,86]. Equally importantly, $CO_2$ is separated from a mixture with different diffusivities of components causing the gas side boundary layer to form which in turn adds to the mass transfer resistance.

There are potential solutions in the academic literature to minimize these resistances that are based on applying additional mixing to reduce the impact of boundary layers on mass transfer. The additional mixing to increase heat transfer have been successfully demonstrated in shell and tube heat exchangers [87]. Using the heat and mass analogy, the mass transfer performance should be enhanced by similar mechanisms [50,88]. These potential solutions are discussed in the following sections.

## 2.6. Potential solutions to reduce solvent side mass transfer resistance

### 2.6.1. Application of oscillating units

Keil and Baird [87] investigated the effect of oscillation on heat transfer performance and observed that oscillating liquid flow enhanced the overall heat transfer coefficient in shell and tube heat exchanger. Karamercan and Gainer [89] introduced appropriate oscillating frequency and amplitude to the liquid boundary layer to facilitate additional mixing and as a result, obtained a greater heat transfer rate [89]. Najarian and Bellhouse [90] investigated the impact of liquid oscillation on the ultrafiltration processes for protein fractionation. They reported an enhancement in the selectivity of the ultrafiltration membrane. Kennedy et al. [88] demonstrated that the application of oscillating reverse osmosis led to 70% increase in the

permeation flux [88]. Blanpain-Avet et al. [91] studied the effect of oscillatory flow on the cross flow microfiltration process. Their experimental work reflected that the oscillation changed the hydrodynamics of the flow upstream of the membrane unit which resulted in the reduction of the membrane fouling resistance (up to 100%). This way the separation performance of the microfiltration process was remarkably enhanced [91]. Similarly, Budzyński et al. applied an oscillating liquid flow to a bubble column and indicated that the mass transfer performance was improved through a change in the hydrodynamics of the flow in the bubble column [92]. Pulsed back and forward cross flow were induced to a membrane emulsification system to eliminate the shear stress outside the membrane as it existed in conventional cross flow membrane emulsification systems. The results of this study indicated that uniform emulsion droplets were obtained using a pulsed back and forward cross flow [93].

Different experimental apparatus have been employed to generate oscillation which unanimously contains an electric motor, a variable speed transmission and a reciprocating pump consisted of a cylinder and a piston (Figure 2.5) [88,89].

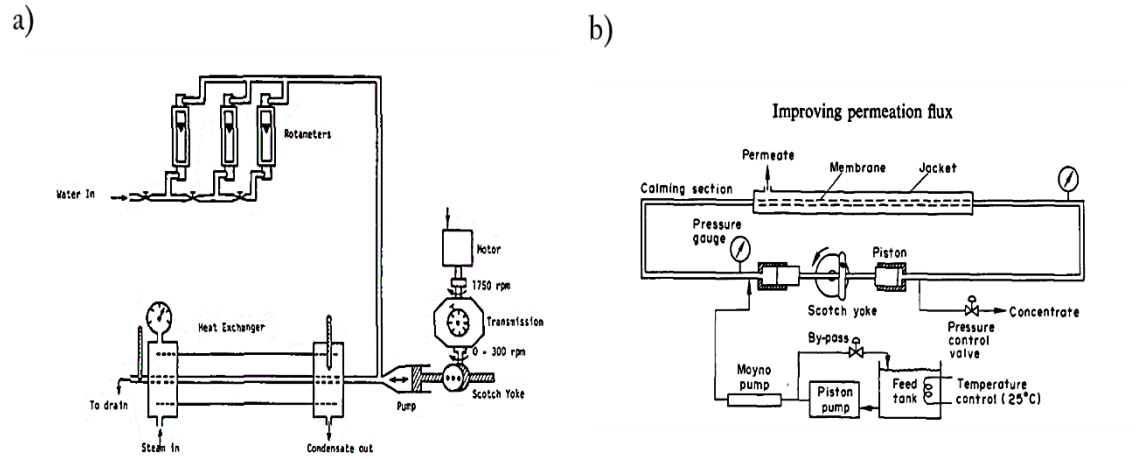


Fig. 2.5. Systems under oscillation: a) application of oscillator in a shell and tube heat exchanger [89], b) application of oscillator in reverse osmosis [88]

## 2.6.2. Application of wavy-walled channels

Nishimura and Matsune [94] used symmetric and asymmetric wavy walled channels (Figure 2.6) to generate pulsatile flow. They showed the time-averaged Sherwood number with the pulsatile flow was improved by a factor of 4.8 relative to the Sherwood number of steady flows. This significant increase was attributed to the formation of vortices that induced additional mixing and reduced the thickness of mass transfer boundary layer.

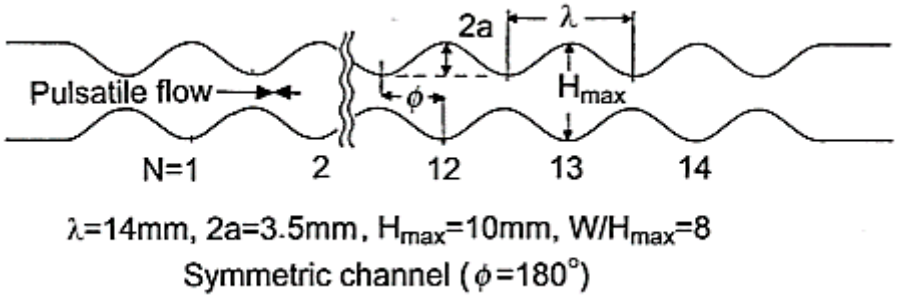


Fig. 2.6. Wavy walled channels used in the Nishimura and Matsune work [94]

Using hollow fibre membrane contactors, Luelf et al. [95] introduced the solvent phase into the hollow fibres whose internal surface was of sinusoidal shape (Figure 2.7). They observed that the oxygen transfer from the shell to the lumen side of the sinusoidal-shaped hollow fibre membrane contactor was significantly enhanced by a factor of 2.5 [95].

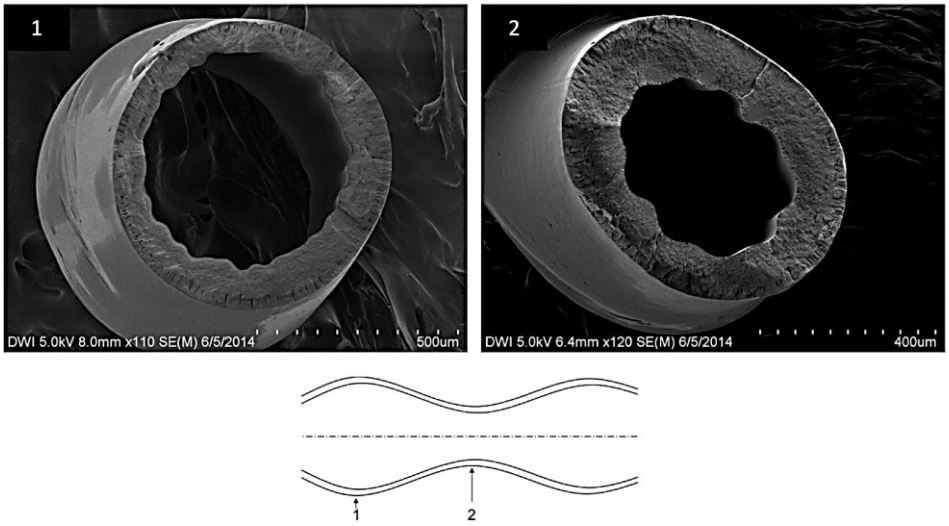


Fig. 2.7. FESEM image of sinusoidal-shaped hollow fibre membranes [95]

### 2.6.3. Application of baffled module

Designed by CELGARD LLC, a central baffle was incorporated into the design of the Liqui-CelTM Extra-Flow membrane contactor (Figure 2.8) [96] where the shell side by-passing was reduced, additional mixing was generated and a higher mass transfer coefficient was provided. Baffled hollow fibre membrane contactor modules provided both counter-current contacting, which in turn increased the number of mass transfer units within the modules, and cross flow configuration, that allowed the flow to be perpendicular to the hollow fibres. In such an

arrangement, the mass transfer coefficient was 5 times greater than that of a non-baffled conventional module [97].

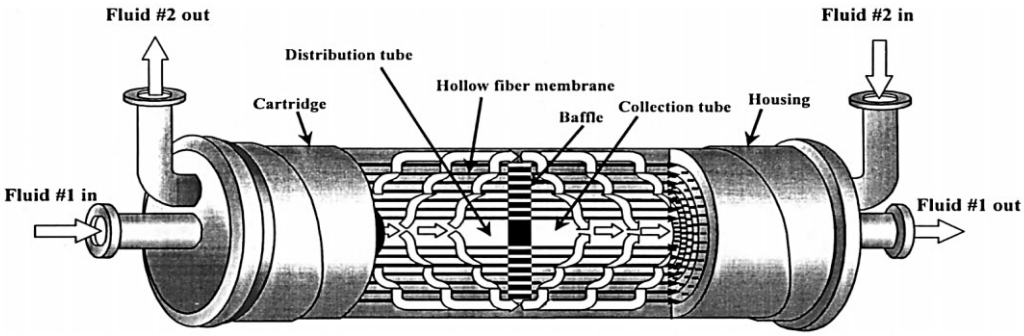


Fig. 2.8. The Liqui-CelTM Extra-Flow membrane contactor designed by CELGARD LLC [96]

## 2.6.4. Application of vibrating units

William B. Krantz et al. [98] evaluated the separation performance of membrane oxygenators under axial membrane vibrations and reported the mass transfer coefficient under the vibrating conditions was at least 2.56 times greater relative to non-vibrating conditions [98]. The vibration perpendicular to the fluid flow was shown to remarkably increase the mass transfer performance of hollow fibre membrane contactors [99]. The advantage of the vibrating hollow fibre membrane contactors was that both mass transfer boundary layers formed on the shell and the lumen side were simultaneously affected which resulted in reducing the overall mass transfer resistance and subsequently increasing the mass transfer rate. Figure 2.9 shows an experimental set-up providing the vibration of fluid flow within hollow fibre membrane contactors. In addition to perpendicular vibration, other vibrational configurations can be induced to the membrane contactor systems. For example, rotational and transverse vibrating units were applied for membrane filtration processes, mitigating membrane fouling, protein separation (Figure 2.10) and water treatment with noticeably enhanced separation performances [100–103].

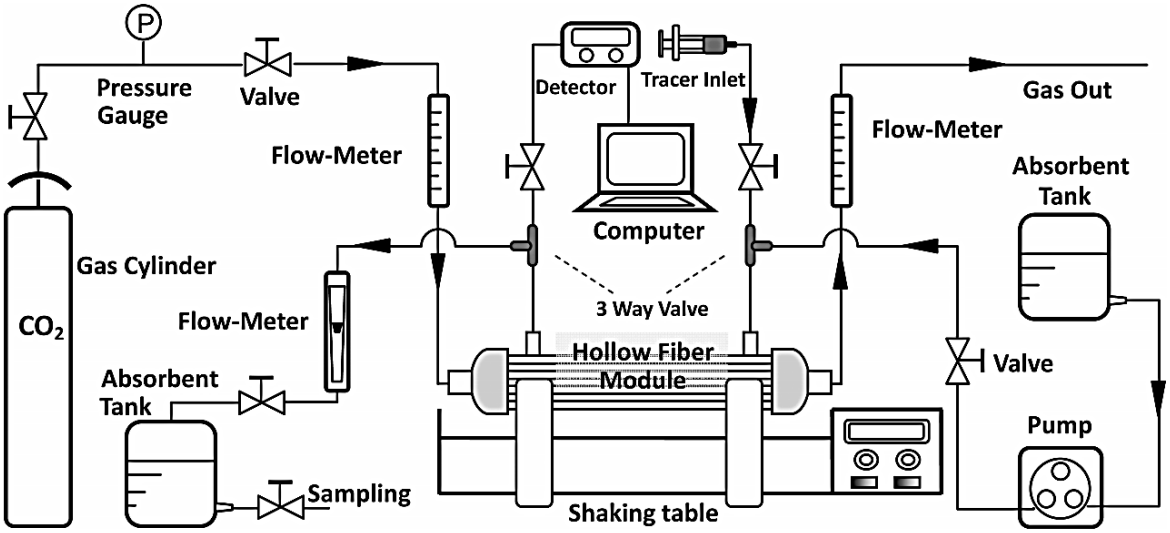


Fig. 2.9. A hollow fibre membrane contactor system under vibrational conditions [99]

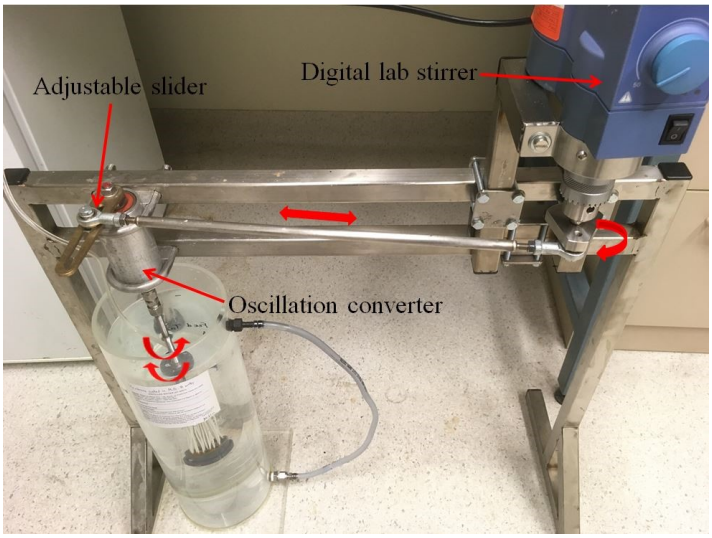


Fig. 2.10. A rotational vibrating system in the bio-separation process[100]

## 2.7. Potential solutions to reduce gas side mass transfer resistance

### 2.7.1. Application of pulsed operation

As mentioned in the previous sections, the gas boundary layer can also form in hollow fibre membrane contactors when separating mixed gases. The formation of gas phase boundary layer adds an extra mass transfer resistance to gas-solvent membrane contactor systems. Inducing the oscillation to the gas phase and generating a pressure wave have been suggested to reduce the effect of gas phase boundary layer resistance on the separation performance [104]. In his pioneering work, Paul [105] introduced a new operation to membrane gas separation through which the upstream pressure was pulsed by opening and closing the valves connected to the

feed and the reject sides (Figure 2.11). The use of pulsed upstream pressure resulted in an increase in the membrane selectivity [105].

In one critical review, Wang et al. [104] discussed pulsed operations (i.e. the short and long class cyclic transient gas separations) and concluded that these methods are too complex to operate, have high operating costs and need high energy consumption.

(a)

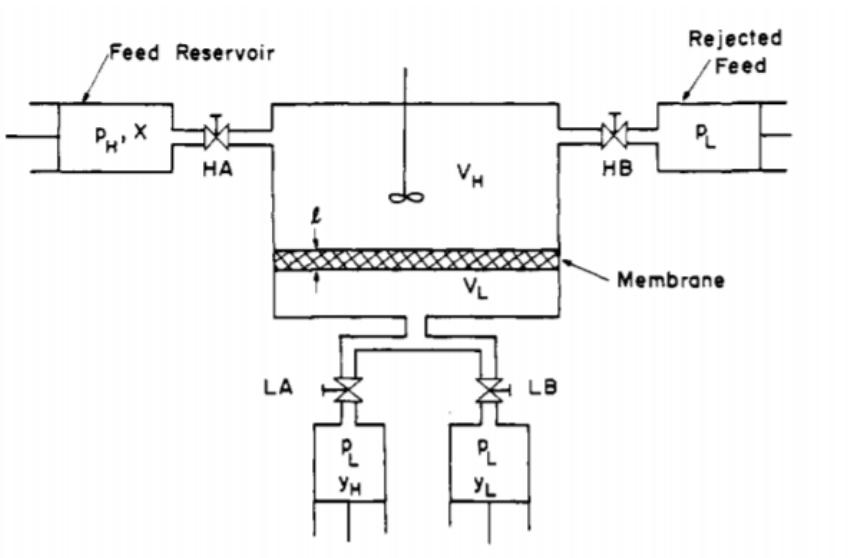


(b)

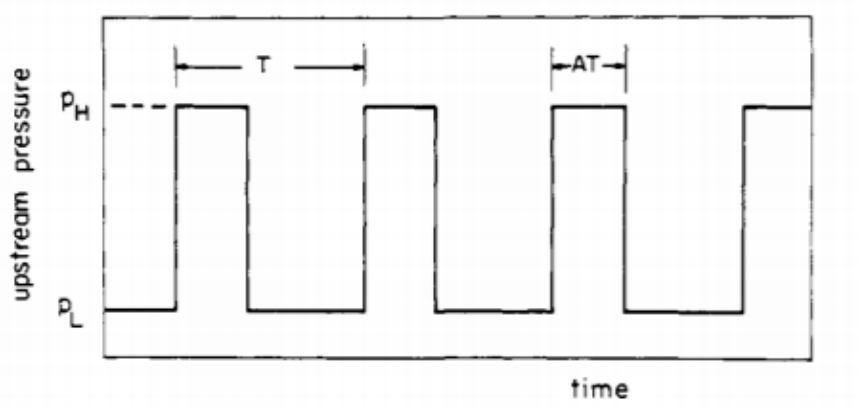


Fig. 2.11. (a) Cyclic transient operation in membrane gas separation proposed by Paul [105] where enhanced separation performances are achieved by introducing pulsation to the upstream pressure, (b) Pulsed upstream pressure (square wave form) as a result of cyclic transient operation.

The enhanced separation performance of membranes was also achieved by retentate pulsed mode where the upstream pressure pulsation was introduced through a valve on the retentate

stream (Figure 2.12) [106]. The pulsed retentate mode was much simpler in operation than the one proposed by Paul and resulted in less loss of membrane productivity.

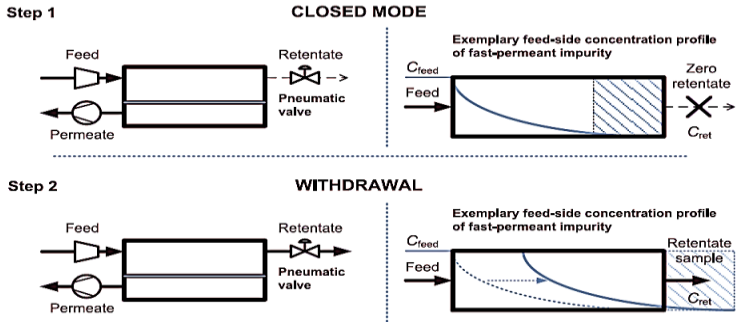


Fig. 2.12. Pulsed retentate mode to introduce pulsation to the upstream pressure [106].

## 2.7.2. Application of pressure oscillating units

The pulsed operation methods in gas phase were based on generating square pressure wave forms (Figure 2.11b) which did not vary the pressure with a certain frequency [105]. In gas-solvent hollow fibre membrane contactors, one approach to achieve enhanced mass transfer in the gas phase is to vary the pressure sinusoidally, similar to introducing oscillation to the solvent phase. With this approach, control over pressure and fluid velocity is enabled by setting frequencies and amplitudes to certain values.

## 2.8. Theory of gas-solvent hollow fibre membrane contactors under oscillating and vibrating conditions

Under oscillating conditions, the pressure and the velocity obey a sinusoidal pattern [87]. Suggested by Keil and Baird [87], the oscillating velocity ($u_{os}$ ,m/s) is defined as a function of the average non-oscillating velocity ($\overline{u_0}$, m/s), the oscillating amplitude (A, m), the oscillating frequency (F, Hz) and the angular frequency (ω, rad/s) [87]:

$$u_{os}(t) = \overline{u_0} + 2\pi AF\sin(\omega t) \tag{2.29}$$

where:

$$\omega = 2\pi F \tag{2.30}$$

Introducing oscillation to the gas-solvent hollow fibre membrane contactors results in unsteady state operation. To model mass transfer phenomenon under such conditions, one effective way is to obtain a time-averaged Sherwood number correlation [94]. A root mean square value

velocity ($u_{os,rms}$) is defined. Based on this velocity, an oscillating Reynolds number is defined, and a Sherwood number correlation is proposed based on this for a given set of experimental data. The oscillating flow root mean square velocity ($u_{os,rms}$) is given by [107,108]:

$$u_{os,rms} = \sqrt{\frac{1}{T}\int_0^T u_{os}^2(t)dt} \tag{2.31}$$

where T is the period of the sinusoidal function. To define the $u_{os,\,rms}$ as a function of F and A (Eq. (2.32)), Eq. (2.29) is substituted into Eq. (2.31).

$$u_{os,rms} = \sqrt{F\int_0^{\frac{1}{F}}(\overline{u_0} + 2\pi AF\sin(\omega t))^2 dt} \tag{2.32}$$

Hino et al. [109] incorporated the oscillating flow parameters (i.e. frequency and amplitude) into the definition of the Reynolds number and used the modified Reynolds number to interpret the fluid dynamics of oscillation systems [109]. This approach is adopted in the current thesis. A general correlation based on the oscillating Reynolds number is proposed to describe mass transfer in the solvent boundary layer given by:

$$Sh_{s,os} = \frac{k_{l,os}d_h}{D_{CO_2}} = f(Re_{s,os}, Sc_s) \tag{2.33}$$

where $Sh_{s,os}$ and $Re_{s,os}$ denote the Sherwood and Reynolds numbers of the solvent (i.e. shell) side under oscillating conditions.

Also, under the oscillating conditions, mass transfer in the gas boundary layer is described as a function of oscillating Graetz number defined by:

$$Sh_{t,os} = f(Gz_{t,os}) \tag{2.34}$$

Under vibrating conditions, Krantz et al. [98] suggested using a dimensionless parameter ($\Pi_v$) to indicate the effect of vibrating frequency and displacement amplitude on the mass transfer correlation [98]. $\Pi_v$ is proposed as:

$$\Pi_v = \frac{A_d F}{\overline{u_0}} \tag{2.35}$$

where $A_d$ and F are the displacement amplitude (m) and frequency (Hz), respectively [98]. The Sherwood number correlation for the solvent ($Sh_{s,v}$) boundary layer under vibrating conditions is proposed by [98]:

$$Sh_{s-vib} = f(\Pi_v, Re_s, Sc_s) \tag{2.36}$$

## 2.9. Scope of this work

One of the cost-effective and efficient technologies for the post-combustion carbon capture is the gas-solvent membrane contactors systems. These systems, however, face critical challenges, such as the gas and the solvent phase boundary layer resistances to overall mass transfer, which restrict their wider use.

This literature review shows that the applications of composite hollow fibre membranes comprised of a non-porous ultra-thin polymer layer supported by a porous polymer and selective solvents in gas-solvent membrane contactor systems are well known. However, to the best of author's knowledge, there is no comprehensive research work addressing limitations imposed by mass transfer resistances of the solvent and gas boundary layers in gas-solvent hollow fibre membrane contactors. Previous studies showed the application of fluid oscillation and vibration to reduce the thickness of boundary layer and subsequently its mass transfer resistance in different applications was successful.

For the first time, this thesis focuses on the influence of boundary layer oscillation and vibration on $CO_2$ capture using gas-solvent hollow fibre membrane contactors. The major difference between oscillation and vibration techniques is in the way that impacts the boundary layers of solvent and gas phases, along with the membrane. Using oscillation, only one of the solvent or gas boundary layers is disturbed, while vibration introduces turbulence to both phases simultaneously along with the membrane. The scope of the current thesis includes:

- Investigating the effect of oscillating solvent flow as a novel approach on the solvent boundary layer mass transfer resistance using pure $CO_2$

- Investigating the influence of oscillating gas flow as a novel method of reducing mass transfer resistance on the gas side using a mixed gas representative of the feed to post-combustion $CO_2$ capture

- Investigating the effect of boundary layer vibration on both solvent and gas side mass transfer resistances for the first time using a novel system inducing linear vibration to membrane contactors

# CHAPTER 3: EXPERIMENTAL

## 3.1. Introduction

Chapter 3 outlines the experimental methods utilised in this thesis. First, the preparation of hollow fibre membrane contactors is described. Next, the design and operation of oscillating and vibrating units are explained in detail. Finally, the operation of the hollow fibre membrane contactor system under oscillating and vibrating conditions is presented and the methods of the analysis of experimental data are discussed. The highlights of this chapter include:

1. Gas-solvent membrane contactors under **oscillating solvent flow conditions**
2. Gas-solvent membrane contactors under **oscillating gas flow conditions**
3. Gas-solvent membrane contactors under **vibrating conditions**

## 3.2. Materials

### 3.2.1. Liquid supplies

Glycine ($NH_2CH_2COOH$, 98.5% purity) and potassium hydroxide (KOH, 85% purity) were provided by Thermo Fisher Co. to prepare potassium glycinate as a solvent for $CO_2$ absorption experiments. Sulfuric acid (95-97% purity, Scharlau) and filtered carbon anode and cathode solution (UIC INC.) were used to measure $CO_2$ content in the rich solvent samples.

### 3.2.2. Gas supplies

Carbon dioxide ($CO_2$, 99.99% purity) and a gas mixture of 10% $CO_2$ in $N_2$ (balanced) were provided by BOC Gas Ltd., Australia to study the $CO_2$ capture by the hollow fibre membrane contactor. Liquid nitrogen was purchased from Liquid Nitrogen Services, Australia to cut the hollow fibre membranes into certain lengths. The use of liquid nitrogen helped the hollow fibres cut precisely without blocking.

### 3.2.3. Membranes

The composite hollow fibre membranes studied in this thesis were composed of a non-porous ultra-thin polydimethylsiloxane (PDMS) on a porous polysulfone (PSf) support supplied by Airrane Co. Ltd. (Daejeon, Korea). The characteristics of Airrane's hollow fibre membranes are shown in Table 3.1.

Table 3.1. Specifications of composite hollow fibre membranes (Airrane Co.)

| | |
|---|---|
| Inside diameter (μm) | 300 |
| Outside diameter (μm) | 470 |
| Thickness of PDMS (μm) | 0.5 |
| Porosity of PSf | 0.5 |
| Tortuosity of PSf | 2.36 |

## 3.3. Methods

### 3.3.1. Potassium glycinate solution preparation

15wt% potassium glycinate solution was prepared from adding equimolar amounts of potassium hydroxide and glycine to water (pH=7, MILLIPORE, Elix®20). It took 2 hours for the prepared solution to reach the ambient temperature before starting the experiments. The pH of the solution was 12 and polyethylene tanks were used to store the solution. Table 3.2 indicates the specifications of the potassium glycinate solution including density, viscosity and

diffusion coefficients obtained from the literature, as well as the enhancement factor and Henry's law constant determined theoretically [69,70].

Table 3.2. Specifications of 15wt% potassium glycinate at 25°C (laboratory temperature)

| | |
|---|---|
| Density ($kg/m^3$) | 1060 |
| Viscosity (kg/m.s) | 0.001323 |
| Diffusion coefficient of $CO_2$ in potassium glycinate ($m^2/s$) | $1.46\times10^{-9}$ |
| Potassium glycinate diffusion coefficient ($m^2/s$) | $4.66\times10^{-10}$ |
| Enhancement Factor | 20.890 |
| Henry's law constant ($Pa.m^3/mol$) | 4224.310 |

### 3.3.2. Hollow fibre membrane contactor preparation

The preparation of hollow fibre membrane contactors is shown in Figure 3.1. Hollow fibre membranes were bundled and inserted into an in-house constructed module. The two ends of the module were glued using an epoxy adhesive (Selley's Araldite Super Strength Epoxy Adhesive, Selleys Pty Ltd, NSW, Australia) to firmly hold the hollow fibre membranes and prevent solvent leakage problems. The glued ends were left for 24 hours to be dried. After drying, extra lengths of the hollow fibres were soaked into the liquid nitrogen, so they were frozen and cut easily. Moreover, with this method, hollow fibres without blockage or deformation were obtained which in turn resulted in unrestricted gas phase entering the fibres. The membrane contactor was thoroughly checked for any solvent leakage before experiments. To do so, the shell side of the membrane contactor was filled with water and no leakage was detected. Additionally, no water leakage was observed from the glued ends of the hollow fibres, so water flowed only on the shell side and was not carried along with the gas phase on the lumen side. This meant that the wetting of the hollow fibres did not occur. The membrane contactors used in this thesis were of 25cm length and constructed from Teflon.

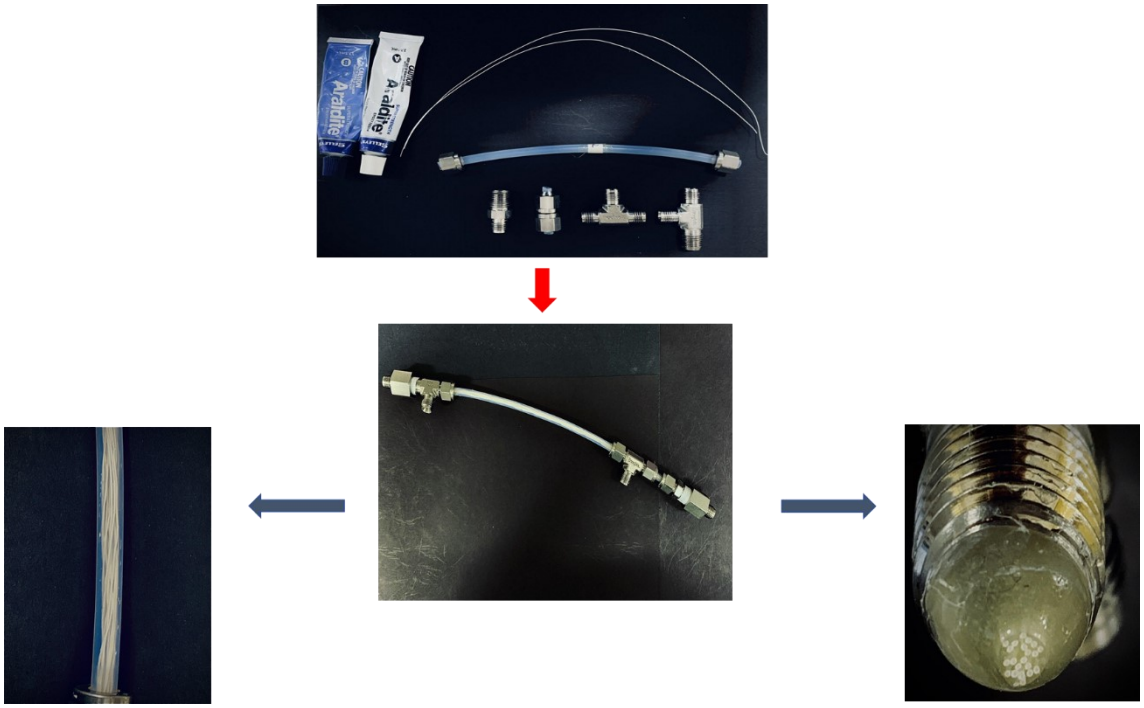


Fig. 3.1. Fabrication of hollow fibre membrane contactor

### 3.3.3. Operation of gas-solvent hollow fibre membrane contactors

The conventional experimental apparatus (Figure 3.2) consisted of hollow fibre membranes contactor, gear pump, solvent tank, $CO_2$/Mixed gas line, needle valve, pressure indicator, gas/solvent flow indicator, temperature indicator, gas meter and separator. The lean solvent was stored in a 20 L tank at ambient temperature. Before the experiments, the rich solvent flow rate was measured manually and the gear pump (Ismatec, 0–0.11 L/min) was calibrated accordingly. In a counter-current fashion, the solvent was entered the flow rotameter (LH-5KA-O (Kytala, Muurame Finland), 0.01-0.13 L/min) and then circulated through the shell side of the membrane module using the gear pump. A needle valve downstream of the module on the solvent stream was used to control the differential pressure across the membrane and to avoid gas bubbling in the solvent phase. The feed gas was introduced to a gas separator to separate out the possible condensable fraction of the gas phase. Then, the gas phase entered the lumen side of the membrane contactor at given pressures and flow rates. The feed gas flow rates and pressures were measured by a gas rotameter (LH-4KD-H (Kytala, Muurame Finland), 0-10 L/min) and a pressure gauge (Swagelok, ranged between 0 and 12 bar), respectively. To ensure that the steady-state process was achieved, the system operated for 1 hour. After that, rich solvent samples were collected and the $CO_2$ concentration was measured by colourimetry titration (CM5015 Coulometer, UIC Inc., USA).

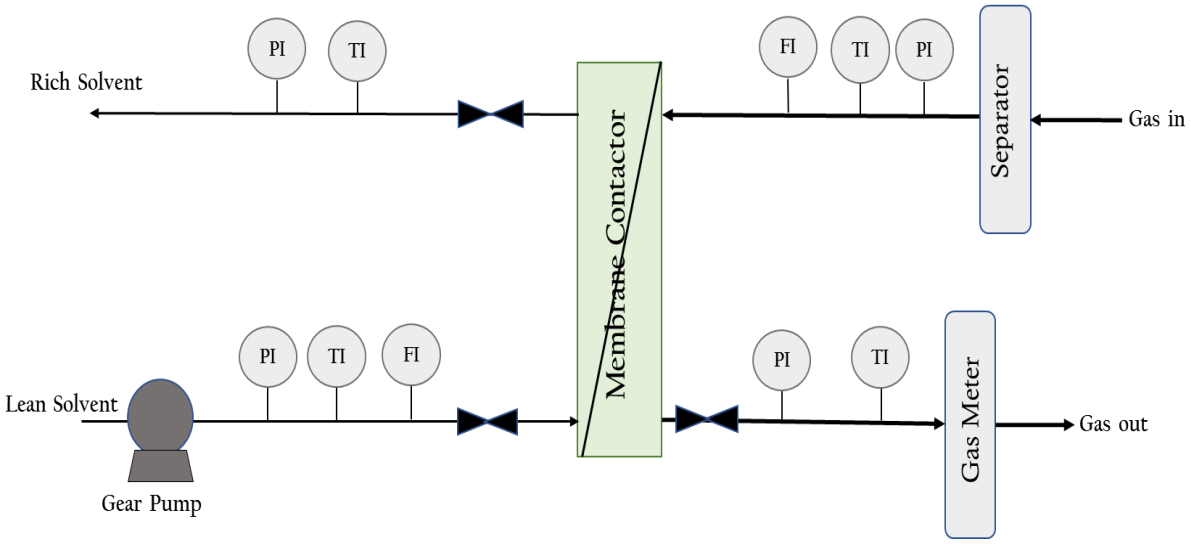


Fig. 3.2. Experimental rig for $CO_2$ capture using conventional hollow fibre membrane contactors

## 3.4. Analysis of $CO_2$ in rich solvent samples

$CO_2$ coulometer equipment was used to obtain the $CO_2$ concentration in the solvent phase. This equipment (Figure 3.3) contained two main parts: acidification module and coulometer. The acidification module was used to acidify the rich solvent samples in a heated reaction vessel by injecting adjusted amount of sulfuric acid (5mL of sulfuric was injected in this research work). After completing the reaction between sulfuric acid and the rich solvent, the products such as dissolved $CO_2$, carbonate ion, bicarbonate ion, and carbonic acid were swept out to a scrubbing system using a free-$CO_2$ carrier after which they were introduced into the $CO_2$ Coulometer for detection. The $CO_2$ reacted with the carbon cathode solution to form a titratable acid. A photodetector device monitored the colour change within the solution during titration. In the final step, the end point of the titration was reported in the coulometer's display. The accuracy of $CO_2$ measurement using the coulometer device is $\pm$5.0 percent.


Fig. 3.3. Colourimetry titration equipment

## 3.5. Oscillating unit

To obtain oscillating flow, an oscillating unit (Figure 3.4) was added to the conventional gas-solvent membrane contactor system. The oscillating unit consisted of a variable frequency drive (Cole-Parmer Co., Masterflex® L/S®), a motor (Cole-Parmer Co., Masterflex® L/S®), a ceramic cylinder and a Teflon piston moving in a sinusoidal motion. The cylinder and piston of the oscillating unit were purchased from Cole-Parmer Co. with the oscillating frequency of 0.002–10 Hz and the stroke lengths of 0-4 cm. This enabled the oscillating solvent/gas flow to be generated by variable speed and stroke length. The accuracy of the adjusted oscillating frequency and amplitude was ±3.0 percent

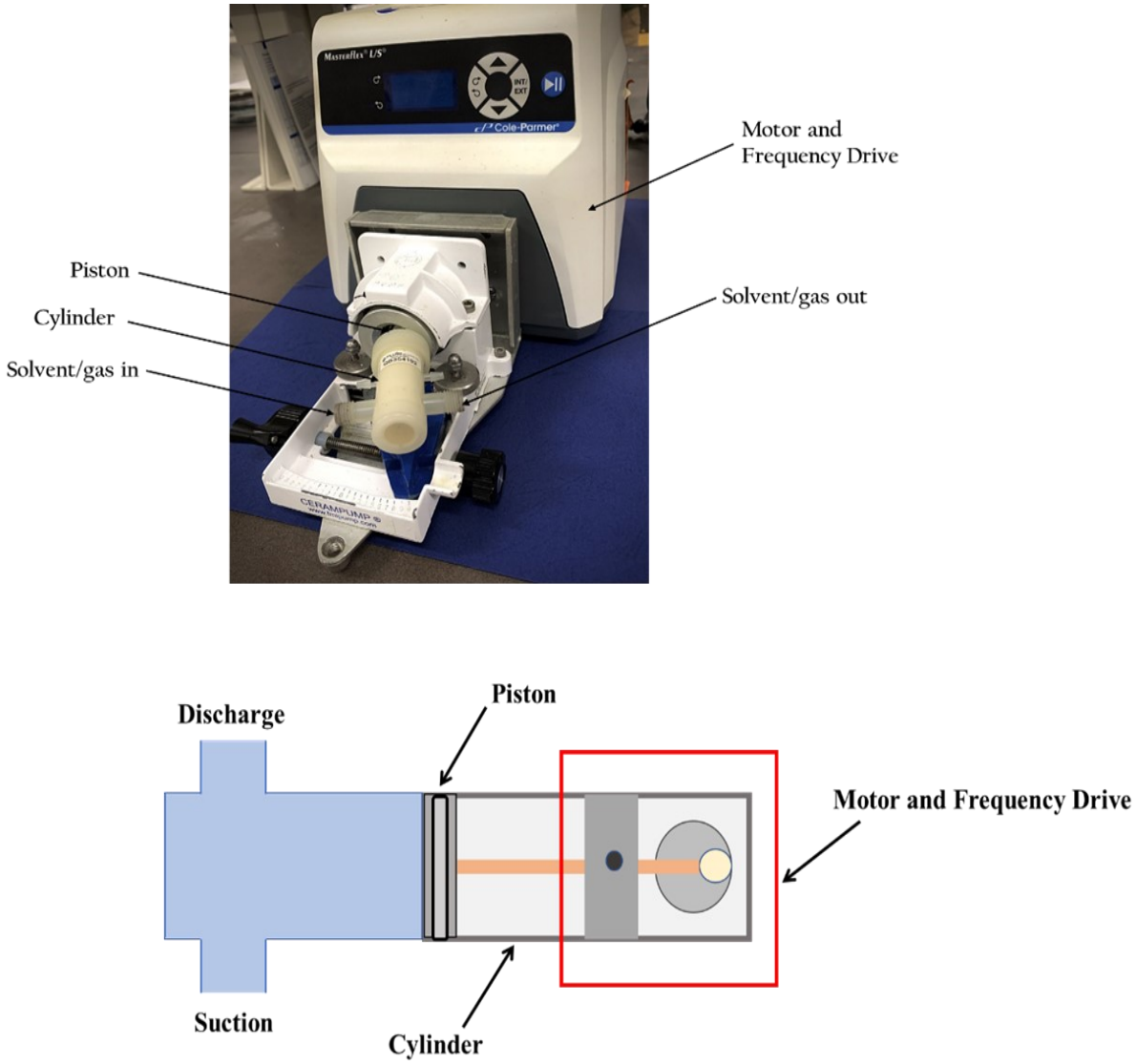


Fig. 3.4. Oscillation generating unit used in the hollow fibre membrane contactor system

## 3.6. Gas-solvent membrane contactors under oscillating solvent flow conditions

The characteristics of the membrane contactor module (Module 1) used in the oscillating solvent flow experiments are listed in Table 3.3. The solvent was introduced to the oscillating unit prior to entering the shell side of the membrane contactor (Figure 3.5) with the flow rate ranging from 0.9 to 8 mL/min. The frequency of the oscillating unit was set to 2.03Hz and the maximum stroke length (4cm) was provided. To obtain the amplitude within the shell side, the outlet solvent flow rate was measured under non-oscillating and oscillating conditions. Considering the calculated shell side cross sectional area, the volume difference between the

non-oscillating and oscillating solvent flow rate was used to determine the amplitude within the shell side of the membrane contactor which was 0.02 cm.

To ensure the change in the mass transfer performance was only due to the oscillating solvent flow, the gas phase was pure $CO_2$ with a flow rate of 0.50 L/min at 1.5 bar. The solvent samples were collected after one-hour operation and then analysed using $CO_2$ coulometer (see section 3.4).

Table 3.3. Characteristics of the hollow fibre membrane contactor module (Module 1) used for the experiments under oscillating solvent flow

| | |
|---|---|
| Number of fibres | 17 |
| Module inside diameter | 4 mm |
| Membrane inside diameter | 300 µm |
| Membrane outside diameter | 470 µm |
| Thickness of PDMS | 0.5 µm |
| Shell material | Teflon |
| Length of module | 25 cm |
| Packing density | 0.3 |

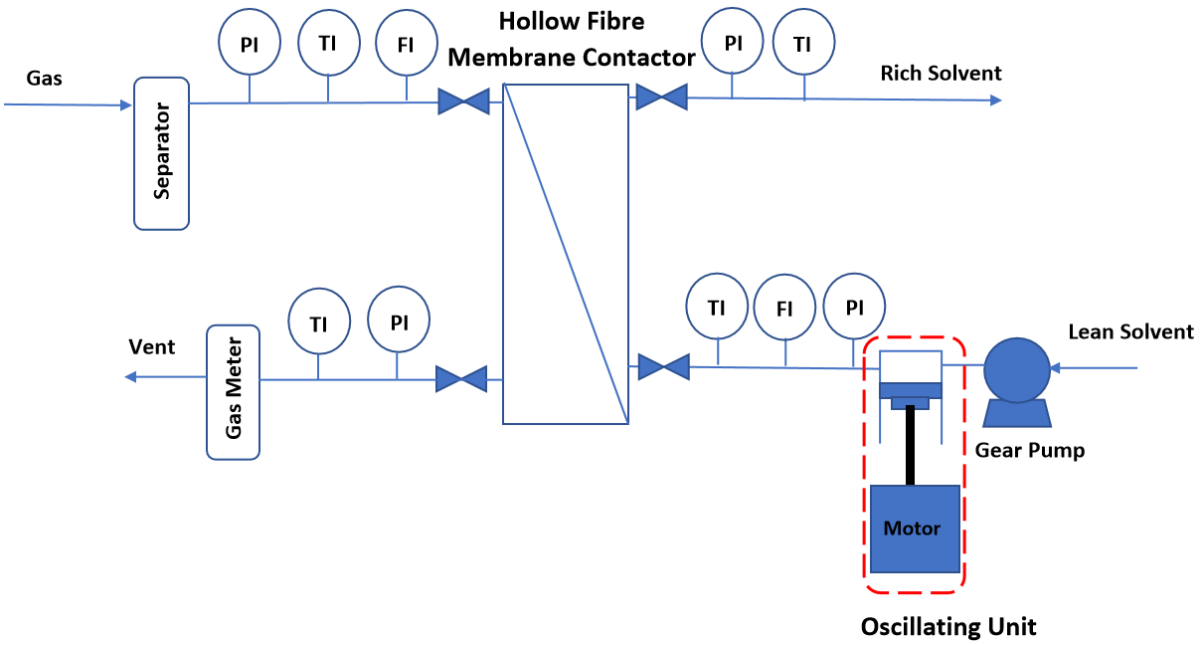


Fig. 3.5. Experimental system for the oscillating unit integrated into the solvent side of the hollow fibre membrane contactor

To analyse the mass transfer performance under oscillating solvent flow conditions, the solvent velocity was measured and compared with Eq. (2.29). For this purpose, the oscillating frequency was set to 0.05 Hz (minimum value for frequency) which provided a time period of 20 s and the oscillating amplitude was set to 0.02 cm (maximum amplitude). The solvent flow rate of the rich solvent stream was measured every 5 s. Then, the oscillating solvent flow velocity ($u_{os,L}$) was determined by having the solvent flow rate and the cross-sectional area of the shell side. The oscillating solvent flow velocity as a function of time is provided in Figure 3.6. The experimental oscillating solvent flow velocities were in a good agreement with Eq. (2.29).

Experiments investigating the effect of frequency on the solvent phase mass transfer coefficient were conducted at the amplitude of 0.02 cm and the frequency range of 0-3Hz. For these experiments, the solvent and gas flow rate were set to 2.4 mL/min and 0.5 L/min, respectively. Moreover, a set of experiments was conducted to evaluate the effect of amplitude on the solvent phase mass transfer coefficient. For this set of experiments, the frequency was set to a constant value of 0.083 Hz and the amplitude was ranged from 0 to 0.02cm.

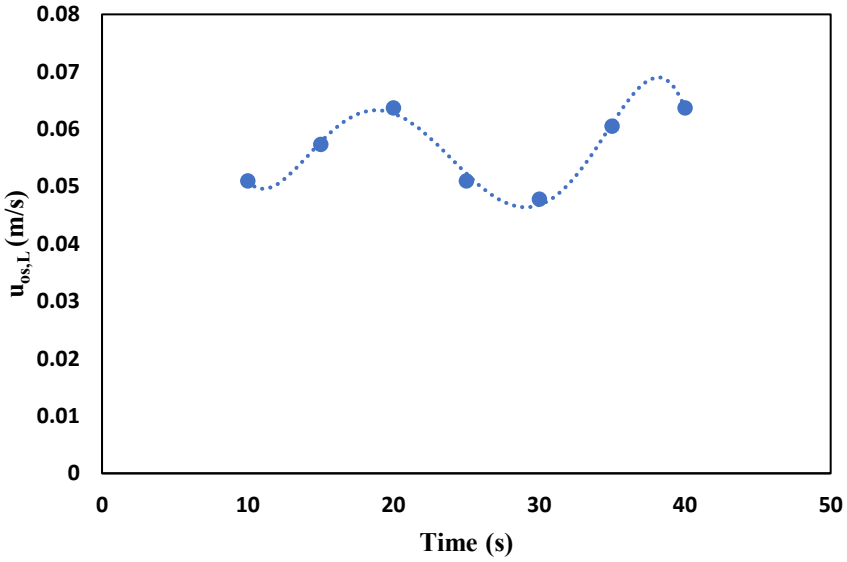


Fig. 3.6. Oscillating solvent flow velocity as a function of time (frequency: 0.05 Hz, amplitude: 0.02 cm)

## 3.7. Gas-solvent membrane contactors under oscillating gas flow conditions

The experimental system of the oscillating gas flow membrane contactor is shown in Figure 3.7. Compared to experiments conducted by oscillating solvent flow, a greater number of hollow fibres were used (Module 2, see Table 3.4). The reason is that greater numbers of hollow

fibres provided lower superficial velocity and higher residence time distribution within every single hollow fibre. Therefore, the gas phase had enough time to show measurable responses to the oscillating unit. Additionally, to maintain packing density identical to the oscillating solvent flow conditions (i.e. the standard packing density of industrial membrane contactors), a module with greater shell inside diameter was selected.

Table 3.4. Characteristics of the hollow fibre membrane contactor module (Module 2) used for the experiments under oscillating gas flow

| | |
|---|---|
| Number of fibres | 123 |
| Module inside diameter | 9.5 mm |
| Membrane inside diameter | 300 µm |
| Membrane outside diameter | 470 µm |
| Thickness of PDMS | 0.5 µm |
| Shell material | Teflon |
| Length of module | 25 cm |
| Packing density | 0.3 |

To introduce oscillation to the gas side, the oscillating unit was placed in the path of the mixed gas (10% $CO_2$ in $N_2$) before entering the membrane contactor module. Once the mixed gas passed through the oscillating unit, the forward and backward movement of the piston, induced oscillation to the gas flow on the lumen side of the contactor system. The gas flow rate was set to 0.3-0.9 L/min using a mass flow controller (MFC, Aalborg 0-7 L/min). The oscillating gas flow frequency and calculated amplitude within the lumen side of the membrane contactor were set to 1.33 Hz and 4 cm, respectively.

The solvent flow rate on the shell side of the membrane contactor was 5 mL/min (equivalent to the Reynolds number of 2.86). The $CO_2$ content of the rich and lean solvent was determined using $CO_2$ coulometer. Assuming the membrane contactor module as a control volume and performing a mass balance for $CO_2$, the mole fraction of $CO_2$ in the gas flow leaving the lumen side was determined. Having calculated the mole fraction of $CO_2$ in the exiting gas flow, the overall gas-based mass transfer coefficient was calculated using Eq. (2.7).

To obtain the changes of oscillating gas flow velocity, the frequency and amplitude were set to 0.083 Hz and 4 cm, respectively. The reason for choosing higher amplitude and lower frequency was to achieve a clear trend for the gas velocity. To find the trend, a camera was

used to record the changes of gas flow rate shown in the MFC display. Then, the gas flow rate data were recorded manually, and plotted as a function of time. The gas flow velocities were calculated and plotted as a function of time (Figure 3.8). A sinusoidal wave was obtained for the velocity, consistent with Eq. (2.29). An oscillating Reynolds number ($Re_{t,os}$) based on the oscillating gas flow velocity ($u_{os,G}$ (t)) could now be established. It was determined that for the experimental conditions studied here, the $Re_{t,os}$ varied between 15.0 and 39.2 which corresponded to laminar flow conditions.

To investigate the effect of amplitude on mass transfer in the gas boundary layer, the frequency was adjusted at 1.33Hz and the amplitude varied in the range of 0-4 cm. For the experiments investigating the effect of frequency, the amplitude was 4 cm and the values of frequency varied from 0 to 3 Hz. For both sets of experiments, the gas and solvent flow rates were set to 0.5 L/min and 2.4 mL/min, respectively.

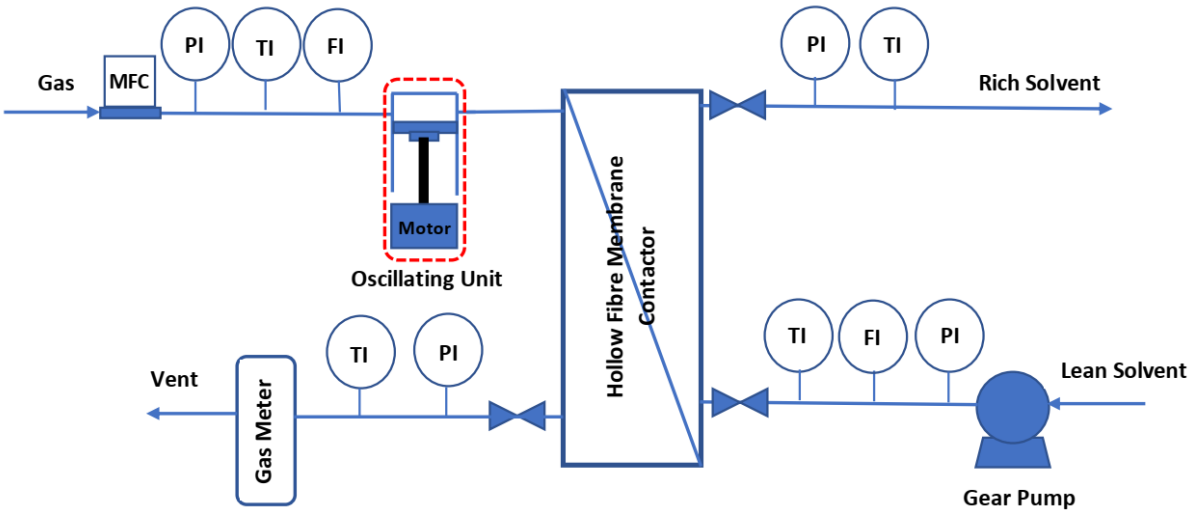


Fig. 3.7. Schematic representative of the experimental system for the oscillating gas flow hollow fibre membrane contactor

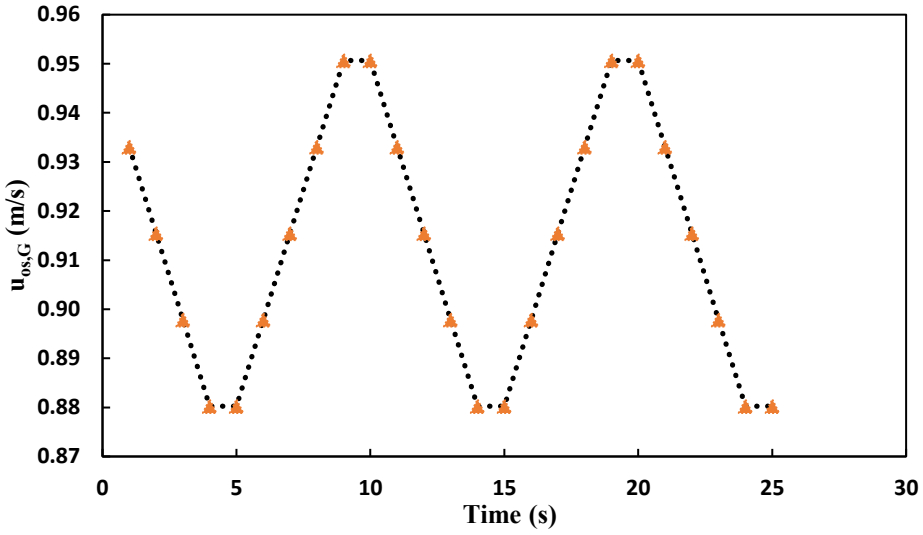


Fig. 3.8. Oscillating gas phase velocity ($u_{os,G}$) as a function of time (frequency: 0.083Hz, amplitude: 4cm).

## 3.8. Vibrating unit

In Figure 3.9 the linear vibrating unit introducing vibration to the solvent and gas flow within the hollow fibre membrane contactor system is illustrated. The characteristics of the membrane contactor system were identical to Module 2 (see Table 3.4). The membrane contactor was connected to a displacement plate, inducing linear vibration (i.e. forward and backward movement). This unit was equipped with a variable frequency drive (GW Instek, DC power supply, GPS-30300), a mechanical shaft, a micromotor (Altronics, J0054 • Micro N20 Geared Motor 150:1 50-200RPM) and a displacement plate to provide adjustable frequencies (0 to 3Hz) and amplitudes (0 to 4 cm). The accuracy of the adjusted vibrational frequency and displacement amplitude was $\pm$3.0 percent

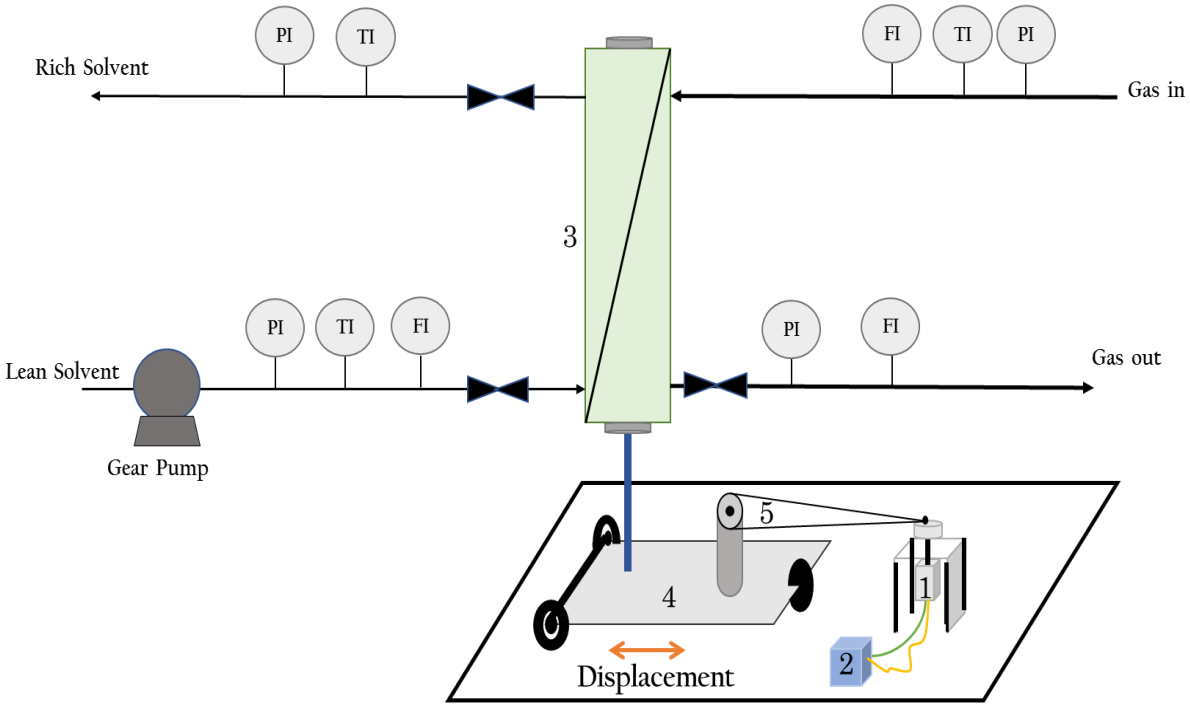


Fig. 3.9. Linear vibrating unit used to introduce vibration to the solvent and gas flow within the membrane contactor. 1) motor, 2) variable frequency drive, 3) membrane contactor on top of holder, 4) displacement plate, 5) connector

## 3.9. Gas- solvent membrane contactors under vibrating conditions

Similar to oscillating gas flow experiments, Module 2 was used to obtain the effect of linear vibration on the solvent and gas boundary layer mass transfer. Under vibrating conditions, the experimental work was divided into two categories. First, the effect of vibration on the solvent phase mass transfer coefficient was investigated. Pure $CO_2$ was introduced to the lumen side of hollow fibre membrane contactor at a flow rate of 0.50 L/min and pressure of 1.5 bar which was identical to the experimental conditions in the oscillating solvent flow experiments (see section 3.6) [110]. The solvent flow rate within the shell side of the membrane contactor was set to 2.5-15 mL/min. The vibrating conditions were applied by adjusting frequency and displacement amplitude at 1.67 Hz and 2 cm, respectively. The solvent samples were taken after 1 hr and the $CO_2$ content was determined using $CO_2$ coulometer equipment. Having calculated the $CO_2$ content of rich solvent, the overall solvent-based mass transfer coefficient was determined. Next, the effect of vibration on the gas phase mass transfer coefficient was explored. A gas mixture of 10% $CO_2$ in $N_2$ (balance) was fed into the lumen side. During the experiments, the mixed gas pressure and flow rate were 1.5 bar and 0.3-0.9 L/min, respectively. To keep the conditions identical to the oscillating gas flow study (section 3.8), the solvent flow

rate in the shell side was 5 mL/min. The frequency was adjusted at 1.67 Hz and the displacement amplitude was set to 2 cm. The overall gas-based mass transfer coefficient was calculated using a procedure identical to that of the oscillating gas flow experiments (see section 3.7).

As mentioned before, the linear vibrating system provided different frequencies and amplitudes of vibration. Table 3.5 lists the operating conditions used for studying the influence of vibrational frequency and amplitude on the overall solvent- and gas-based mass transfer coefficients. The range of frequency (0-3Hz) and displacement amplitude (0-4cm) was determined according to the vibrating system design and characteristics.

Table 3.5. The experimental operating condition for investigating the effects of vibrational frequency and displacement amplitude on the mass transfer performance of hollow fibre membrane contactor

| Type of experiment | Displacement amplitude | Frequency | Gas flow rate | Solvent flow rate |
|---|---|---|---|---|
| Effect of amplitude | 0-4 cm | 1.67 Hz | 0.5 L/min | 5 mL/min |
| Effect of frequency | 2 cm | 0-3 Hz | 0.5 L/min | 5 mL/min |

The effect of module packing density was incorporated into the Sherwood number correlation for the solvent side to achieve a more robust mass transfer correlation. To study the effect of packing density on the mass transfer performance, modules with four different packing densities (i.e. 0.1, 0.2, 0.3 and 0.4, see Table 3.6) were prepared. The studied solvent side Reynolds numbers were 0.68, 1.35, 2.70 and 4.05 and the flow rate of pure $CO_2$ was 0.5 L/min.

Table 3.6. Hollow fibre membrane contactors with different packing densities used in the experiments to obtain the effect of packing density on the solvent boundary layer mass transfer

| Packing density | 0.1 | 0.2 | 0.3 | 0.4 |
|---|---|---|---|---|
| Number of fibres | 41 | 82 | 123 | 164 |
| Module inside diameter (mm) | 9.5 | 9.5 | 9.5 | 9.5 |
| Membrane inside diameter (μm) | 300 | 300 | 300 | 300 |
| Membrane outside diameter (μm) | 470 | 470 | 470 | 470 |
| Thickness of PDMS (μm) | 0.5 | 0.5 | 0.5 | 0.5 |
| Porosity of PSf | 0.5 | 0.5 | 0.5 | 0.5 |
| Tortuosity of PSf | 2.36 | 2.36 | 2.36 | 2.36 |
| Module's shell material | Teflon | Teflon | Teflon | Teflon |
| Length of module (cm) | 25 | 25 | 25 | 25 |

## 3.10. Conclusion

This study of membrane contactor technology was aimed at identifying improvements in mass transfer performance specifically for the field of carbon capture. Potassium glycinate was prepared and used as a solvent due to its good $CO_2$ absorption properties and low environmental footprints. The solvent was employed on in-house constructed hollow fibre membrane contactors. A new experimental system was designed to introduce oscillation to these conventional gas-solvent hollow fibre membrane contactors. The effect of oscillating flow on the solvent and gas phase boundary layer mass transfer was quantified using the measurement of overall solvent- and gas-based mass transfer coefficients. A novel apparatus was designed to induce simultaneous vibration to the solvent and gas flow within the membrane contactors. The oscillating and vibrating units allowed the frequency and amplitude of oscillation and vibration to vary through which the sensitivity of $CO_2$ absorption to the frequency and the amplitude was captured. The accuracy of the adjusted oscillating/vibrating frequency and oscillating/displacement amplitude was $\pm 3.0$ percent and the error percentage of the experimental data was reported in the result chapters.

# CHAPTER 4: MEMBRANE GAS-SOLVENT CONTCATORS UNDERGOING OSCLLATING SOLVENT FLOW FOR ENHANCED CARBON DIOXIDE CAPTURE

The solvent side boundary layer mass transfer resistance is the predominant resistance in membrane contactor systems. The main aim of this chapter is to investigate the effect of oscillating solvent flow on the solvent side boundary layer mass transfer resistance. For the first time, the results of this chapter indicated the mass transfer performance of gas-solvent hollow fibre membrane contactors was significantly enhanced using the oscillation technique.

This chapter has been published in **Separation and Purification Technology** as follows:

**Elaheh Hosseini**, Geoffrey W. Stevens, Colin A. Scholes. "Membrane Gas-Solvent Contactors Undergoing Oscillating Solvent Flow for Enhanced Carbon Dioxide Capture". Journal of Separation and Purification Technology Vol.227 (2019) 115

## 4.1. Introduction

Carbon dioxide emissions from the fossil fuel industry is the primary cause of anthropogenic climate change. Post- combustion carbon capture is an approach to reduce carbon dioxide ($CO_2$) emissions from large scale sources, such as power stations, by separating $CO_2$ from flue gas [111]. The conventional technology for post combustion is reversible solvent absorption, but this technology has a number of drawbacks in terms of operation, such as flooding, weeping, foaming or entrainment problems and size limitations [13,23]. Membrane contactors, which combine the benefits of membrane technology with a $CO_2$-selective solvent, overcome these operational difficulties and achieve small size of equipment for $CO_2$ capture due to their high gas- solvent interfacial area. These contactors also allow for the independent control of gas and solvent flow rates [6,23,24,112].

The choice of the solvent is crucial for membrane contactors, as the solvent-$CO_2$ reaction kinetic has a strong impact on absorption [6,113]. The most commonly used solvent is monoethanolamine (MEA). However, MEA has a number of drawbacks, such as toxicity, degradation in the presence of oxygen and the formation of heat stable salts [114]. For these reasons, alternative solvents are an active area of research in solvent absorption, which also

benefits membrane contactors. Amino acid salt- based solvents, e.g. sodium glycinate and potassium glycinate, have strong potential to replace MEA, as they display a high reactivity to $CO_2$, low volatility, and low reactivity to oxygen, $SO_x$ and $NO_x$ [43]. For the membrane contactors, the membrane acts as additional mass transfer resistance layer, and hence it is imperative to reduce this resistance. This is achieved with a non-porous ultra-thin polymeric layer on a porous support (i.e. composite membrane). The non-porous layer separates the gas and solvent phases and provides some selectivity for $CO_2$ transport relative to other gases. Being ultra-thin the mass transfer resistance is minimised, while the porous support also provides minimal resistance. Hence, for non-porous membrane contactors, the solvent boundary layer becomes the dominant mass transfer resistant stage [29,38,86]. As a result, there is a strong interest in developing strategies to minimise the mass transfer resistance of the solvent boundary layer.

To enhance the mass transfer through the solvent boundary layer, it is necessary to induce additional mixing [115]. This can be achieved by operating at higher Reynolds numbers and transitioning to a turbulent flow regime. Karamercan et al. [116] showed that by establishing appropriate oscillating frequency and amplitude, convection forces can also be introduced to the solvent boundary layer, facilitating additional mixing. Furthermore, Nishimura and Matsune [94] demonstrated the effect of oscillating flow in symmetric and asymmetric wavy walled channel's mass transfer performance and showed that application of oscillating flow caused an improvement in mass transfer performance. Hence, the application of oscillating flow to membrane contactor process holds the potential to increase mixing within the solvent boundary layer and increase mass transfer.

To the best of the authors' knowledge, there has been no comprehensive study addressing the effect of oscillating solvent flow on the $CO_2$ capture efficiency of membrane contactors. Here, oscillating solvent flow in a gas- solvent membrane contactor is applied for the first time for the stated purpose of $CO_2$ capture. The system studied used 15 wt% potassium glycinate as the selective solvent, while the composite hollow fibre membranes consisted of a non-porous ultra-thin polydimethylsiloxane (PDMS) on a porous poly sulfone (PSf) support. The overall mass transfer coefficients ($K_{ov}$) obtained from the oscillating flow conditions were compared with the non- oscillating solvent flow case. To study the $CO_2$ removal efficiency of the membrane contactor, the influence of the amplitude and frequency of solvent flow on $K_{ov}$ was investigated. The improvement in capture efficiency also enabled membrane contactor mass

transfer theory to be extended for oscillating flow conditions and an appropriate mass transfer correlation established.

## 4.2. Theory

In a membrane contactor module, the molar mass transfer flux of $CO_2$ (N) is determined from:

$$N = \frac{(C_{out}-C_{in})L}{A} = K_{ov}C_{LM} \quad (4.1)$$

where L is the inert solution flowrate ($m^3/s$), A is the mass transfer area ($m^2$), $C_{out}$ is the outlet molar concentration of $CO_2$ in the solution ($mol/m^3$) and $C_{in}$ is the inlet molar concentration of $CO_2$ in the solution ($mol/m^3$). $C_{LM}$ represents the log mean average of the concentration driving force between the solvent and bulk gas phases and $K_{OV}$ is the overall liquid- phase mass transfer coefficient (m/s) which is expressed based on the film theory as Eq. (4.2) [61,64]:

$$\frac{1}{K_{ov}} = \frac{Hd_{out}}{k_g d_{in}} + \left(\frac{Hd_{out}}{k_m d_{ln}}\right)_{porous} + \left(\frac{Hd_{out}}{k_m d_{ln}}\right)_{active\ layer} + \frac{1}{Ek_l} \quad (4.2)$$

In Eq. (4.2), $k_g$ is the mass transfer coefficient of $CO_2$ across the gas boundary layer (m/s), $k_m$ is mass transfer coefficient of $CO_2$ through membrane (m/s), $d_{in}$ is the inside diameter of fibre (m), $d_{out}$is outside diameter of fibre (m), $d_{ln}$ is logarithmic mean diameter of membrane (m) and $k_l$ is the mass transfer coefficient of $CO_2$ through the solvent boundary layer (m/s). H is the Henry's law constant of $CO_2$ in the solvent and E is enhancement factor related to the reaction between $CO_2$ and potassium glycinate [6,61,64,65]. The Henry's law constant for $CO_2$ in the solvent is calculated using salting out effect theory proposed by the Sechenov correlation at high concentrations of amino acid salt [69,70]. The enhancement factor can be modelled depending on the absorption rate. For intermediate regime, Decoursey [66], Van Swauij et al. [67] and Versteky et al. [68] suggested an enhancement factor (E) as a function of Hatta number (Ha) and infinite enhancement factor ($E_\infty$).

$$Ha = \frac{\sqrt{k_{ov}D_{CO_2}}}{k_l} \quad (4.3)$$

$$E_\infty = \sqrt{\frac{D_{CO_2}}{D_s}} + \frac{C_{PG}}{v_{CO_2}\frac{P_{CO_2}}{H_{CO_2}}}\sqrt{\frac{D_{PG}}{D_{CO_2}}} \quad (4.4)$$

$$E = -\frac{Ha^2}{2(E_\infty\text{-}1)} + \sqrt{\frac{Ha^4}{4(E_\infty\text{-}1)^2} + \frac{E_\infty.Ha^2}{E_\infty\text{-}1} + 1} \quad (4.5)$$

where $D_{PG}$ is the potassium glycinate diffusion coefficient ($m^2/s$), $D_{CO_2}$ is diffusion coefficient of $CO_2$ in potassium glycinate ($m^2/s$), $v_{CO_2}$ is the stoichiometric coefficient of $CO_2$ and $k_{ov}$ is the overall kinetic constant of $CO_2$ reacting with potassium glycinate ($s^{-1}$) and is defined as [43,60]:

$$k_{ov} = 2.42*10^{16} \exp\left(\frac{-8544}{T}\right) \exp(0.44C_{PG})\, C_{PG} \quad (4.6)$$

where $C_{PG}$ is the molar concentration of potassium glycinate solution ($mol/m^3$) and T is the temperature of solution (K).

The membrane mass transfer coefficient can be determined from the non-oscillating solvent flow conditions using the method of Wilson plot [61]:

$$\frac{1}{K_{ov}} = C_1 u^{-\alpha} + \frac{Hd_{out}}{k_m d_{ln}} \quad (4.7)$$

where u is solvent velocity (m/s) and α is a fitting parameter providing the best linear relationship. Therefore, the membrane mass transfer resistance can be determined by a linear fitting of $\frac{1}{K_{ov}}$ versus $u^{-\alpha}$ [61].

Sherwood number for the shell side of the membrane contactor is taken as an empirical correlation, that corresponds to the Reynolds number and module parameters of this study. For the PDMS membrane contactor system studied here, the following mass transfer correlation was considered**.** According to published membrane mass transfer correlations, it is assumed that the exponent of Sc number is 0.33 [72].

$$Sh = \Upsilon Sc^{0.33} Re^{\beta} \quad (4.8)$$

where:

$$Re = \frac{\rho \bar{u} d_h}{\mu} = \frac{4\rho L}{n\pi d_{out}\mu} \quad (4.9)$$

$$d_h = \frac{d_{cin}^2 - n d_{out}^2}{n d_{out}} \quad (4.10)$$

where $\bar{u}$ is the average solvent velocity, $d_{cin}$ is the contactor inner diameter (m) and $d_h$ is hydraulic dimeter (m). $\Upsilon$ and β can determined through the relationship between Reynolds and Sherwood numbers for mass transfer, through standard approaches [72].

For the membrane contactor system under oscillating conditions, it is important that non-oscillating solvent velocity and the oscillating solvent velocity to be described separately. This enables a comparison on performance between non-oscillating and oscillating systems in terms of Reynolds number. The oscillating solvent velocity ($u_{os}(t)$) can be described as [87]:

$$u_{os}(t) = \overline{u_0} + 2\pi af\sin(\omega t) \tag{4.11}$$

where $\overline{u_0}$ is average non-oscillating velocity (m/s), a is oscillating amplitude (m), f is oscillating frequency (Hz) and ω is angular frequency (rad/s) given by:

$$\omega = 2\pi f \tag{4.12}$$

The waveform parameters can be characterized through a root mean square value. Here, oscillating flow velocity is defined based on root mean square value ($u_{os,rms}$) and used for developing oscillating Reynolds number ($Re_{os}$) [107,108]:

$$u_{os,rms} = \sqrt{\frac{1}{T}\int_0^T u_{os}^2(t)dt} \tag{4.13}$$

where T is the period of sinusoidal function.

## 4.3. Experimental

### 4.3.1. Chemicals

Glycine (98.5% purity) and potassium hydroxide (85% purity) were provided by Thermo Fisher Co. Hollow fibre membranes were supplied by Airrane Co. $CO_2$ gas (99.99% purity) was supplied by Core gas.

### 4.3.2. Potassium glycinate solution preparation

The solvent was aqueous 15 wt% potassium glycinate solution, prepared from adding equimolar amounts of potassium hydroxide and glycine to deionized water. The solution was stored in polyethylene tanks. Details of the solvent properties at the ambient temperature (25°C) are provided in Table 4.1.

Table 4.1. Characteristics of 15 wt% potassium glycinate at operating temperature (25°C).

| | |
|---|---|
| Density (kg/m$^3$) | 1060 |
| Viscosity (kg/m.s) | 0.001323 |
| Diffusion coefficient of $CO_2$ in potassium glycinate (m$^2$/s) | 1.46x10$^{-9}$ |
| Potassium glycinate diffusion coefficient (m$^2$/s) | 4.66x10$^{-10}$ |
| Enhancement Factor | 20.890 |
| Henry's law constant (Pa.m$^3$/mol) | 4224.310 |

### 4.3.3. Experimental set-up

The experimental apparatus (schematic in Figure 4.1) consisted of hollow fibre membranes with non-porous PDMS on PSf support. Details of the membranes and module used in this research are provided in Table 4.2.

Table 4.2. Membrane contactor characteristics (oscillating solvent flow studies)

| | |
|---|---|
| Number of fibres | 17 |
| Module inside diameter | 4 mm |
| Membrane inside diameter | 300 µm |
| Membrane outside diameter | 470 µm |
| Thickness of PDMS | 0.5 µm |
| Module's shell composition | Teflon |
| Length of module | 25 cm |
| Packing density | 0.3 |

The gas was introduced to the lumen side of the membrane contactor. The solvent was stored in a 20 litres tank at ambient temperature. In a counter-current fashion, the solvent was circulated through the shell side of the membrane module. A needle valve downstream of the module on the solvent stream was used to control the differential pressure across the membrane and avoid gas bubbling in the solvent phase.

To achieve oscillating solvent flow, an oscillating unit was added to a non-oscillating flow system. This consisted of a variable frequency drive, a motor, a cylinder and a piston moving in a sinusoidal motion. All parts of the oscillating unit were purchased from Cole- Parmer Co. with the oscillating frequency of 0.002 to 10 Hz and the oscillating amplitude of 0 to 0.2mm. This enabled the oscillating solvent flow to be generated by variable speed and stroke length. The solvent was pumped using a gear pump (Ismatec, 0-0.11 L/min) and introduced to the

oscillating unit prior to entering the shell side of the membrane contactor. In this study, the range of solvent flow rate was 0.9 to 8 mL/min. The rotation speed during solvent oscillation was set between 0.66 and 2.5 Hz. The piston provided the amplitude of 0.0 to 0.2 mm. The feed gas flow rate and pressure were measured by a gas rotameter (Kytala (Muurame Finland), 0- 10 L/min) and a pressure gauge (Swagelok, ranged between 0- 12 bar), respectively. To ensure mass transfer change is only due to the oscillating solvent flow, the gas phase was pure $CO_2$, at a flow rate of 0.50 L/min and pressure of 1.5 bara.

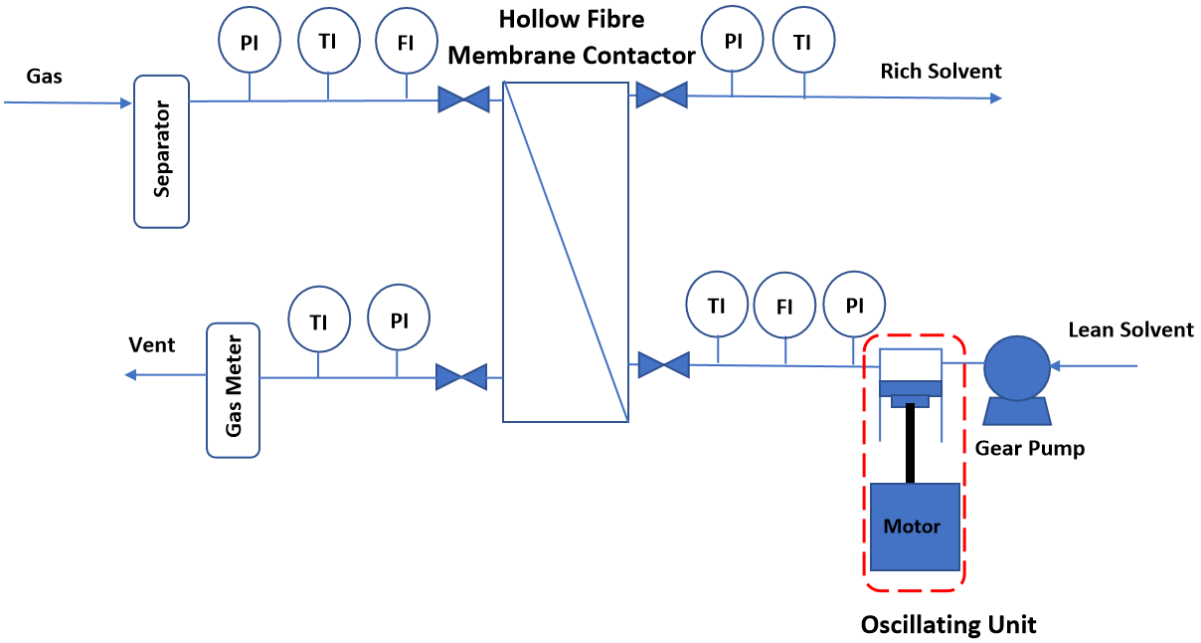


Fig. 4.1. Schematic diagram of oscillating solvent flow membrane contactor (experimental system).

After the processing time, solvent sampling was obtained by collection of loaded solvent and $CO_2$ loading was measured by colourimetry titration (CM5015 Coulometer, UIC Inc., USA).

### 4.3.4. Oscillating solvent velocity measurement

For the current study, the velocity was measured and compared with Eq. (4.11). To do this, the oscillating frequency was fixed at 0.05 Hz which provides a time period of 20s. The oscillating amplitude was set at 0.2 mm. Here, a lower frequency value (0.05 Hz) was applied to measure the solvent flow rate in every 5s. The oscillating flow velocity was demonstrated in Figure 4.2 as a function of time. The sinusoidal trend of this figure showed that the oscillating solvent flow velocity of the current system was in a good agreement with Eq. (4.11).

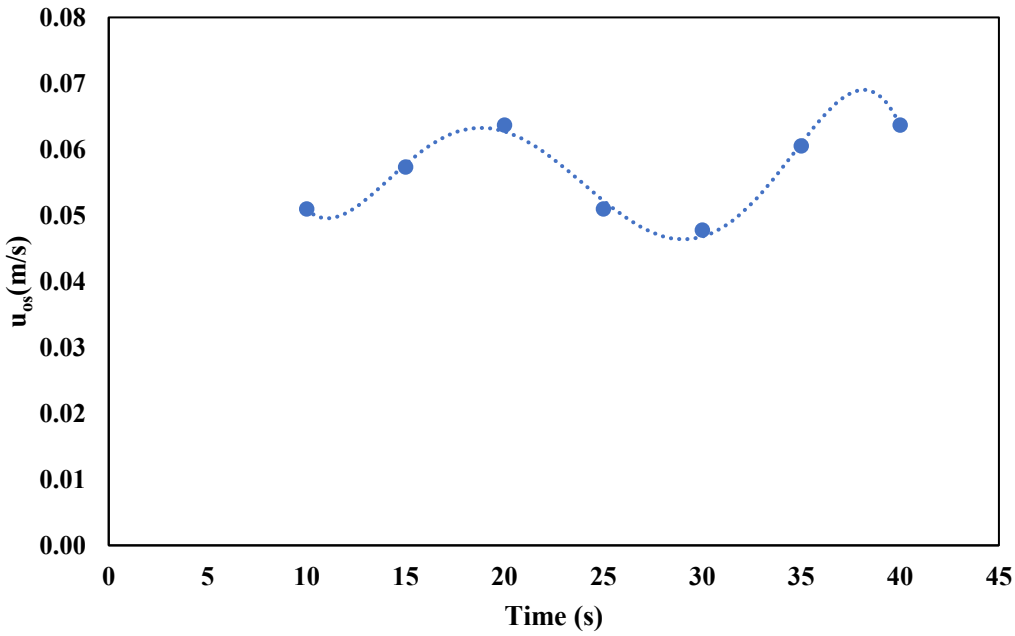


Fig. 4.2. $u_{os}$ as a function of time (frequency: 0.05 Hz, amplitude: 0.2 mm)

## 4.4. Results and discussion

### 4.4.1. Mass transfer performance under oscillating and non-oscillating solvent conditions

The $CO_2$ flux and $K_{ov}$ of the non-oscillating system are provided in Figures 4.3 and 4.4, respectively, as a function of the non-oscillating Reynolds number ($Re_{non\text{-}oscillating}$). There was a clear trend of increasing $CO_2$ flux and $K_{ov}$ with increasing $Re_{non\text{-}oscillating}$ (i.e. solvent flow rate). This is a standard behaviour for membrane contactors, and reported extensively in the literature [62]. The range of the obtained solvent side Reynolds number agreed with the literature as Scholes et al. [6] showed that the range of solvent side Reynolds number at a pilot plant scale could be lower than 1. The mixing over the solvent side is increased at higher Reynolds numbers resulting in a reduction of solvent side boundary layer resistance. However, providing higher solvent flow rates (i.e., Reynolds numbers) is not practically viable in terms of power consumption and membrane wetting problem. Therefore, oscillating unit was applied to improve mixing at low solvent side Reynolds numbers. The flux and $K_{ov}$ of $CO_2$ under oscillating flow conditions are also provided in Figures 4.3 and 4.4, respectively. For the current study, the $K_{ov}$ and $CO_2$ flux were calculated using $u_{os,rms}$ and therefore, they did not follow a sinusoidal trend. The use of the $Re_{non\text{-}oscillating}$ enabled the comparison of the oscillating and non-oscillating systems. A comparison of the two systems clearly demonstrated that the

application of oscillating flow resulted in an increase in $CO_2$ flux and a corresponding increase in $K_{ov}$ compared to non-oscillating solvent flow. The enhancement can be described by comparing $u_{os,rms}$ with the average non-oscillating velocity. The $u_{os,rms}$ was greater than the average non-oscillating velocity. This resulted in greater solvent flow rate for the oscillating conditions than the non-oscillating conditions. Consequently, the $CO_2$ flux and $K_{ov}$ increased. This reflected the improvement of the overall $CO_2$ absorption due to increased mixing in the solvent boundary layer. However, the improvement in mass transfer performance with oscillation diminished as the $Re_{non\text{-}oscillating}$ increased. Mass transfer improvement was greatest for the $Re_{non\text{-}oscillating}$ of 1.92 and decreased as $Re_{non\text{-}oscillating}$ increased. Extrapolation of this oscillating trend with increasing solvent flow rate implies that the oscillating and non-oscillating operations have comparable performance at the $Re_{non\text{-}oscillating}$ of 21.3. This behaviour was attributed to the dampening of the cyclic mixing at higher solvent flow rates.

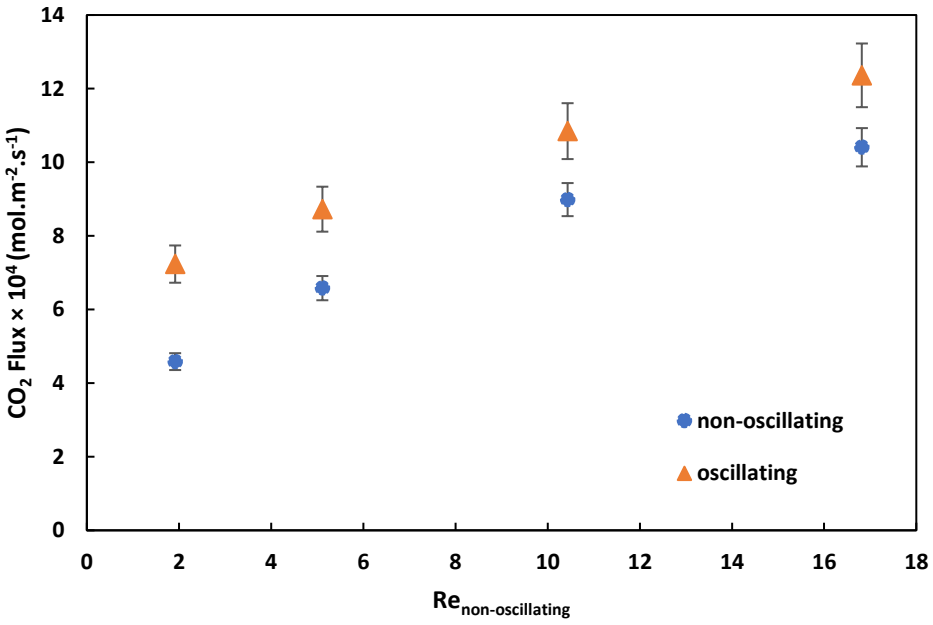


Fig. 4.3. $CO_2$ flux under non-oscillating and oscillating conditions as a function of $Re_{non\text{-}oscillating}$ (frequency: 2.03 Hz, amplitude: 0.2 mm)

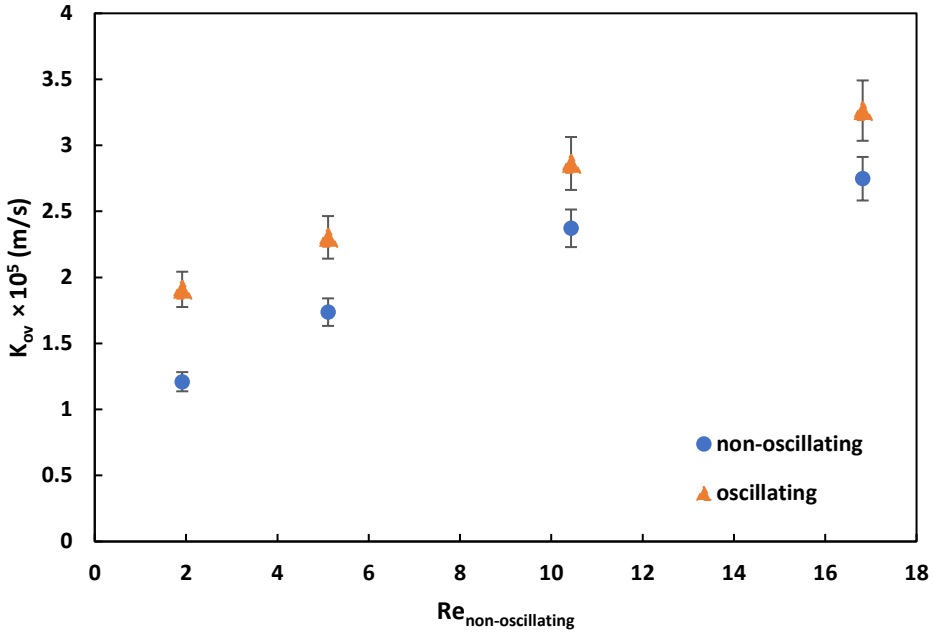


Fig. 4.4. $K_{ov}$ under non-oscillating and oscillating conditions as a function of $Re_{non\text{-}oscillating}$ (frequency: 2.03 Hz, amplitude: 0.2 mm)

The enhancement in the $K_{ov}$ resulted in increasing the mass transfer coefficient of the solvent side ($k_l$) obtained by Eq. (4.2). The term including gas boundary layer mass transfer resistance ($\frac{Hd_{out}}{k_g d_{in}}$) was negligible, as pure $CO_2$ was present on the lumen side of the membrane contactor. The Wilson plot is provided in Figure 4.5 for the non-oscillating data and the corresponding best fit is described as:

$$\frac{1}{K_{ov}} = 5928.1u^{-0.39} + 892.43 \qquad (4.14)$$

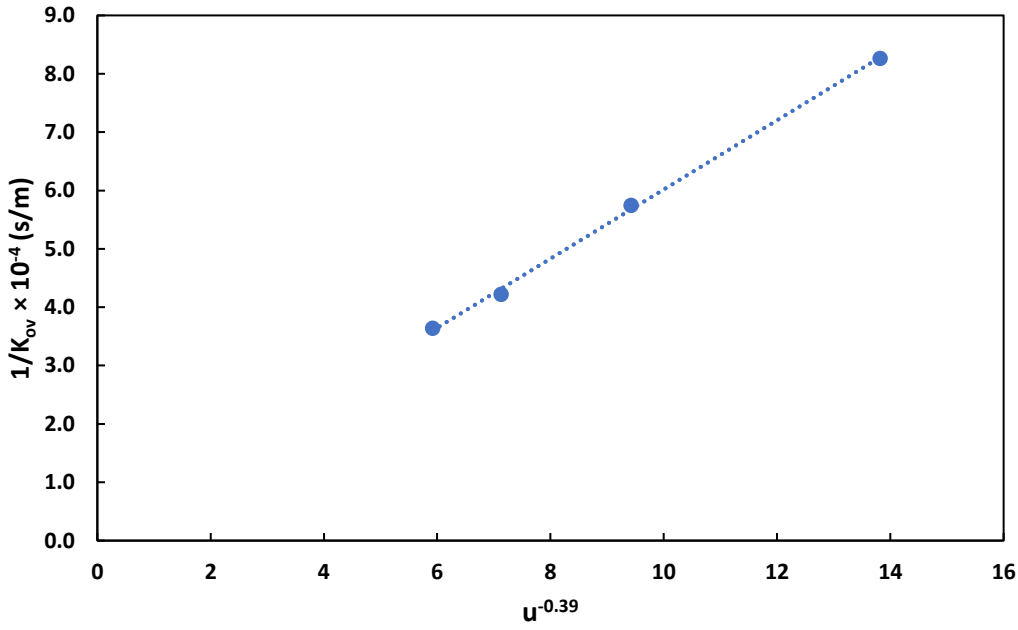


Fig. 4.5. The regression of $\frac{1}{K_{ov}}$ versus $v^{-\alpha}$ based on Wilson's method [61]. ($R^2$=0.9987)

From Eq. (4.14), the term including the membrane mass transfer resistance is 892.43 s/m. This value was used in Eq. (4.2) to calculate the $k_l$ (Figure 4.6). Compared to the non-oscillating data, the oscillating solvent enhanced $k_l$ by 20 to 50% as the $Re_{non\text{-}oscillating}$ decreased.

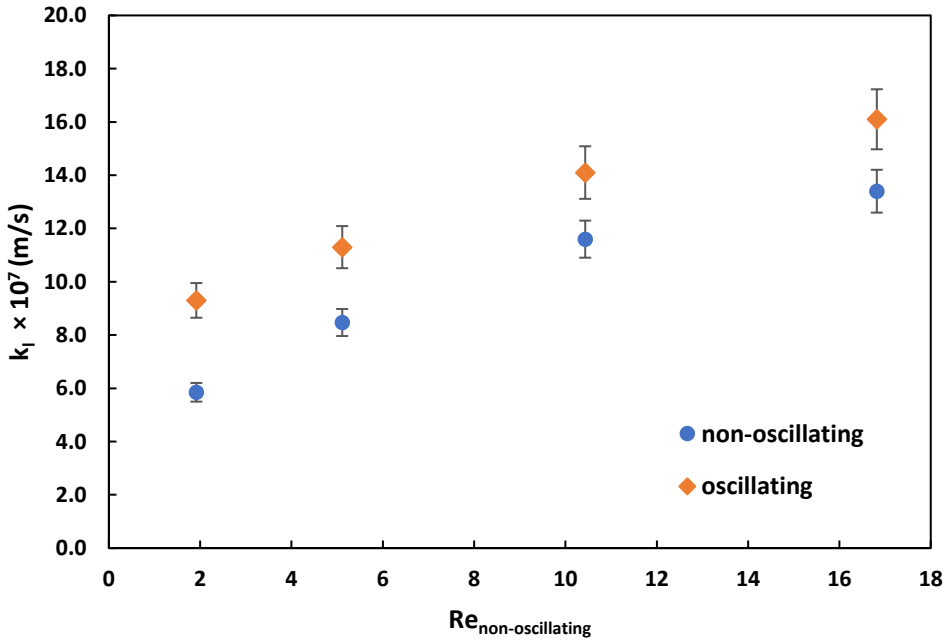


Fig. 4.6. Solvent mass transfer coefficient ($k_l$) under non-oscillating and oscillating conditions as a function of $Re_{non\text{-}oscillating}$ (frequency: 2.03 Hz, amplitude: 0.2 mm)

### 4.4.2. Effect of oscillating frequency and amplitude on $K_{ov}$

The effects of oscillating frequency and amplitude on the $CO_2$ flux and $K_{ov}$ were demonstrated independently in Figure 4.7 and 4.8, respectively. The $CO_2$ flux and mass transfer coefficients obviously increased with increasing oscillating frequency at the fixed oscillating amplitude (0.2 mm). The enhancement can be explained by the oscillating solvent pressure wave initiating additional mixing between the bulk and boundary layer. This is associated with changing the thickness of the solvent boundary layer (δ) which is described by [109]:

$$\delta = \left(\frac{2\nu}{\omega}\right)^{0.5} \tag{4.15}$$

where the thickness of the solvent boundary layer is inversely proportional to the square root of oscillating frequency. Hence, an increase in the oscillating frequency results in a decrease in the boundary layer thickness and an enhancement of mass transfer between the bulk phase and boundary layer. This reduced the mass transfer resistance of the solvent boundary layer. The $K_{ov}$ increased by 53% as the oscillating frequency increased from 0.83 Hz to 2.03 Hz.

The improved $CO_2$ flux and $K_{ov}$ were observed (Figure 4.8) at a fixed oscillating frequency (2.03 Hz) where doubling the oscillating amplitude corresponded to a 30% increase in the $K_{ov}$. For the current study, the change in the oscillating frequency had a larger impact on the $K_{ov}$ than the change in the oscillating amplitude.

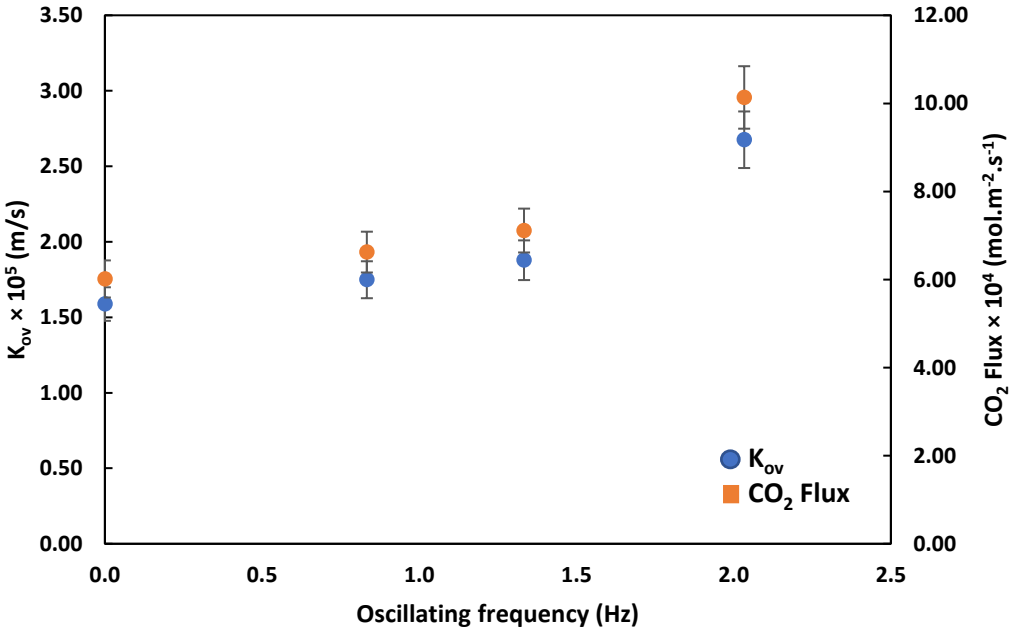


Fig. 4.7. Effect of oscillating frequency on $K_{ov}$ and $CO_2$ flux. The oscillating amplitude was fixed at 0.2 mm. The $Re_{non\text{-}oscillating}$ was 4.9.

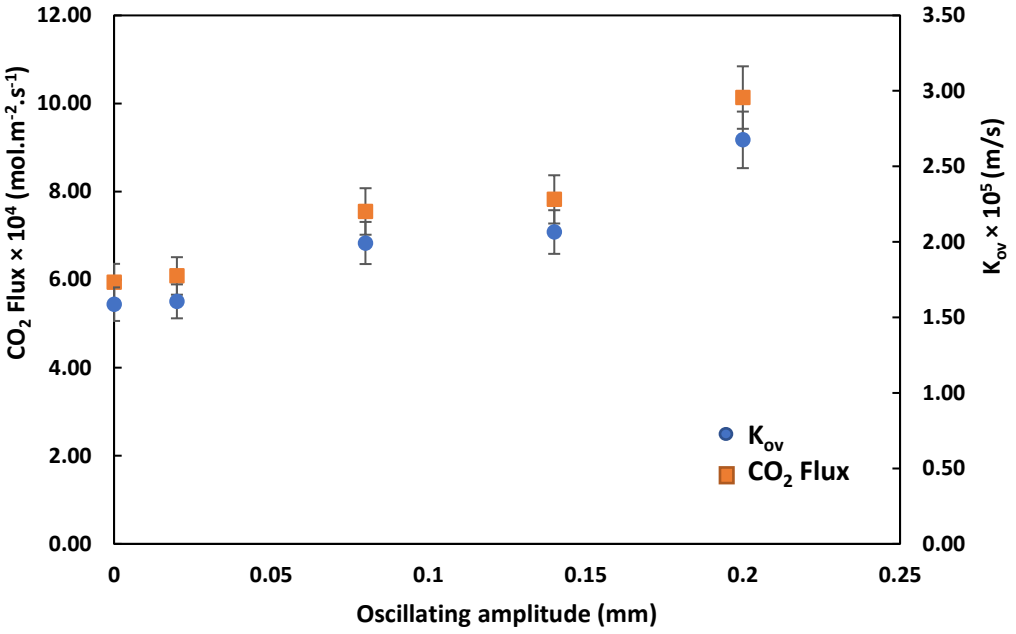


Fig. 4.8. Effect of oscillating amplitude on $K_{ov}$ and $CO_2$ flux. The oscillating frequency was fixed at 2.03 Hz. The $Re_{non\text{-}oscillating}$ was 4.9.

### 4.4.3. Determination of Sherwood number for oscillating solvent conditions

A mass transfer correlation in terms of the $Re_{os}$ is described here. The $Re_{non\text{-}oscillating}$ was modified to account for the solvent oscillating frequency and amplitude. The effects of these two parameters were condensed into the definition of $u_{os,rms}$ and the $Re_{os}$ was defined as:

$$Re_{os} = \frac{4\rho u_{os,rms} A'}{\pi n d_{out} \mu} \tag{4.16}$$

where A´ represents the cross sectional area of the solvent flow.

The Sherwood numbers of the non-oscillating and oscillating conditions were calculated using $k_l$ obtained from the experimental data (see Section 4.4.1).

Figure 4.9 shows the non-oscillating Sherwood number ($Sh_{non\text{-}oscillating}$) as a funcion of the $Re_{non\text{-}oscillating}$. The non-oscillating mass transfer coefficient was evaluated and $Sh_{non\text{-}oscillating}$ was dependent on:

$$Sh_{non\text{-}oscillating} = 0.035 Sc^{0.33} Re^{0.39} \tag{4.17}$$

In Figure 4.10, the Sherwood number of the oscillating conditions ($Sh_{os}$) is provided as a function of the $Re_{os}$. The $Sh_{os}$ was determined as:

$$Sh_{os} = 0.05\, Re_{os}^{0.3} Sc^{0.33} \quad (4.18)$$

Compared to the non-oscillating condition (Eq. 4.17), the exponent of the Reynolds number was reduced to 0.3 for the oscillating condition. This indicated an increase in the absolute value of the Reynolds number under the oscillating flow condition at a fixed solvent flow rate.The constant factor (0.05) increased by 40% in the oscillating flow correlation compared to the non-oscillating flow correlaton. The comparison between the Sherwood numbers of the oscillating and non-oscillating conditions are indicated in Figure 4.11. Since all operating conditions were constant in oscillating and non-oscillating experiments, the increase in the $Sh_{os}$ was associated with the increased mixing between the bulk and solvent boundary layer. Moreover, the low values of the Sherwood numbers of the solvent (i.e., 0.4 to 1.2) show that convective mass transfer controls the mass transfer process. Therefore, generation of oscillating solvent flow enhanced mixing between bulk side and boundary layer.

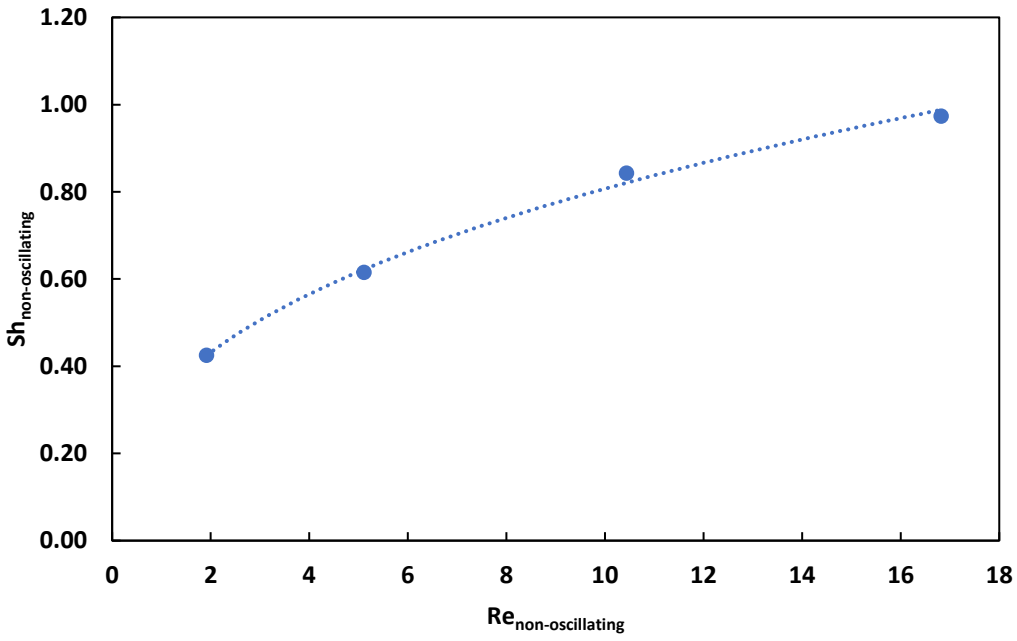


Fig. 4.9. $Sh_{non\text{-}oscillating}$ as a function of the $Re_{non\text{-}oscillating}$

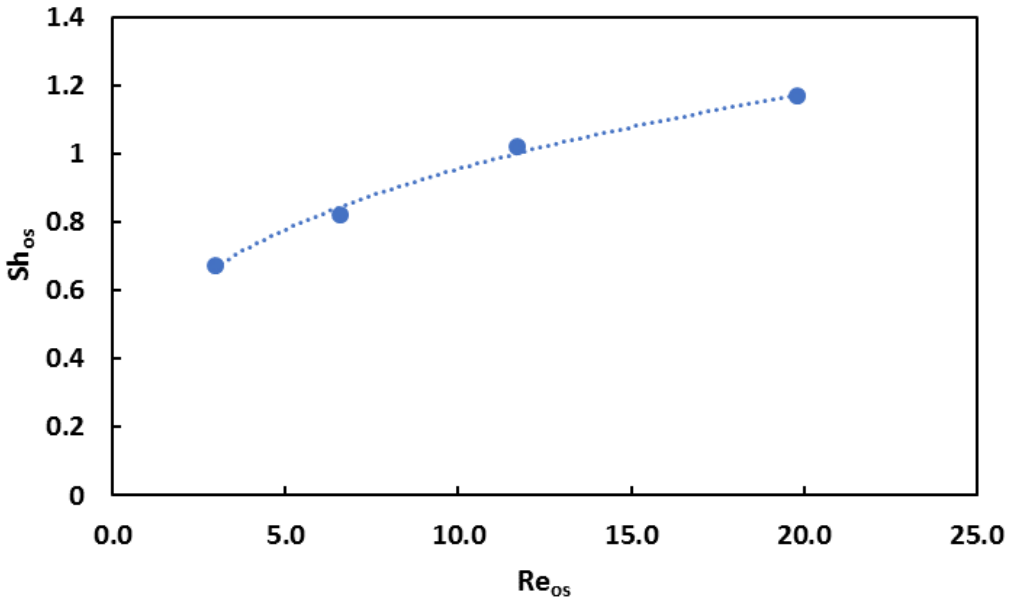


Fig. 4.10. $Sh_{os}$ as a function of the $Re_{os}$ (frequency: 2.03 Hz, amplitude: 0.2 mm)

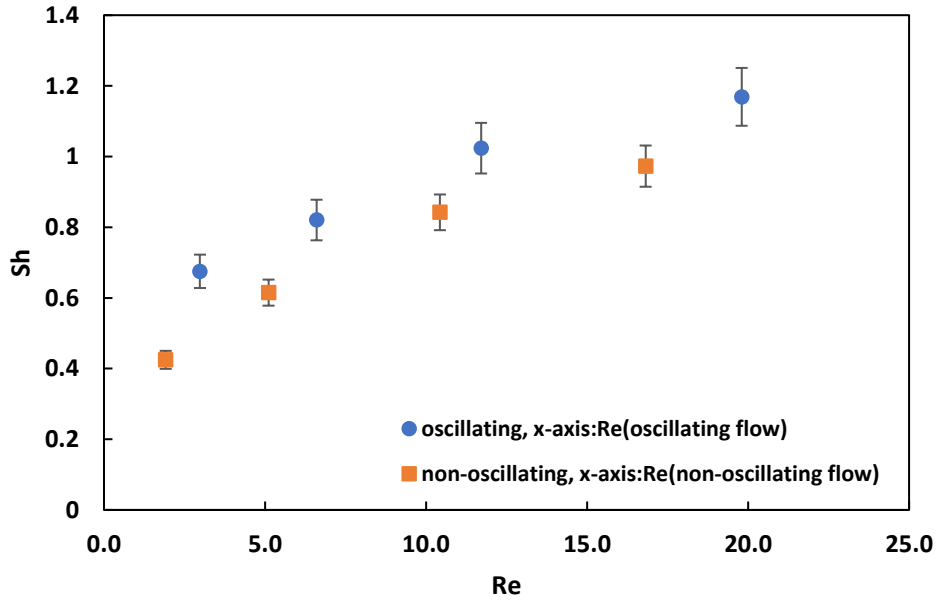


Fig. 4.11. Comparison between the Sherwood number (Sh) of the oscillating and non-oscillating conditions as a function of Reynolds number (Re)

## 4.5. Conclusion

The mass transfer performance of a hollow fibre membrane contactor module was evaluated under oscillating and non-oscillating solvent flow conditions. The increase in $CO_2$ flux from the gas phase to the solvent demonstrated that the solvent side mass transfer coefficient

increased with oscillating flow. Additionally, the mass transfer coefficient of the solvent side also increased under oscillating condition. The effects of oscillating frequency and amplitude were investigated on $K_{ov}$. The $K_{ov}$ increased by increasing the oscillating frequency and amplitude. The oscillating frequency, however, had a stronger impact relative to the oscillating amplitude. A modified Reynolds number was defined for the oscillating condition using the concept of root mean square velocity. Based on the $Re_{os}$, a new correlation for the Sherwood number was proposed and compared with the $Sh_{non\text{-}oscillating}$. The $Sh_{os}$ was clearly greater than the $Sh_{non\text{-}oscillating}$.

# CHAPTER 5: ABSORPTION OF $CO_2$ FROM FLUE GAS UNDER OSCILLATING GAS FLOW CONDITIONS IN GAS-SOLVENT HOLLOW FIBRE MEMBRANE CONTACTOR

Gas-solvent membrane contactors are intended to separate mixed gases that may impose a measurable mass transfer resistance on the gas side. This chapter focuses on the use of oscillation to reduce the gas-based mass transfer resistance in gas-solvent hollow fibre membrane contactors.

This chapter has been published in **Separation and Purification Technology** as follows:

**Elaheh Hosseini**, Ehsan Soroodan Miandoab, Geoffrey W. Stevens, Colin A. Scholes. "Absorption of $CO_2$ from Flue Gas under Oscillating Gas Flow Conditions in Gas-Solvent Hollow Fibre Membrane Contactors". Journal of Separation and Purification Technology Vol.249 (2020) 117151

## 5.1. Introduction

The emission of $CO_2$ from fossil fuel based power plants is a major environmental concern due to anthropogenic climate change [111]. Post-combustion carbon capture is one strategy that has potential for making significant reductions in carbon emissions from these power plants. Various approaches have been employed for $CO_2$ separation and purification, including conventional solvent absorption, membrane gas separation, cryogenic distillation, etc [57,24]. Membrane gas-solvent contactor technology is a hybrid approach, that incorporates the advantages of membrane gas separation, phase regime flow control and the compact nature of membrane modules, with the highly $CO_2$ selective solvent [57,117,118]. This enables greater mass transfer of $CO_2$ per unit volume to be achieved than either conventional solvent absorption or standard membrane gas separation approaches alone [62,119]. Membrane gas-solvent contactors have three mass transfer resistance stages, the gas phase boundary layer, the membrane layer and the solvent phase boundary layer. The membrane layer can be further differentiated into the non-porous active layer and the porous support layer [62,120]. To improve the separation performance of the membrane contactors, it is necessary to decrease the resistance of each respective mass transfer layer. In our recent work, ultra-thin composite

hollow fibre membranes and oscillating solvent flow were implemented in the membrane contactor system to minimize the membrane layer resistance and solvent boundary layer resistance, respectively [25]. In that study, the gas was pure $CO_2$ and the mass transfer resistance of the gas boundary layer was therefore negligible [25,121]. However, in industrial applications where the $CO_2$ volumetric percentage in the flue gas can vary between 5 to 30 % [122], there is the potential for the gas boundary layer resistance to impact overall mass transfer. One possible solution to this problem can be achieved by introducing oscillating gas flow, i.e. cyclic transient flow. An early study into the effect of oscillating feed gas on the separation performance of membranes was undertaken by Paul [105]. He exposed a flat sheet gas separation membrane to an upstream square wave oscillating gas flow and reported an increase in membrane selectivity. However, the system came with a loss in permeability. Trubyanov et al. [106] applied a pneumatic valve to the retentate side of the flat sheet gas separation membrane module to generate pulsed retentate flow and observed an increase in separation efficiency. Wang et al. [104] critically reviewed the short and long class cyclic transient membrane gas separation. They concluded that the cyclic transient method is too complex to operate, has high operating costs and energy consumption.

The potential of gas phase oscillation to membrane gas-solvent contactor system has not been established, to the best of the authors' knowledge, though there is clear need to increase mixing within the gas phase of contactor modules. Hence, this investigation is focused on reducing the gas boundary layer resistance in membrane contactor systems by generating additional mixing within this boundary layer. This is achieved through oscillating the gas phase flow, generating a pressure wave and therefore altering the flow dynamics of the gas boundary layer. This is a complementary study to the authors' recent investigation into inducing mixing within the solvent phase through oscillating flow [25].

In the present work, a gas mixture of 10% $CO_2$ in $N_2$ (balance), representative of flue gas in post-combustion $CO_2$ capture, was fed into the lumen side of the membrane contactor. Although there is a range of solvents that hold promise to $CO_2$ capture, such as novel amine based solvents [123–126], a $CO_2$-selective solvent based on 15wt% potassium glycinate was used in this investigation to keep conditions consistent with the authors' previous study on oscillation solvent flow. The solvent was introduced to the shell side of the membrane contactor. A gas mixture consisted of 10% $CO_2$ in $N_2$ (balance) was fed into the lumen side of the membrane. The composite hollow fibre membranes were non-porous ultra-thin polydimethylsiloxane (PDMS) on a porous polysulfone (PSf) support, which were also utilised

in the authors' previous study. The overall mass transfer coefficients ($K_{ov}$) for $CO_2$ separation under oscillating gas flow system were determined and compared with non-oscillating gas flow. The corresponding oscillating gas flow Reynolds number ($Re_{os}$) and Graetz number ($Gz_{os}$) were then employed to establish a mass transfer correlation for membrane contactors under gas phase oscillating flow. This correlation will enable similar membrane contactor systems to be modelled for enhanced performance under oscillating gas flow conditions.

## 5.2. Theory

The $CO_2$ molar flow rate through the membrane ($\dot{n}$) and molar flux (N) in membrane contactor module are given by [62]:

$$\dot{n} = NA \tag{5.1}$$

$$N = \frac{(Y_{in} - Y_{out})G}{A} = K_G C_{LM} \tag{5.2}$$

where G is gas molar flow rate ($mol_{mixture}/s$), A is the mass transfer area based on internal diameter of lumen side ($m^2$), Y is mole ratio of $CO_2$ in gas phase ($mol_{CO2}/mol_{mixture}$) and $C_{LM}$ is the log mean average of inlet and outlet concentrations of $CO_2$ in the bulk gas phase ($mol_{CO2}/m^3$). $K_G$ represents the overall gas-phase mass transfer coefficient (m/s) and is expressed as [61]:

$$\frac{1}{K_G} = \frac{1}{EHk_l} + \frac{d_o}{k_m d_{ln}} + \frac{d_o}{k_g d_i} \tag{5.3}$$

where $k_g$, $k_m$ and $k_l$ are the gas side, membrane and solvent side mass transfer coefficients (m/s), respectively, $d_i$ is the internal diameter of the hollow fibre membranes (m), $d_o$ is the outer diameter of the hollow fibre membranes (m), and $d_{ln}$ is the logarithmic mean diameter of the hollow fibre membranes (m); with the fibres consisting of porous and non-porous layers. H is Henry's law constant for $CO_2$ in the solvent and E represents the solvent enhancement factor [61,73,127].

The membrane non-porous layer mass transfer resistance is 0.0008 s/m as determined in the authors' previous study [25,61], while the porous layer mass transfer resistance is related to its thickness (δ, m), pore tortuosity (τ), porosity (ε), and gas diffusivity into the pores ($D_{CO_2}, m^2/s$) [62,127]:

$$\left(\frac{1}{k_m}\right)_{porous} = \frac{\delta\tau}{D_{CO_2}\varepsilon} \quad (5.4)$$

For the laminar flow, the Sherwood number (Sh) in the gas phase boundary layer (lumen side) is obtained from the Graetz- Lévêque correlations [62,73]:

$$Sh = 1.62Gz^{\frac{1}{3}} \qquad Gz > 6 \quad (5.5)$$

$$Sh = 0.5Gz \qquad Gz < 6 \quad (5.6)$$

where the Graetz number (Gz) is defined as [62]:

$$Gz = Re.\,Sc.\left(\frac{d_{in}}{l}\right) \quad (5.7)$$

Here, l is the length of the hollow fibre membranes, Re and Sc are the Reynolds and Schmidt numbers, respectively, and defined by [64,73]:

$$Re = \frac{\rho\bar{u}d_{in}}{\mu} \quad (5.8)$$

$$Sc = \frac{\mu}{\rho D_{CO_2}} \quad (5.9)$$

where $\mu$ and $\rho$ represent the viscosity (Pa.s) and density (kg/m$^3$) in the gas boundary layer, respectively, and $\bar{u}$ is the mean (average) gas velocity (m/s). However, Wickramasinghe et al. [74] has shown that the Graetz-Lévêque correlation overestimates the Sherwood number at low flow conditions, i.e. $Gz < 6$. This is because the Graetz- Lévêque analysis assumes that the concentration of component remains constant in the centre of fibres [74]. The asymmetric PDMS membrane contactors studied here operated at low Graetz numbers ($Gz < 0.1$), and therefore a generic form for validating the Sherwood number of the gas boundary layer was used:

$$Sh = \alpha Gz^{\beta} \quad (5.10)$$

for which $\alpha$ and $\beta$ are two adjustable parameters and determined from the experimental data.

To clarify the difference between oscillating and non-oscillating gas flow conditions, it is important to define a correlation for oscillating gas flow velocity. The oscillating gas flow velocity ($u_{os}(t)$) is assumed as [87,128]:

$$u_{os}(t) = \overline{u_0} + 2\pi f A \sin(2\pi f t) \quad (5.11)$$

where $\overline{u_0}$ indicates average non-oscillating gas flow velocity (m/s). f and A are oscillating gas flow frequency (Hz) and amplitude (m), respectively. To obtain the Reynolds and subsequently Sherwood numbers of the oscillating gas flow on the lumen side, an appropriate approach is employed to calculate the mean (average) gas velocity ($\bar{u}$). For oscillating gas flow, $\bar{u}$ is replaced by the root mean square velocity ($u_{os,rms}$) which is given by [25,107]:

$$u_{os,rms} = \sqrt{\frac{1}{T}\int_0^T u_{os}^2(t)dt} \quad (5.12)$$

Here, T is the period of sinusoidal function in Eq. (5.11). The root mean square approach enables the Reynolds and Sherwood numbers to be determined as a function of the oscillating gas flow parameters, i.e. f and A.

## 5.3. Experimental

### 5.3.1. Chemicals

Glycine (98.5% purity) and potassium hydroxide (85% purity) were supplied by Thermo Fisher Co. (Australia). Hollow fibre membranes were provided by Airrane Co. (South Korea). Fibres were bundled into an in-house constructed module. The membrane active layer mass transfer resistance of the hollow fibres has been previously determined for $CO_2$ absorption, 0.0008 s/m [25,61].

The gas mixture of 10% $CO_2$ in $N_2$ was provided by BOC (Australia).

### 5.3.2. Experimental set-up

The schematic diagram of the membrane contactor experimental apparatus is shown in Figure 5.1. The characteristics of the membrane contactor module are provided in Table 5.1. In the current apparatus, the mixed gas (10% $CO_2$ in $N_2$) was introduced to an oscillating unit and then fed into the lumen side of the membrane contactor. The feed gas flow was within 0.3-0.9 L/min and set by a mass flow controller (MFC, Aalborg 0-7 L/min). The feed gas pressure was measured by a pressure gauge (Swagelok, 0-12 bar). The oscillating unit was supplied by Cole-Parmer Co. (Australia) and consisted of a reciprocating piston inside a fixed cylinder. It was also equipped with a motor and a variable frequency drive to provide the reciprocating motion of the piston. Once the mixed gas passed through the oscillating unit, the piston introduced the oscillating gas flow into the system. The oscillating gas frequency and amplitude were set to 0-3 Hz and 0-4 cm, respectively.

In the present work, 15wt% of potassium glycinate was used, although the common concentration of commercialized solvents such as monoethanolamine (MEA) is 30wt% [8]. The choice in solvent is because of safety and environmental concerns, as potassium glycinate is less toxic and environmentally benign while having comparable reaction kinetics to conventional MEA [43].The solvent was prepared by adding equimolar amounts of potassium hydroxide and glycine to deionized water (pH=7). Table 5.2 indicates characteristics of the potassium glycinate solution at 25°C (lab temperature), with density, viscosity and diffusion coefficients taken from literature, while the enhancement factor and Henry's law constant determined from theory [69,70]. The solvent was introduced into the shell side through a gear pump (Ismatec, 0–0.11 L/min) and circulated in the system with a counter-current mode of operation. The solvent flow rate was 5 mL/min (equivalent to the Reynolds number of 2.86).

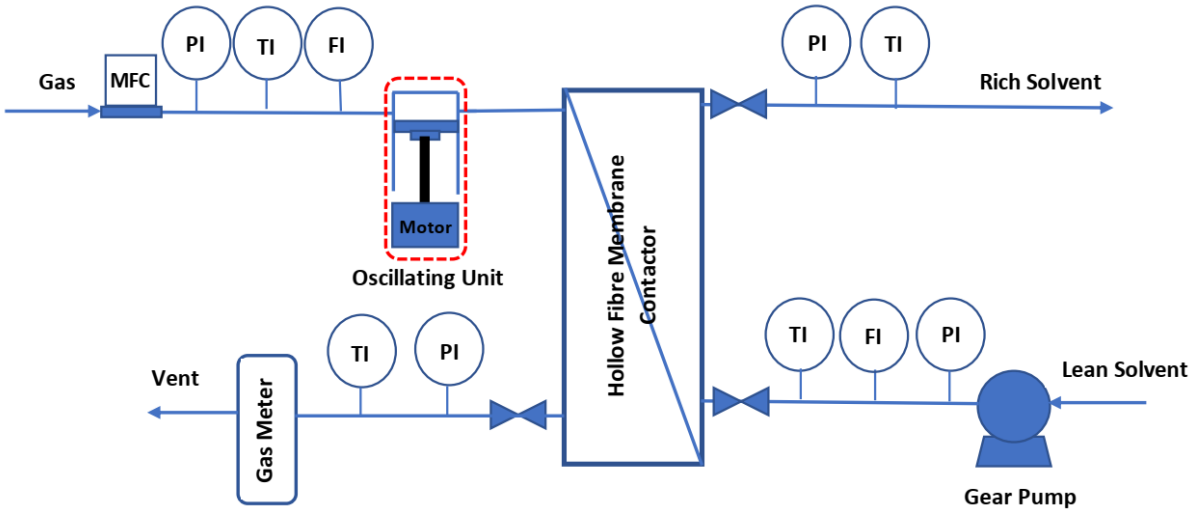


Fig. 5.1. Schematic diagram of oscillating gas flow membrane contactor apparatus

Table 5.1. Gas-solvent hollow fibre membrane contactor characteristics (oscillating gas flow studies)

| | |
|---|---|
| Number of fibres | 123 |
| Module inside diameter | 9.5 mm |
| Membrane inside diameter | 300 µm |
| Membrane outside diameter | 470 µm |
| Thickness of PDMS | 0.5 µm |
| Module's shell composition | Teflon |
| Length of module | 25 cm |
| Packing density | 0.3 |
| Porous membrane mass transfer resistance | 0.019 m/s |

Table 5.2. Characteristics of 15wt% potassium glycinate at 25°C

| | |
|---|---|
| Density ($kg/m^3$) | 1060 |
| Viscosity (kg/m.s) | 0.001323 |
| Diffusion coefficient of $CO_2$ in potassium glycinate ($m^2/s$) | $1.46\times10^{-9}$ |
| Potassium glycinate diffusion coefficient ($m^2/s$) | $4.66\times10^{-10}$ |
| Enhancement Factor | 20.890 |
| Henry's law constant ($Pa.m^3/mol$) | 4224.310 |

To ensure that the steady-state process has achieved, the system operated for 1 hour. After which samples were collected from the solvent side and the amount of $CO_2$ loading was measured by colourimetry titration (CM5015 Coulometer, UIC Inc., USA). The gas-solvent membrane contactor operation and colourimetry titration was done at 25°C. Once the $CO_2$ content of the solvent was determined, an overall mass balance for $CO_2$ was performed to calculate the $CO_2$ mole fraction in the outlet gas stream ($Y_{out}$).

### 5.3.3. Oscillating gas flow velocity measurement

The gas flow velocity under oscillating conditions is provided in Figure 5.2 and demonstrated as a sinusoidal wave (Eq. (5.11)). This sinusoidal wave correlated with the amplitude and frequency configuration. An oscillating Reynolds number ($Re_{os}$) based on the oscillating gas flow velocity ($u_{os}(t)$) could now be established. It was determined that for the experimental conditions studied here, the $Re_{os}$ varied between 15.0 and 39.2; which corresponded to laminar flow conditions. These low Re numbers are comparable to other membrane contactor processes, given the focus here is on the gas phase [74].

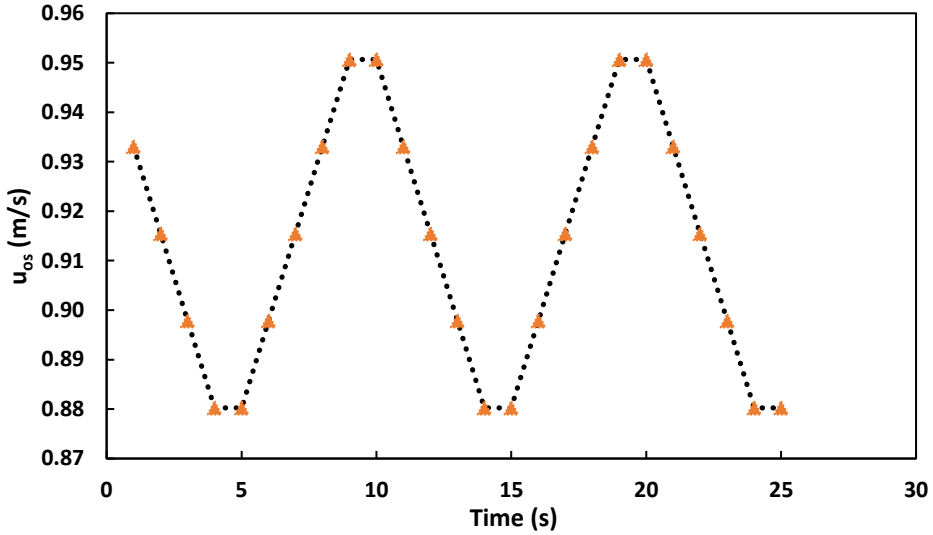


Fig. 5.2. Oscillating gas phase velocity ($u_{os}$) as a function of time (frequency: 0.083Hz, amplitude: 4cm)

## 5.4. Results and discussion

### 5.4.1. Comparison of the mass transfer performances under oscillating and non-oscillating gas flow conditions

The values of $K_G$ for oscillating and non-oscillating conditions are shown in Figures 5.3. $Re_{non\text{-}oscillating}$ was calculated based on the average flow velocity entering the module:

$$Re_{non-oscillating} = \frac{\rho \overline{u_0} d_{in}}{\mu} \quad (5.13)$$

Reporting both oscillating and non-oscillating flow as a function of $Re_{non\text{-}oscillating}$ enables the performance comparison to be clearly observed and quantified. For both flow conditions, as feed flow rate increased, $Re_{non\text{-}oscillating}$ also increased resulting in an increase in the $CO_2$ flux and $K_G$ (see Eq. (5.2)). This is standard behaviour for membrane contactors, associated with a reduction in the boundary layer thickness and increased mixing [129]. The $CO_2$ flux and $K_G$ under oscillating gas flow conditions were enhanced relative to the non-oscillating flow, from 14 to 28% at studied Reynolds numbers. This reflected the existence of additional mixing in the gas phase boundary layer, as the oscillating flow disrupted the boundary layer thickness and flow regime around this layer.

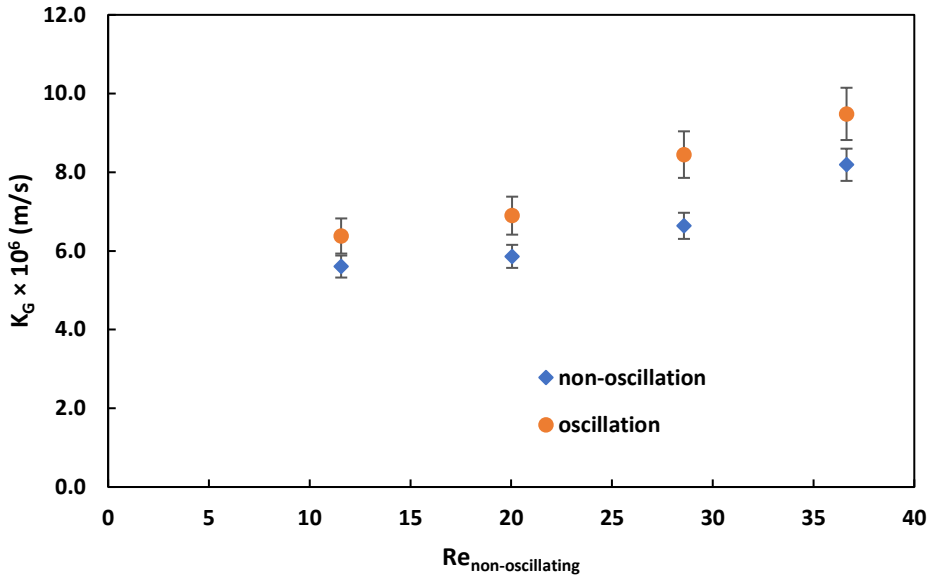


Fig. 5.3. Overall mass transfer coefficient ($K_G$) under oscillating and non-oscillating gas flow condition (frequency: 1.33Hz, amplitude: 4cm)

The mass transfer coefficient for $CO_2$ through the non-porous PDMS membrane and porous layer has been previously established by the authors (see Chapter 4) [25]. Similarly, the mass transfer correlation of $CO_2$ transfer in the solvent boundary layer under non-oscillating conditions has been established by the authors (see Chapter 4) [25]. Therefore, the mass transfer coefficient in the gas phase boundary layer ($k_g$) was calculated from Eq. (5.3) and a comparison of $k_g$ for oscillating and non-oscillating system is provided in Figure 5.4. $k_g$ clearly increased under oscillating flow conditions relative to non-oscillating flow, confirming the presence of additional mixing in the gas phase to improve separation performance.

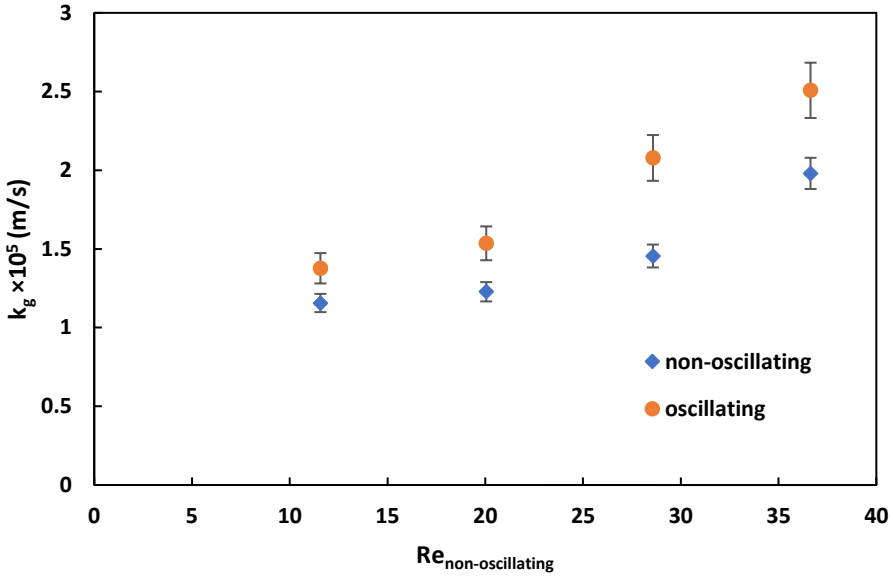


Fig. 5.4. Gas phase mass transfer coefficient ($k_g$ for oscillating and non-oscillating conditions as a function of $Re_{non\text{-}oscillating}$ (frequency: 1.33Hz, amplitude: 4cm))

### 5.4.2. Influence of oscillating frequency and amplitude on overall mass transfer coefficient ($K_G$)

The effect of oscillating gas flow frequency for a fixed amplitude on $K_G$ is provided in Figure 5.5. The $K_G$ increased by 15 % with the oscillating frequency increasing from 0 to 2Hz, with the majority of this increase occurring in transition from steady-state condition (f=0) to a frequency of 1.33 Hz. This indicates that only a small fluctuation in the gas phase flow is necessary to induce mixing [128]. The differences in $K_G$ values for frequencies higher than 2 Hz are not significant given the experimental error, hence increasing the rate of the gas fluctuation has only a minor impact. This behaviour was independent of module characteristics as indicated in Figure 5.5, where the performance of two different length modules is reported. This result indicates that inducting oscillation and therefore mixing is important for increased mass transfer, but the rate of oscillation is not a significant factor above a limiting frequency.

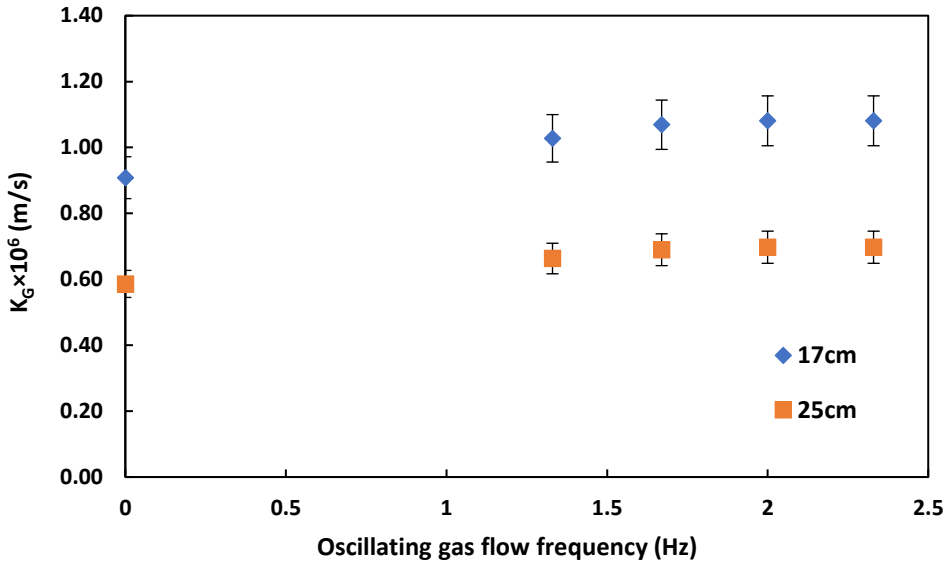


Fig. 5.5. Effect of oscillating gas flow frequency on the mass transfer rate of $CO_2$ for different membrane contactor modules (amplitude: 4cm, $Re_{non\text{-}oscillating}$: 11.57)

The influence of oscillating gas flow amplitude for a fixed frequency on $K_G$ is provided in Figure 5.6. The gas phase is a compressible fluid, therefore the correlation between oscillating amplitude and the fluctuation of the gas flow was not linear. It was observed that at fixed oscillating frequency of 1.33 Hz, an increase in the oscillating amplitude from 0.4 cm to 4 cm, resulted in essentially a doubling of $K_G$ from $3.53\times10^{-6}$ m/s to $6.89\times10^{-6}$ m/s. This increase is partly explained by an increase in the driving force across the membrane, which is the difference in the partial pressure of $CO_2$ in the feed and the equilibrium partial pressure above the solvent. As the oscillating amplitude generated a pressure wave in the gas phase flow; there will correspondingly be regions within the contactor of high pressure, and subsequently higher partial pressure of $CO_2$ than used in the driving force calculation, which is based on average conditions. As a result, the mass transfer of $CO_2$ increased and reflected as an increase in overall mass transfer coefficient.

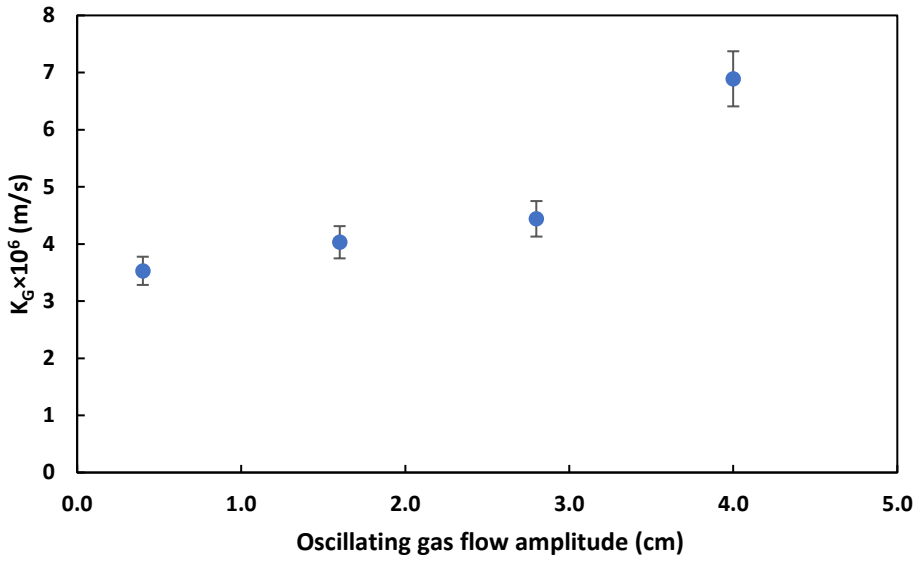


Fig. 5.6. Effect of oscillating amplitude on overall mass transfer coefficient ($K_G$) (frequency: 1.33 Hz, $Re_{non\text{-}oscillating}$: 11.57)

### 5.4.3. Determination of Sherwood number correlation for oscillating and non-oscillating gas flow conditions

To develop a mass transfer correlation in the gas phase boundary layer, the Sherwood number was calculated using $k_g$ obtained from oscillating and non-oscillating gas flow experiments. Contrary to the Graetz-Lévêque analysis, the relationship between Gz and Sh numbers did not obey a linear relationship, as shown in Figure 5.7. This behaviour was in agreement with the experimental and theoretical study by Wickramasinghe et al. [74]. The experimental values of oscillating Sherwood number ($Sh_{os}$) and non-oscillating Sherwood number ($Sh_{non\text{-}oscillating}$) can therefore not be presented from the mass transfer correlations reported in Graetz-Lévêque correlation (Eq.(5.5) and (5.6)) [74,130]. A new more robust mass transfer correlation (Eq. (5.10)) was developed as a function of the Gz number for the oscillating and non-oscillating conditions, i.e. $Sh_{non\text{-}oscillating}$ and $Sh_{os}$. The difference between $Sh_{non\text{-}oscillating}$ and $Sh_{os}$ was related to the definitions of $Gz_{os}$ and $Gz_{non\text{-}oscillating}$; while $Gz_{os}$ was defined based on the oscillating gas flow root mean square velocity ($u_{os,rms}$), $Gz_{non\text{-}oscillating}$ was calculated by the aid of the non-oscillating average velocity ($\overline{u_0}$). Figure 5.7 illustrated the experimental Sherwood numbers under the non-oscillating and oscillating flow conditions along with the line of best fit to Eq. (5.10). The experimental data of oscillating and non-oscillating conditions was simultaneously fitted to Eq. (5.10) to estimate statistically valid fitting parameters (α and β). The predicted

values of α and β were 0.0026 and 0.57, respectively. Therefore, the non-oscillating and oscillating Sherwood numbers were described by:

$$Sh_{non-oscillating} = 0.0026 Gz_{non-oscillating}^{0.57} \quad (5.14)$$

$$Sh_{os} = 0.0026 Gz_{os}^{0.57} \quad (5.15)$$

where, $Gz_{non\text{-}oscillating}$ and $Gz_{os}$ were accordingly defined by:

$$Gz_{non-oscillating} = Re_{non-oscillating}. Sc. \left(\frac{d_{in}}{l}\right) \quad (5.16)$$

$$Gz_{os} = Re_{os}. Sc. \left(\frac{d_{in}}{l}\right) \quad (5.17)$$

In Eq. (5.17), $Re_{os}$ was the oscillating gas flow Reynolds number given by:

$$Re_{os} = \frac{\rho u_{os,rms} d_{in}}{\mu} \quad (5.18)$$

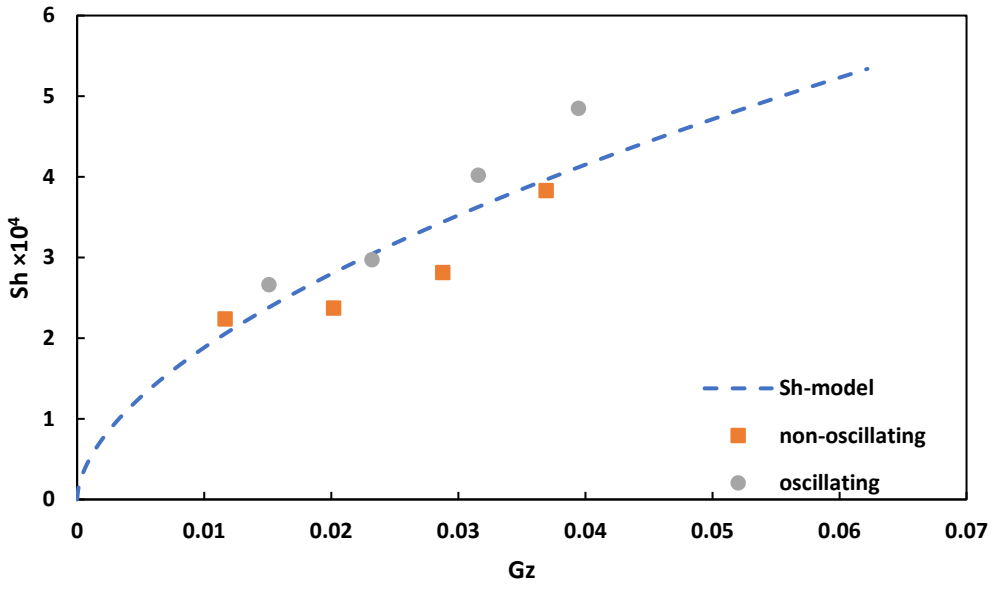


Fig. 5.7. Sh as a function of Gz for oscillating and non-oscillating gas flow conditions

## 5.5. Conclusion

This investigation applied oscillating gas phase flow to a gas-solvent membrane contactor undertaking $CO_2$ capture, to enhance mass transfer from gas to solvent phase. The performance of the membrane contactor under oscillating gas flow conditions indicated an increase in mixing within the gas phase boundary layer and hence, greater mass transfer coefficients were obtained in comparison with non-oscillating gas flow conditions. Higher oscillating gas flow

amplitude led to more improvement in mass transfer rate of $CO_2$ capture module, because the compressible phase created conditions of increased mass transfer driving force. In contrast, overall mass transfer coefficient increased when oscillation occurred, but remained constant irrespective of frequency. Importantly, the improvement in overall mass transfer coefficient under oscillating gas phase conditions revealed that the gas phase boundary layer has a measurable impact on overall mass transfer in membrane contactor systems.

# CHAPTER 6: VIBRATION-INDUCED ENHANCED MASS TRANSFER WITHIN MEMBRANE CONTACTORS FOR EFFICIENT $CO_2$ CAPTURE

## 6.1. Introduction

In gas-solvent membrane contactor systems, the mass transfer resistance of the respective phases (gas boundary layer, membrane layer, porous support layer and solvent boundary layer) all play key roles in the overall mass transfer process. To reduce the mass transfer resistance of the membrane, the application of ultra-thin composite membranes with porous support has achieved significant performance improvements and are now the standard for the technology [131,132]. Chapter 4 and 5 demonstrated that oscillating flow conditions reduced mass transfer resistance and enhanced $CO_2$ separation [25,110]. This was achieved by the oscillating flow disrupting the gas phase and solvent phase boundary layer profiles. However, two separate processes were needed to apply oscillation to the respective boundary layers. Therefore, an alternative approach was required to agitate both phases' boundary layers. The application of vibration was a strong candidate, given vibrations have been demonstrated to enhance mass transfer for oxygenation applications by a factor of 2.56 [98].

This study investigated the influence vibration had on mass transfer performance in gas-solvent membrane contactor systems undertaking $CO_2$ absorption into a chemical solvent, as the agitation from the vibration influences the flow regimes present within the membrane configuration as well as the transfer of chemical species through the respective boundary layers.

In the experimental work, hollow fibre membranes consisting of a non-porous ultra-thin polydimethylsiloxane (PDMS) on a porous polysulfone (PSf) support were utilised, which demonstrated in industry pilot plant trials for high performance $CO_2$ capture [38]. The $CO_2$ selective solvent was 15 wt% potassium glycinate and pure $CO_2$ and a mixture of 10%$CO_2$ in $N_2$ were used as the gas.

The measured $CO_2$ flux and subsequent mass transfer through the various stages of the membrane contactor enabled the overall solvent-based mass transfer coefficient ($K_L$) to be determined for vibrating and non-vibrating systems, which enabled analysis of mass transfer enhancement under various vibrational conditions. Subsequently, the membrane contactor

mass transfer performance was described through a Sherwood number correlation, utilising a dimensionless vibration number to account for enhancement in mass transfer. Additionally, this study presented the first quantitative analysis of vibrational induced mass transfer in membrane contactor systems, achieving a significant improvement in the technology's performance.

## 6.2. Theory

The theory of gas-solvent hollow fibre membrane contactor systems was described in chapter 2 (see section 2.4).

The mass transfer in the solvent boundary layer can be established by a shell side correlation based on the dimensionless Sherwood number ($Sh_s$), which is generally defined as a function of the shell side Reynolds ($Re_s$) and Schmitt ($Sc_s$) numbers, as well as the packing density ($\Phi$) of membrane contactors (the packing density is the ratio of cross-sectional hollow fibres area to the cross-sectional shell area) [72]:

$$Sh_s = \frac{k_l d_h}{D_{CO_2}} = f(\Phi) Re_s^{\alpha} Sc_s^{\beta} \tag{6.1}$$

where $d_h$ is the hydraulic diameter.

The influence of vibration on the mass transfer in the solvent or gas boundary layer is dependent on the vibrating frequency (F) and displacement amplitude ($A_d$), which can be accounted for by a new dimensionless number ($\Pi_{v,L}$). Hence, the Sherwood number correlation for the solvent boundary layer (shell side) under vibrating conditions ($Sh_{s\text{-}vib}$) is based on Reynolds, Schmidt and vibrational dimensionless numbers:

$$Sh_{s-vib} = \frac{k_l d_h}{D_{CO_2}} = f(\Pi_{v,L}) f(\Phi) Re_s^{\alpha} Sc_s^{\beta} \tag{6.2}$$

where $\alpha$, $\beta$, $f(\Pi_{v,L})$ and $f(\Phi)$ are obtained from fitting the corresponding non-vibrating and vibrating experimental data to Eq. (6.1) and Eq. (6.2), respectively.

## 6.3. Experimental

In this chapter, experiments were conducted to show the effect of vibrating unit on the solvent side and gas side boundary layers. The design of the vibrating unit and the experimental procedure have been presented in chapter 3 (see 3.8 and 3.9).

## 6.4. Results and discussion

### 6.4.1. Solvent boundary layer mass transfer

#### 6.4.1.1. Effect of vibrational frequency and amplitude

Pure $CO_2$ as the feed gas enabled the effect of vibrating frequency on the overall solvent-based mass transfer coefficient to be determined which is provided in Figure 6.1, for a solvent Reynolds number of 1.35, also included is the overall mass transfer coefficient when there was no vibration. Compared to the non-vibrating system, $K_L$ was enhanced under vibrating conditions. This enhancement of vibration can be considered from both flow dynamics and boundary layer perspectives. The vibrating frequency resulted in the vibration of the membrane fibres, as well as the solvent phase that disrupted the solvent boundary layer, resulting in enhanced mixing. There was a clear trend of increased enhancement in mass transfer at higher frequencies. A shift from 0.5 to 2.3 Hz corresponded to the overall solvent-based mass transfer coefficient enhanced from 3% to 20%, respectively. These improvements in mass transfer performance by frequency can be quantitatively linked with the solvent boundary layer thickness (see Eq. (4.15))

From Eq. (4.15), as the vibrating frequency increases, the boundary layer thickness correspondingly decreases, which for the membrane contactor system represented a decrease of over 50% in boundary layer thickness between 0.5 and 2.3 Hz measurements. As a consequence, an enhancement in mass transfer was observed.

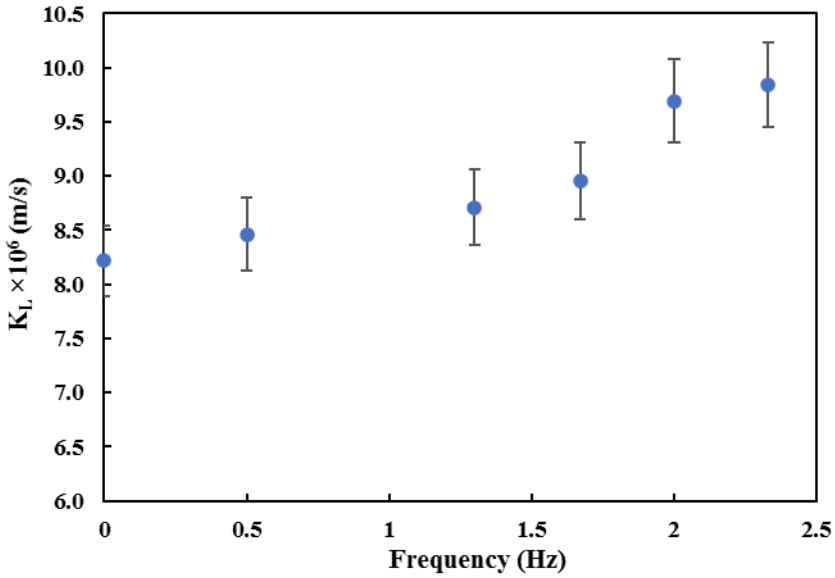


Fig. 6.1. Overall solvent-based mass transfer coefficient ($K_L$) as a function of vibrating frequency at the fixed displacement amplitude of 2cm (displacement per module length of 8%) and a solvent Reynolds No of 1.35. The feed is pure $CO_2$.

The effect of displacement amplitude (i.e., module displacement) on the overall solvent-based mass transfer coefficient of $CO_2$ is provided in Figure 6.2. Again, the non-vibrating measurement was provided for reference and there was clear evidence that displacement amplitude improved mass transfer, with an increase in mass transfer coefficient of 9% for a displacement amplitude of just 1cm. Importantly, the mass transfer coefficient was further enhanced as the displacement amplitude increased, with an enhancement of 21% measured for the largest displacement possible on the apparatus. displacement amplitude impacted the flow dynamics within the membrane module, with the size of the amplitude propagating a pressure displacement wave through the module and generating secondary flow characteristics that enhanced mixing [99].

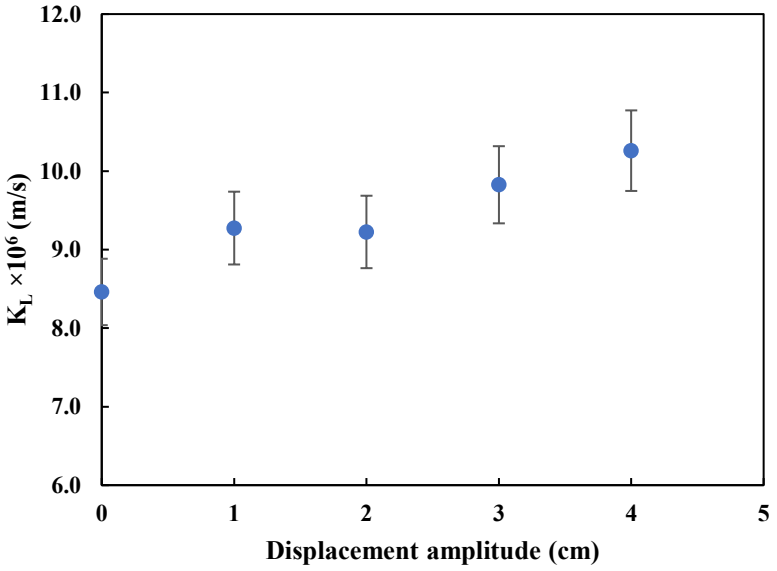


Fig. 6.2. Overall solvent-based mass transfer coefficient ($K_L$) as a function of displacement amplitude at the fixed vibrating frequency of 1.67 Hz and a solvent Reynolds No of 1.35. The feed is pure $CO_2$.

### 6.4.1.2. Effect of module packing density and solvent flow rate

The membrane packing density within the contactor module impacts the mass transfer of $CO_2$ into the solvent phase, as packing density influences the shell side flow regimes within the module. The mass transfer performance of the non-vibrating membrane contactor as a function of solvent Reynolds number and packing density is provided in Figure 6.3. The overall solvent-based mass transfer coefficient increased with the solvent Reynolds number, which is a standard behaviour for contactor systems [62]. This increase was associated with increased mixing within the solvent boundary layer at higher Reynolds numbers. There was also an obvious increase in overall solvent-based mass transfer coefficient with increased packing density of the module [79]. This is a direct result of the reduction in cross-sectional area on the shell side of the module due to an increase in the number of membrane fibres present. This resulted in a greater solvent velocity around and across the fibres, corresponding to a reduction in solvent boundary layer and increase in mass transfer. Increasing the packing density at higher Reynolds numbers had greater impact on the mass transfer coefficient. This was because the effect of solvent disturbance was higher at the increased Reynolds numbers which was added to the effect of higher packing densities.

Although the mass transfer coefficient is enhanced with increasing the solvent flow rate, this, at least, has two major limitations. First and foremost, an increase in the flow rate comes at the cost of reduced $CO_2$ loading in the solvent, as the higher flow rate decreases the retention time

of the solvent in the membrane module, subsequently, reduces the amount of $CO_2$ absorption. This behaviour of membrane contactors has been proved by numerous studies. Secondly, the solvent flow rate cannot be increased endlessly and there is an operational range for the solvent flow rate beyond which the use of membrane contactors (or perhaps any other technology) is not practical. Therefore, the aim of this chapter was to investigate the effect of vibrating unit on the performance of gas-solvent membrane contactor considering these limitations. The effect vibration has on membrane contactors for different Reynolds numbers is provided in Figure 6.4, for a packing density of 0.3 and a frequency of 1.67 Hz and amplitude displacement of 8%. Figure 6.4 shows that inducing vibration enhances the performance of membrane contactors compared to that of conventional modules that operate under identical conditions.

The presence of vibration enhanced the mass transfer coefficient of the system, with an increase of 11% at the lowest Reynolds number that tapered off to below the error margins for the experiment at the highest Reynolds number, at this frequency and amplitude. Considering figure 6.1 and 6.2, higher mass transfer enhancements can be achieved by increasing the vibrating frequency and displacement amplitude. Hence, vibrational effects had their strongest impact on mass transfer when the solvent velocity (Reynolds number) was low. This observation is similar to the results of chapter 4 investigating the effect of oscillating solvent flow on gas-solvent membrane contactor systems [110]. This tapering off in vibrational enhancement with increased solvent velocity was more likely attributed to thinner boundary layer at higher solvent velocities which result in reducing the effect of vibration. The comparison of the solvent side mass transfer enhancement under oscillating and vibrating unit conditions showed that the oscillating unit had a greater impact on the solvent side mass transfer coefficient. The difference between the impact of oscillating and vibrating unit is due to the limitation of vibration equipment which had no direct contact with the solvent flow, thereby the effect of vibration was not as pronounced as that of oscillation in which the solvent flow was directly disturbed by the piston movement.

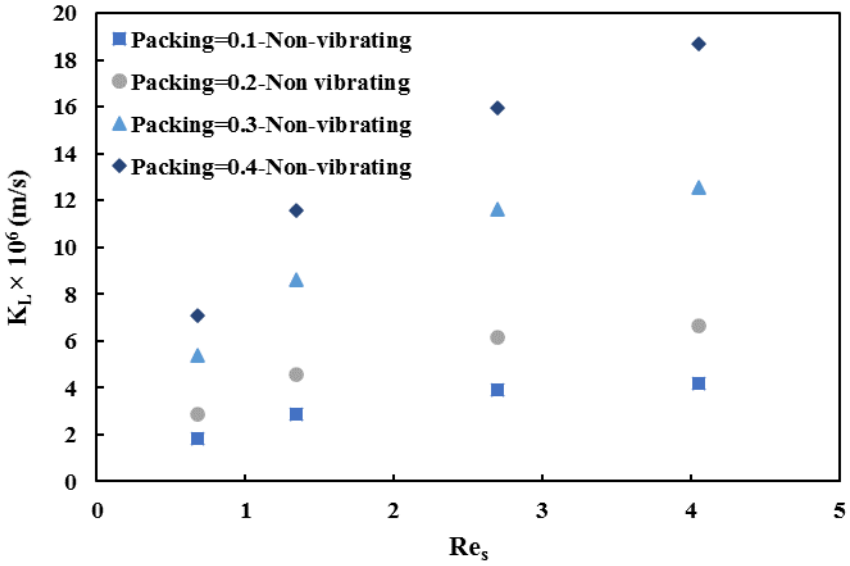


Fig. 6.3. Effect of solvent Reynolds number ($Re_s$) and packing density on overall solvent-based mass transfer coefficient ($K_L$) under non-vibrating conditions. Symbols and lines are experimental data and the lines of best fit to Eq. (6.1), respectively. The error of experiments was 4%.

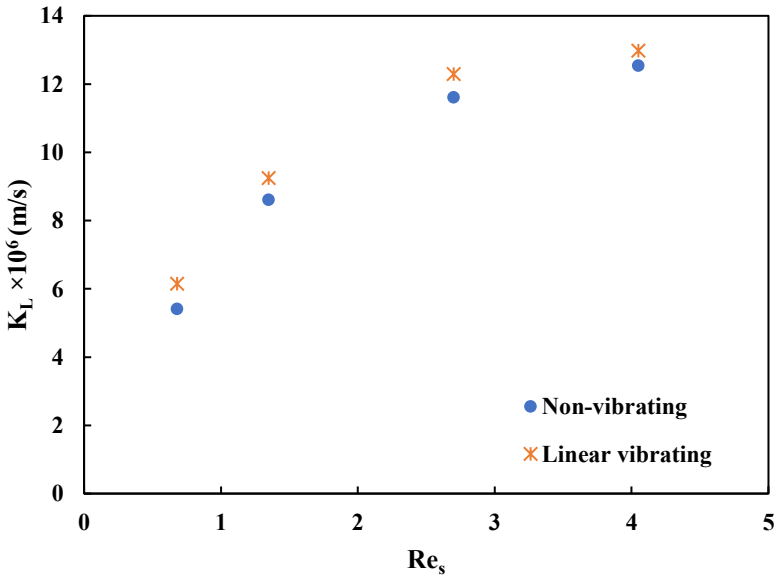


Fig. 6.4. Overall solvent-based mass transfer coefficient ($K_L$) as a function of shell side Reynolds number ($Re_s$) under vibrating and non-vibrating conditions. The vibration was at a frequency of 1.67 Hz and displacement amplitude of 2cm. The packing density of module is 0.3 and the error of experiments was 4%.

The effect module packing density has on the vibrational enhancement of mass transfer is demonstrated in Figure 6.5, for a vibrating frequency of 1.67 Hz and displacement amplitude of 2cm. For a module packing density of 0.1, vibration enhanced the overall solvent-based mass transfer coefficient by 35%, but as the packing density of the module increased the vibrational enhancement effects reduced until there was no enhancement for a packing density

of 0.4. This behaviour was also associated with the solvent velocity, as for constant solvent flowrates the smaller packing density had a lower solvent velocity (higher shell side cross-sectional area) than high packing density (lower cross-sectional area). Hence, as solvent velocity increased within the shell side of the module, the enhancement in mass transfer coefficient was significantly reduced, because the agitation generated by the vibration was unable to disturb the solvent boundary layer at higher solvent flow rates. Moreover, the hollow fibres had more freedom of movement inside lower packing density modules. Therefore, the influence of vibration was more pronounced for the modules with lower packing densities.

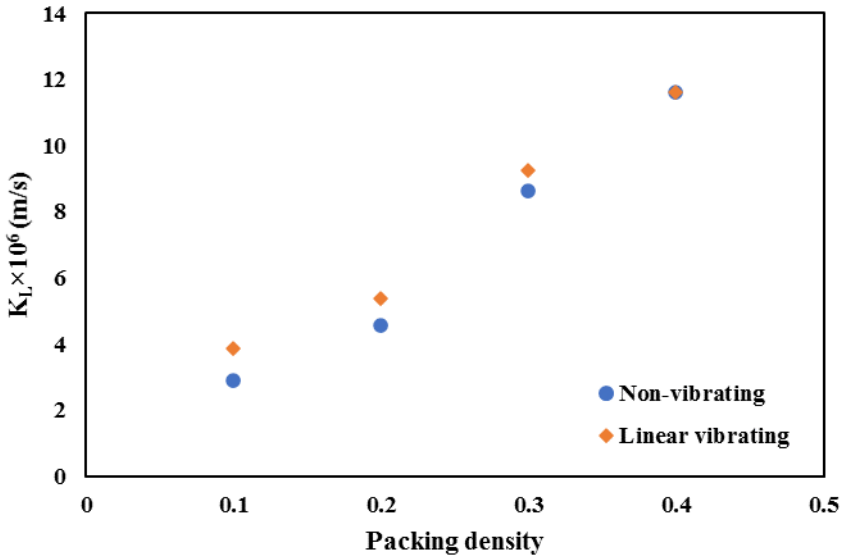


Fig. 6.5. Overall solvent-based mass transfer coefficient ($K_L$) as a function of packing density under linear vibrating and non-vibrating conditions. The vibration was at a frequency of 1.67 Hz and displacement amplitude of 2cm. The Reynolds number fixed at 1.35 and the error of experiments was 4%.

### 6.4.1.3. Sherwood number correlation under vibrating conditions

Mass transfer in gas-solvent membrane contactors is influenced by solvent and gas phase Reynolds numbers, Schmidt number, as well as the geometric characteristics of the contactors described through packing density (Φ), as clearly demonstrated in the previous section [72]. For the gas-solvent contactor systems studied here, the non-vibrating data (Figure 6.4) was fitted to the standard correlation expression (Eq. (6.1)) and the following correlation was established:

$$Sh_s = (0.03 - 0.0136\Phi)Re_s^{0.48}Sc_s^{0.33} \qquad 0.1<\Phi<0.5 \qquad (6.3)$$

The dependence of Sherwood number on Φ (i.e. f(Φ)) is generally expressed by a polynomial [72], which for this system was best modelled by a linear relationship. This correlation was comparable to the mass transfer correlations obtained in chapter 4 for membrane contactors in terms of the Reynolds and Schmidt number exponents.

As shown in figures 6.1 and 6.2, an increase in displacement amplitude and frequency resulted in the solvent side mass transfer enhancement. Therefore, for vibrating conditions, the mass transfer correlation must account for the vibrating agitation on the system which was expressed through the vibrating dimensionless number ($\Pi_{v,L} = \frac{A_d F}{u_{0,L}}$). The dimensionless number was constructed as a multiplication of the frequency and displacement amplitude of the vibration, an indication of the vibrational force being applied to the system, divided by the phase velocity, an indication of the inertial forces.

Figure 6.6 indicated that an increase in $\Pi_{v,L}$ (i.e., an increase in frequency, displacement amplitude or both of them) improved the solvent side Sherwood number. Consequently, the vibrational dimensionless number contribution to the Sherwood number mass transfer correlation was determined from the enhancement to mass transfer in the membrane contactor system. According to the reported data in Figure 6.6, the Sherwood number correlation under vibrating conditions was established as:

$$Sh_{s-vib} = (1 + \frac{A_d F}{u_{0,L}})^{0.03}(0.03 - 0.0136\Phi)Re^{0.48}Sc^{0.33} \qquad 0.1 < \Phi < 0.5 \qquad (6.4)$$

The dimensionless vibration number took the form $(1+\frac{A_d F}{u_{0,L}})$ in the correlation to ensure the correlation accurately described the system when no vibration was present, e.g. at $\frac{A_d F}{u_{0,L}} = 0$ and Eq. (6.4) reduced to Eq. (6.3). Hence, the enhancement in the mass transfer performance due to the vibrational effects on the solvent phase can be modelled purely as $(1 + \frac{A_d F}{u_{0,L}})^{0.03}$.

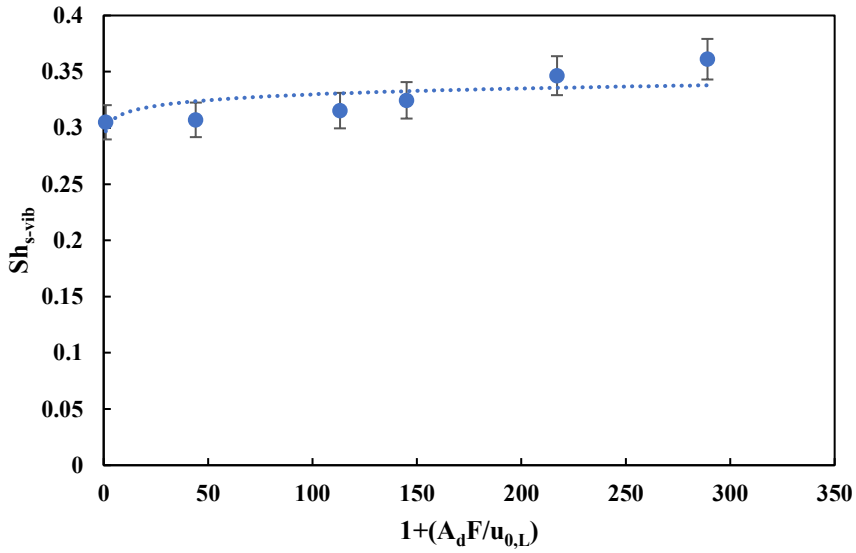


Fig. 6.6. Experimental Sherwood numbers for the solvent boundary layer under linear vibrating conditions as a function of the dimensionless vibration number $1+A_dF/u_{0,\,L}$. The experimental data were fitted to Eq. (6.2).

## 6.4.2. Gas boundary layer mass transfer

### 6.4.2.1. Effect of vibration frequency and amplitude

Using 10% $CO_2$ in $N_2$ as the feed gas, the effect of vibration on mass transfer through the gas phase boundary layer was quantified in terms of the overall gas-based mass transfer coefficient as a function of amplitude displacement (Figure 6.7) and frequency (Figure 6.8). The displacement amplitude was varied between 1 and 4 cm, at a fixed frequency of 1.67 Hz, and demonstrated an enhancement in overall mass transfer coefficient, which increased with greater displacement amplitude. At the maximum displacement amplitude, the overall mass transfer coefficient increased by 38%. Similarly, for variable frequency (constant amplitude) there was a significant increase in overall mass transfer coefficient for the contactor system, with an increase of 36% from non-vibration at 2.3 Hz measurement. Again, this indicated that vibration frequency influenced mass transfer in the gas phase, as the enhancement of solvent-based mass transfer coefficient due to frequency increase was 20%. The increase in mass transfer was attributed to the vibration agitation significantly propagating through the gas phase and inducing additional mixing. Moreover, the additional mixing was most likely split between the gas phase boundary layer as well as within the membrane's porous support where mass transfer was diffusivity limited and therefore benefit from increased agitation. The fact that this additional mixing was occurring within two locations of the contactor system meant that

extrapolation to mass transfer theory was extremely difficult, as it was not possible to determine how much each location was contributing to the mass transfer enhancement. Hence, no attempt can be made of developing a consistent mass transfer correlation for this gas phase behaviour under vibrational conditions.

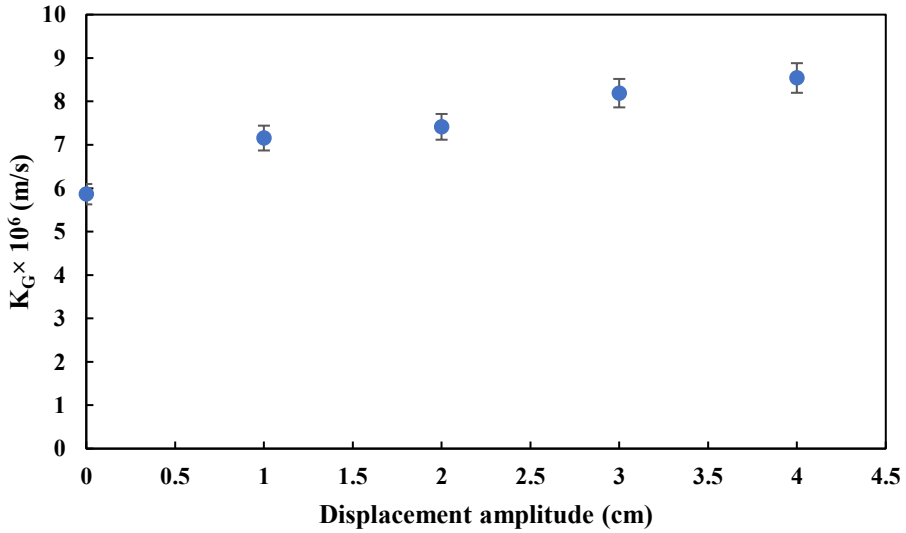


Fig. 6.7. Overall gas-based mass transfer coefficient ($K_G$) as a function of displacement amplitude at the fixed vibrating frequency of 1.67 Hz and a solvent Reynolds No of 1.35 and gas Reynolds No of 20.

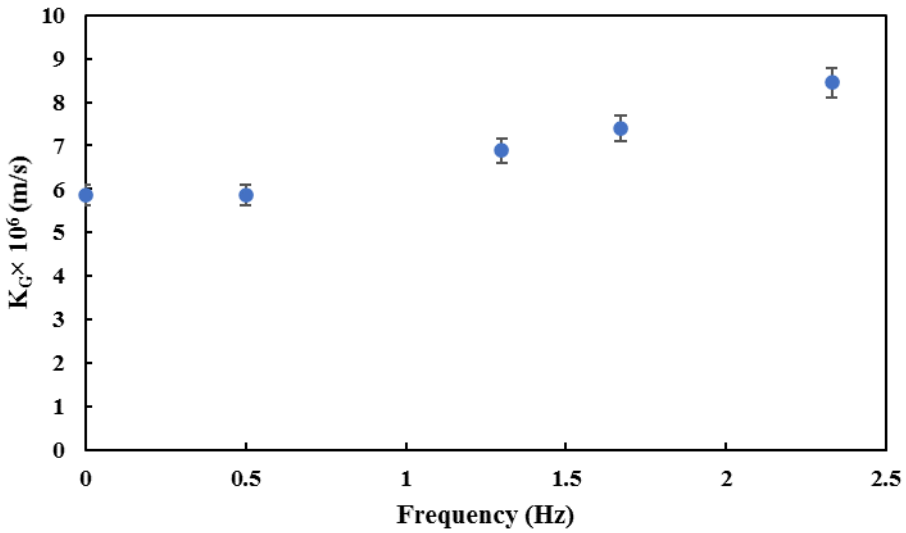


Fig. 6.8. Overall gas-based mass transfer coefficient ($K_G$) as a function of vibrating frequency at the fixed displacement amplitude of 2 cm (displacement per module length of 8%) and a solvent Reynolds No of 1.35 and gas Reynolds No of 20.

### 6.4.2.2. Effect of gas phase velocity

To quantify the influence gas velocity has on the performance of membrane contactors under vibration, the overall mass transfer coefficient as a function of gas phase Reynolds number is provided in Figure 6.9, for both non-vibrating and vibrating conditions. This is based on a vibrating displacement amplitude of 2cm and a frequency of 1.7 Hz. The membrane contactor had similar overall mass transfer coefficients between non-vibration and vibration conditions at low Reynolds numbers, but vibrating conditions produced an improved mass transfer performance at higher Reynolds number, corresponding to a 30% increase at the highest measurement. Hence, at the experimental conditions studied, as the gas phase velocity increased through the membrane fibres, the influence of vibration resulted in an increase in performance, contrasting what was observed for the solvent phase (Section 6.4.1.2). The reason for these observations can be explained by considering the individual mass transfer resistances within the gas and solvent boundary layers ($1/k_g$ and $1/k_l$). Assuming $1/k_l$ was identical to the values used in the experiments with pure $CO_2$ as the feed gas (Section 6.4.1), $1/k_g$ can be calculated using Eq. (2.8). These calculations showed the gas boundary layer share of the overall mass transfer resistance was ranged from ~ 53% at $Re_t$=11.6 to ~ 23% at $Re_t$=36.6. The greater share (~ 53%) is most likely an evidence of stronger concentration polarization effect at lower flowrates [133]. As a result, at low Reynolds number, vibration was unable to effectively impact the gas boundary layer and insignificant enhancement in $K_G$ was observed. At increased Reynolds numbers, vibration introduced more turbulence to the gas boundary layer which in turn alleviated the concentration polarization effect and resulted in significant improvements in $K_G$. These results agreed with the gas-solvent membrane contactor behaviour under oscillating gas flow conditions (i.e., Chapter 5).

As the gas phase is on the lumen side of the membrane fibres, analysis of the impact of module packing density on performance provided no meaningful insight.

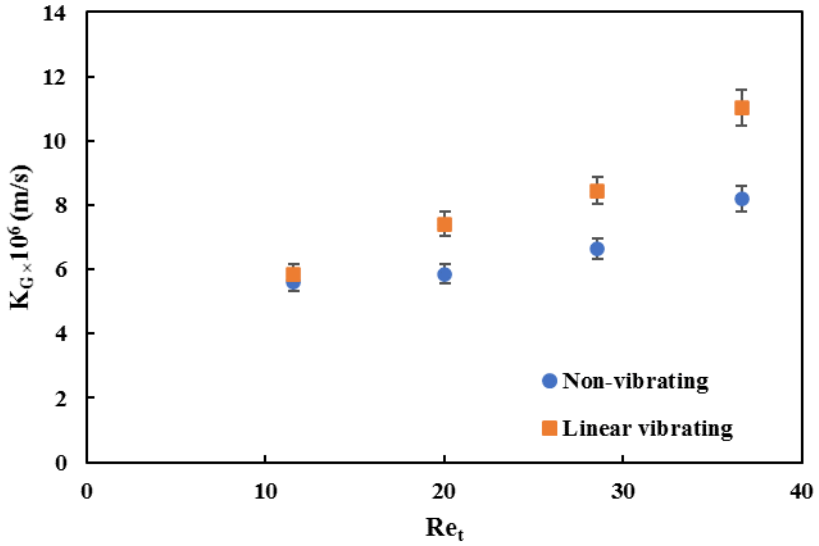


Fig. 6.9. Overall gas-based mass transfer coefficient ($K_G$) as a function of lumen side Reynolds number ($Re_t$) under vibration and non-vibration conditions. The vibration frequency was 1.67 Hz and displacement amplitude displacement was 2cm.

## 6.5. Conclusion

This study demonstrated that the selective separation performance of gas-solvent hollow fibre membrane contactors was improved up to 38% by introducing vibration to system. The separation performance of the membrane contactor systems was enhanced by both the frequency and amplitude of the vibration, which had different effects on the solvent and gas phases. In the solvent phase, vibration enhanced mass transfer by more than 20% compared to non-vibrating conditions but tapered off with increasing solvent Reynolds number. This was due to the disruption caused to the solvent boundary layer and the subsequent reduction in thickness lowering the mass transfer resistance. Vibration had a greater improvement in mass transfer on the gas phase, compared to the solvent, with the increase in performance expanding at higher amplitudes and frequencies. This effect was possibly attributed to the compressible characteristics of gas flow relative to the solvent, which enabled the propagation of the displacement wave through the gas phase. To define the effect of vibrating unit on the performance of gas-solvent membrane contactor system, a new vibrational dimensionless number (i. e. , $\Pi_{v,L}$) was introduced. The resulting solvent phase mass transfer was described through modified Sherwood number correlation that link packing density, Reynolds and Schmidt numbers with a vibrational dimensionless number. This mass transfer correlation therefore enabled the impact of vibration on the membrane contactor systems to be expanded beyond that which was studied here. Considering the strong effect of vibrating unit on the gas

phase, membrane contactor technology has significant potential for separation applications, with the addition of non-invasive vibration beneficial for enhanced performance.

The outcome of this chapter indicates the mass transfer resistance of gas and solvent boundary layers are simultaneously reduced by a vibration-induced membrane contactor system. The enhancement of mass transfer is significant using vibration, thus this vibration approach can be extended to industrial uses, given most of the commercial hollow fibre membrane modules are not too large allowing effective vibration of whole system to achieve.

# CHAPTER 7: CONCLUSION AND FUTURE PERSPECTIVE

## 7.1. Conclusion

Gas-solvent hollow fibre membrane contactors hold promise to mitigate $CO_2$ emissions from industrial processes. While hollow fibre membranes composed of an ultra-thin non-porous polymer have been introduced to minimize the mass transfer resistance of membranes, the mass transfer resistances of gas and solvent phase boundary layers remain significant challenges in achieving a high mass transfer performance in gas-solvent membrane contactors. This thesis investigated three novel approaches to reduce the mass transfer resistances of solvent and gas boundary layers and improve the $CO_2$ mass transfer rate in gas-solvent membrane contactor systems.

**- Membrane gas-solvent contactors undergoing oscillating solvent flow for enhanced carbon dioxide capture**

The reduction of solvent phase mass transfer resistance is of considerable importance in improving the mass transfer performance of gas-solvent membrane contactors, as the mass transfer resistance of solvent boundary layer dominates the overall mass transfer resistance. An oscillating unit was fabricated and integrated into a membrane contactor system to add disturbance and mixing into the solvent boundary layer and reduce its thickness which in turn lowered the mass transfer resistance of the solvent boundary layer. The experimental set-up was operated with 15wt% potassium glycinate as a solvent with a higher kinetic constant and lower viscosity in comparison with 30wt% MEA. It was indicated that the oscillating unit induced a sinusoidal trend to the solvent flow resulting in an increase in the root mean square velocity of solvent flow. Therefore, the oscillating solvent flow enhanced the solvent phase mass transfer coefficient compared to that of the non-oscillating solvent flow. There was a 53% enhancement in overall solvent-based mass transfer coefficient once the oscillating solvent flow frequency increased from 0.83Hz to 2.03Hz. Doubling the value of amplitude resulted in a 30% enhancement in overall solvent-based mass transfer coefficient. The oscillating solvent flow Reynolds number was defined to involve the oscillating flow parameters and a Sherwood number correlation was proposed using a modified Reynolds number to predict the mass transfer behaviour of gas-solvent membrane contactor system under oscillating conditions.

**- Absorption of $CO_2$ from flue Gas under oscillating gas flow conditions in gas-solvent hollow fibre membrane contactors**

This thesis showed that an oscillating unit could also apply oscillation to the gas phase flow. Therefore, the effect of oscillating gas flow on the mass transfer performance of the gas-solvent membrane contactor system was investigated for $CO_2$ capture from a simulated flue gas (i.e. 10% $CO_2$ in $N_2$). When mixing was induced by the oscillating unit, it was found that there was an average increase of 28% in the gas phase mass transfer coefficient. Increasing the value of oscillating gas flow amplitude enhanced the overall gas-based mass transfer coefficient by a factor of two as the pressure wave was generated in the gas phase resulting in higher $CO_2$ driving force. However, it was observed that the gas phase oscillating frequencies above 2Hz had only a minor impact on the performance. Using the concept of root mean squared velocity again, the oscillating gas flow Reynolds number was defined, and the mass transfer performance was described by a Sherwood number correlation. The proposed Sherwood number was valid for both oscillating and non-oscillating gas flow conditions.

**- Vibration-induced enhanced mass transfer within membrane contactors for efficient $CO_2$ capture**

A vibrating unit was designed and integrated into the gas-solvent membrane contactor system to study the reduction of solvent and gas phase mass transfer resistances simultaneously. In experiments with pure $CO_2$, the overall solvent-based mass transfer coefficient was significantly enhanced due to the disturbance of the solvent boundary layer and the generation of secondary flow on the solvent side. The gas phase boundary layer on the lumen side was also affected by the vibrating unit. This reflected the existence of extra mixing in the gas phase boundary layer and membrane porous support. The results indicated that the overall gas-based and solvent-based mass transfer coefficients increased by enhancing the frequency and amplitude of the vibrating unit. The impact of vibrating unit parameters on the solvent side boundary layer was explained using a dimensionless vibration number. Finally, the new correlation was proposed for the solvent side Sherwood number in terms of Reynolds number, Schmitt number and dimensionless vibration number.

In summary, this thesis quantified the enhanced mass transfer performance of gas-solvent hollow fibre membrane contactor systems for $CO_2$ removal from flue gas under oscillating and vibrating conditions. Both oscillating and vibrating units reduced the mass transfer resistance of the gas and solvent boundary layers. Frequency and amplitude were introduced as the main adjustable parameters of the designed units enabled proposing new mass transfer correlations for the gas and solvent boundary layer mass transfers. The outcome of this thesis demonstrated

that the oscillating unit had a greater impact on the solvent side mass transfer coefficient in comparison to the gas side. However, the vibrating unit had a greater impact on the mass transfer enhancement of the gas phase boundary layer.

## 7.2. Future perspective

The following suggestions can be considered for future research:

- Computational fluid dynamic (CFD) simulations which take mass and momentum diffusions into account under oscillating/vibrating solvent and gas phases. These simulations will enable validating experimental mass transfer performance data with more mathematically sound models
- Industrial trials of gas-solvent hollow fibre membrane contactor system undergoing oscillating and vibrating conditions are likely considerable future works.
- An energy study of the $CO_2$ absorption process using membrane contactor under oscillating and vibrating modes is suggested. This way the cost-effectiveness of adding extra mixing to the membrane contactor system is determined.
- The solvent boundary layer mass transfer resistance exists in the liquid-liquid membrane contactors. The application of oscillating and vibrating unit is suggested to investigate whether the same approaches work for other processes.
- The application of sinusoidal-shaped shell in gas-solvent membrane contactors is recommended to induce the sinusoidal pattern to the solvent velocity from internal sources. This enables a comparison between the results of the oscillating solvent flow generated by internal and external sources.

# CHAPTER 8: References


[1] I.P. Koronaki, L. Prentza, V. Papaefthimiou, Modeling of $CO_2$ capture via chemical absorption processes − An extensive literature review, Renewable and Sustainable Energy Reviews. 50 (2015) 547–566. https://doi.org/10.1016/j.rser.2015.04.124.

[2] M.A. González-Salazar, Recent developments in carbon dioxide capture technologies for gas turbine power generation, International Journal of Greenhouse Gas Control. 34 (2015) 106–116. https://doi.org/10.1016/j.ijggc.2014.12.007.

[3] Z. (Henry) Liang, W. Rongwong, H. Liu, K. Fu, H. Gao, F. Cao, R. Zhang, T. Sema, A. Henni, K. Sumon, D. Nath, D. Gelowitz, W. Srisang, C. Saiwan, A. Benamor, M. Al-Marri, H. Shi, T. Supap, C. Chan, Q. Zhou, M. Abu-Zahra, M. Wilson, W. Olson, R. Idem, P. (PT) Tontiwachwuthikul, Recent progress and new developments in post-combustion carbon-capture technology with amine based solvents, International Journal of Greenhouse Gas Control. 40 (2015) 26–54. https://doi.org/10.1016/j.ijggc.2015.06.017.

[4] Katherine Richardson, Will Steffen, Diana Liverman, Climate Change: Global Risks, Challenges and Decisions, Cambridge University Press, New York, 2011.

[5] S.C. Page, A.G. Williamson, I.G. Mason, Carbon capture and storage: Fundamental thermodynamics and current technology, Energy Policy. 37 (2009) 3314–3324. https://doi.org/10.1016/j.enpol.2008.10.028.

[6] C.A. Scholes, A. Qader, G.W. Stevens, S.E. Kentish, Membrane Gas-Solvent Contactor Pilot Plant Trials of $CO_2$ Absorption from Flue Gas, Separation Science and Technology. 49 (2014) 2449–2458. https://doi.org/10.1080/01496395.2014.937499.

[7] L. Zheng, Oxy-Fuel Combustion for Power Generation and Carbon Dioxide ($CO_2$) Capture, Elsevier, 2011.

[8] S. Zhao, P.H.M. Feron, L. Deng, E. Favre, E. Chabanon, S. Yan, J. Hou, V. Chen, H. Qi, Status and progress of membrane contactors in post-combustion carbon capture: A state-of-the-art review of new developments, Journal of Membrane Science. 511 (2016) 180–206. https://doi.org/10.1016/j.memsci.2016.03.051.

[9] T.C. Merkel, H. Lin, X. Wei, R. Baker, Power plant post-combustion carbon dioxide capture: An opportunity for membranes, Journal of Membrane Science. 359 (2010) 126–139. https://doi.org/10.1016/j.memsci.2009.10.041.

[10] K. Kumar, D. Banerjee, D. Das, Carbon dioxide sequestration from industrial flue gas by Chlorella sorokiniana, Bioresource Technology. 152 (2014) 225–233. https://doi.org/10.1016/j.biortech.2013.10.098.

[11] M.M.F. Hasan, R.C. Baliban, J.A. Elia, C.A. Floudas, Modeling, Simulation, and Optimization of Postcombustion CO2 Capture for Variable Feed Concentration and Flow Rate. 1. Chemical Absorption and Membrane Processes, Ind. Eng. Chem. Res. 51 (2012) 15642–15664. https://doi.org/10.1021/ie301571d.

[12] S. Yan, M.-X. Fang, W.-F. Zhang, S.-Y. Wang, Z.-K. Xu, Z.-Y. Luo, K.-F. Cen, Experimental study on the separation of $CO_2$ from flue gas using hollow fiber membrane contactors without wetting, Fuel Processing Technology. 88 (2007) 501–511. https://doi.org/10.1016/j.fuproc.2006.12.007.

[13] J.-L. Li, B.-H. Chen, Review of $CO_2$ absorption using chemical solvents in hollow fiber membrane contactors, Separation and Purification Technology. 41 (2005) 109–122. https://doi.org/10.1016/j.seppur.2004.09.008.

[14] M. Fang, N. Yi, W. Di, T. Wang, Q. Wang, Emission and control of flue gas pollutants in $CO_2$ chemical absorption system – A review, International Journal of Greenhouse Gas Control. 93 (2020) 102904. https://doi.org/10.1016/j.ijggc.2019.102904.

[15] A. Basile, F. Gallucci, P. Morrone, 6 - Advanced carbon dioxide ($CO_2$) gas separation membrane development for power plants, in: D. Roddy (Ed.), Advanced Power Plant Materials, Design and Technology, Woodhead Publishing, 2010: pp. 143–186. https://doi.org/10.1533/9781845699468.2.143.

[16] P. Luis, Chapter 5 - Membrane contactors, in: P. Luis (Ed.), Fundamental Modelling of Membrane Systems, Elsevier, 2018: pp. 153–208. https://doi.org/10.1016/B978-0-12-813483-2.00005-8.

[17] S. Boributh, S. Assabumrungrat, N. Laosiripojana, R. Jiraratananon, A modeling study on the effects of membrane characteristics and operating parameters on physical absorption of $CO_2$ by hollow fiber membrane contactor, Journal of Membrane Science. 380 (2011) 21–33. https://doi.org/10.1016/j.memsci.2011.06.029.

[18] P.H.M. Feron, A.E. Jansen, $CO_2$ separation with polyolefin membrane contactors and dedicated absorption liquids: performances and prospects, Separation and Purification Technology. 27 (2002) 231–242. https://doi.org/10.1016/S1383-5866(01)00207-6.

[19] R. Klaassen, P.H.M. Feron, A.E. Jansen, Membrane Contactors in Industrial Applications, Chemical Engineering Research and Design. 83 (2005) 234–246. https://doi.org/10.1205/cherd.04196.

[20] O. Falk-Pedersen, M.S. Grønvold, P. Nøkleby, F. Bjerve, H.F. Svendsen, $CO_2$ Capture with Membrane Contactors, International Journal of Green Energy. 2 (2005) 157–165. https://doi.org/10.1081/GE-200058965.

[21] R. Klaassen, Achieving flue gas desulphurization with membrane gas absorption, Filtration & Separation. 40 (2003) 26–28. https://doi.org/10.1016/S0015-1882(03)00033-8.

[22] M. Hedayat, M. Soltanieh, S.A. Mousavi, Simultaneous separation of $H_2S$ and $CO_2$ from natural gas by hollow fiber membrane contactor using mixture of alkanolamines, Journal of Membrane Science. 377 (2011) 191–197. https://doi.org/10.1016/j.memsci.2011.04.051.

[23] E. Chabanon, R. Bounaceur, C. Castel, S. Rode, D. Roizard, E. Favre, Pushing the limits of intensified $CO_2$ post-combustion capture by gas–liquid absorption through a membrane contactor, Chemical Engineering and Processing: Process Intensification. 91 (2015) 7–22. https://doi.org/10.1016/j.cep.2015.03.002.

[24] E. Chabanon, E. Kimball, E. Favre, O. Lorain, E. Goetheer, D. Ferre, A. Gomez, P. Broutin, Hollow Fiber Membrane Contactors for Post-Combustion $CO_2$ Capture: A Scale-Up Study from Laboratory to Pilot Plant, Oil & Gas Science and Technology – Revue d'IFP Energies Nouvelles. 69 (2014) 1035–1045. https://doi.org/10.2516/ogst/2012046.

[25] E. Hosseini, G.W. Stevens, C.A. Scholes, Membrane gas-solvent contactors undergoing oscillating solvent flow for enhanced carbon dioxide capture, Separation and Purification Technology. 227 (2019) 115653. https://doi.org/10.1016/j.seppur.2019.05.095.

[26] P.H.M. Feron, A.E. Jansen, R. Klaassen, Membrane technology in carbon dioxide removal, Energy Conversion and Management. 33 (1992) 421–428. https://doi.org/10.1016/0196-8904(92)90039-Y.

[27] V.V. Usachov, V.V. Teplyakov, A.Yu. Okunev, N.I. Laguntsov, Membrane contactor air conditioning system: Experience and prospects, Separation and Purification Technology. 57 (2007) 502–506. https://doi.org/10.1016/j.seppur.2006.09.021.

[28] M. Vogt, R. Goldschmidt, D. Bathen, B. Epp, H. Fahlenkamp, Comparison of membrane contactor and structured packings for $CO_2$ absorption, Energy Procedia. 4 (2011) 1471–1477. https://doi.org/10.1016/j.egypro.2011.02.013.

[29] H.B. Al-saffar, B. Ozturk, R. Hughes, A Comparison of Porous and Non-Porous Gas-Liquid Membrane Contactors for Gas Separation, Chemical Engineering Research and Design. 75 (1997) 685–692. https://doi.org/10.1205/026387697524182.

[30] H.A. Rangwala, Absorption of carbon dioxide into aqueous solutions using hollow fiber membrane contactors, Journal of Membrane Science. 112 (1996) 229–240. https://doi.org/10.1016/0376-7388(95)00293-6.

[31] J.-G. Lu, Y.-F. Zheng, M.-D. Cheng, Wetting mechanism in mass transfer process of hydrophobic membrane gas absorption, Journal of Membrane Science. 308 (2008) 180–190. https://doi.org/10.1016/j.memsci.2007.09.051.

[32] C.A. Scholes, S.E. Kentish, G.W. Stevens, D. deMontigny, Comparison of thin film composite and microporous membrane contactors for $CO_2$ absorption into monoethanolamine, International Journal of Greenhouse Gas Control. 42 (2015) 66–74. https://doi.org/10.1016/j.ijggc.2015.07.032.

[33] M. Mavroudi, S.P. Kaldis, G.P. Sakellaropoulos, A study of mass transfer resistance in membrane gas–liquid contacting processes, Journal of Membrane Science. 272 (2006) 103–115. https://doi.org/10.1016/j.memsci.2005.07.025.

[34] R. Naim, S. Abdullah, Membrane Wetting in Membrane Contactor System: A Review, Journal of Applied Membrane Science & Technology. 17 (2015). https://doi.org/10.11113/amst.v17i1.10.

[35] A. Mansourizadeh, S. Mousavian, Structurally developed microporous polyvinylidene fluoride hollow-fiber membranes for $CO_2$ absorption with diethanolamine solution, J Polym Res. 20 (2013) 99. https://doi.org/10.1007/s10965-013-0099-3.

[36] H. Kreulen, C.A. Smolders, G.F. Versteeg, W.P.M. van Swaaij, Microporous hollow fibre membrane modules as gas-liquid contactors Part 2. Mass transfer with chemical reaction, Journal of Membrane Science. 78 (1993) 217–238. https://doi.org/10.1016/0376-7388(93)80002-F.

[37] B. Belaissaoui, E. Favre, Evaluation of a dense skin hollow fiber gas-liquid membrane contactor for high pressure removal of $CO_2$ from syngas using Selexol as the absorbent, Chemical Engineering Science. 184 (2018) 186–199. https://doi.org/10.1016/j.ces.2018.02.028.

[38] C.A. Scholes, S.E. Kentish, G.W. Stevens, D. deMontigny, Asymmetric composite PDMS membrane contactors for desorption of CO2 from monoethanolamine, International Journal of Greenhouse Gas Control. 55 (2016) 195–201. https://doi.org/10.1016/j.ijggc.2016.10.008.

[39] V.Y. Dindore, D.W.F. Brilman, F.H. Geuzebroek, G.F. Versteeg, Membrane–solvent selection for CO2 removal using membrane gas–liquid contactors, Separation and Purification Technology. 40 (2004) 133–145. https://doi.org/10.1016/j.seppur.2004.01.014.

[40] H. Thee, N.J. Nicholas, K.H. Smith, G. da Silva, S.E. Kentish, G.W. Stevens, A kinetic study of CO2 capture with potassium carbonate solutions promoted with various amino acids: Glycine, sarcosine and proline, International Journal of Greenhouse Gas Control. 20 (2014) 212–222. https://doi.org/10.1016/j.ijggc.2013.10.027.

[41] M. Ehsan Hamzehie, H. Najibi, Carbon dioxide absorption in aqueous solution of potassium glycinate + 2-amino-2-methyl-1-propanol as new absorbents, RSC Advances. 6 (2016) 62612–62623. https://doi.org/10.1039/C6RA09600J.

[42] S. Yan, Q. He, S. Zhao, H. Zhai, M. Cao, P. Ai, $CO_2$ removal from biogas by using green amino acid salts: Performance evaluation, Fuel Processing Technology. 129 (2015) 203–212. https://doi.org/10.1016/j.fuproc.2014.09.019.

[43] A.F. Portugal, P.W.J. Derks, G.F. Versteeg, F.D. Magalhães, A. Mendes, Characterization of potassium glycinate for carbon dioxide absorption purposes, Chemical Engineering Science. 62 (2007) 6534–6547. https://doi.org/10.1016/j.ces.2007.07.068.

[44] I.M. Bernhardsen, L. Ansaloni, H.K. Betten, L. Deng, H.K. Knuutila, Effect of liquid viscosity on the performance of a non-porous membrane contactor for CO2 capture, Separation and Purification Technology. 222 (2019) 188–201. https://doi.org/10.1016/j.seppur.2019.04.024.

[45] S. Mazinani, A. Samsami, A. Jahanmiri, A. Sardarian, Solubility (at Low Partial Pressures), Density, Viscosity, and Corrosion Rate of Carbon Dioxide in Blend Solutions of Monoethanolamine (MEA) and Sodium Glycinate (SG), J. Chem. Eng. Data. 56 (2011) 3163–3168. https://doi.org/10.1021/je2002418.

[46] D. Aaron, C. Tsouris, Separation of CO2 from Flue Gas: A Review, Separation Science and Technology. 40 (2005) 321–348. https://doi.org/10.1081/SS-200042244.

[47] N. McCann, D. Phan, X. Wang, W. Conway, R. Burns, M. Attalla, G. Puxty, M. Maeder, Kinetics and Mechanism of Carbamate Formation from CO2(aq), Carbonate Species, and Monoethanolamine in Aqueous Solution, J. Phys. Chem. A. 113 (2009) 5022–5029. https://doi.org/10.1021/jp810564z.

[48] P.S. Kumar, J.A. Hogendoorn, G.F. Versteeg, P.H.M. Feron, Kinetics of the reaction of CO2 with aqueous potassium salt of taurine and glycine, AIChE Journal. 49 (2003) 203–213. https://doi.org/10.1002/aic.690490118.

[49] M. A. Abd El-Ghaffar, Hossam A. Tieama, A Review of Membranes Classifications, Configurations, Surface Modifications, Characteristics and Its Applications in Water Purification, Chemical and Biomolecular Engineering. 2 (2017) 57–82. https://doi.org/10.11648/j.cbe.20170202.11.

[50] Z. Cui, D. deMontigny, Part 7: A review of $CO_2$ capture using hollow fiber membrane contactors, Carbon Management. 4 (2013) 69–89. https://doi.org/10.4155/cmt.12.73.

[51] P.T. Nguyen, E. Lasseuguette, Y. Medina-Gonzalez, J.C. Remigy, D. Roizard, E. Favre, A dense membrane contactor for intensified $CO_2$ gas/liquid absorption in post-combustion capture, Journal of Membrane Science. 377 (2011) 261–272. https://doi.org/10.1016/j.memsci.2011.05.003.

[52] V.Y. Dindore, D.W.F. Brilman, G.F. Versteeg, Modelling of cross-flow membrane contactors: physical mass transfer processes, Journal of Membrane Science. 251 (2005) 209–222. https://doi.org/10.1016/j.memsci.2004.11.017.

[53] S. Eslami, S.M. Mousavi, S. Danesh, H. Banazadeh, Modeling and simulation of $CO_2$ removal from power plant flue gas by PG solution in a hollow fiber membrane contactor, Advances in Engineering Software. 42 (2011) 612–620. https://doi.org/10.1016/j.advengsoft.2011.05.002.

[54] P.S. Kumar, J.A. Hogendoorn, P.H.M. Feron, G.F. Versteeg, New absorption liquids for the removal of $CO_2$ from dilute gas streams using membrane contactors, Chemical Engineering Science. 57 (2002) 1639–1651. https://doi.org/10.1016/S0009-2509(02)00041-6.

[55] C.A. Scholes, S.E. Kentish, A. Qader, Membrane gas-solvent contactor pilot plant trials for post-combustion CO2 capture, Separation and Purification Technology. 237 (2020) 116470. https://doi.org/10.1016/j.seppur.2019.116470.

[56] C.A. Scholes, M. Simioni, A. Qader, G.W. Stevens, S.E. Kentish, Membrane gas–solvent contactor trials of $CO_2$ absorption from syngas, Chemical Engineering Journal. 195–196 (2012) 188–197. https://doi.org/10.1016/j.cej.2012.04.034.

[57] P. Kosaraju, A.S. Kovvali, A. Korikov, K.K. Sirkar, Hollow Fiber Membrane Contactor Based $CO_2$ Absorption−Stripping Using Novel Solvents and Membranes, Ind. Eng. Chem. Res. 44 (2005) 1250–1258. https://doi.org/10.1021/ie0495630.

[58] S. Nii, H. Takeuchi, K. Takahashi, Removal of $CO_2$ by Gas Absorption across a Polymeric Membrane, Journal of Chemical Engineering of Japan. 25 (1992) 67–72. https://doi.org/10.1252/jcej.25.67.

[59] K. Li, W.K. Teo, An Ultrathin Skinned Hollow Fibre Module for Gas Absorption at Elevated Pressures, Chemical Engineering Research and Design. 74 (1996) 856–862. https://doi.org/10.1205/026387696523157.

[60] A.F. Portugal, F.D. Magalhães, A. Mendes, Carbon dioxide removal from anaesthetic gas circuits using hollow fiber membrane contactors with amino acid salt solutions, Journal of Membrane Science. 339 (2009) 275–286. https://doi.org/10.1016/j.memsci.2009.04.055.

[61] S. Khaisri, D. deMontigny, P. Tontiwachwuthikul, R. Jiraratananon, Comparing membrane resistance and absorption performance of three different membranes in a gas absorption membrane contactor, Separation and Purification Technology. 65 (2009) 290–297. https://doi.org/10.1016/j.seppur.2008.10.035.

[62] C.A. Scholes, M. Simioni, A. Qader, G.W. Stevens, S.E. Kentish, Membrane gas–solvent contactor trials of $CO_2$ absorption from syngas, Chemical Engineering Journal. 195–196 (2012) 188–197. https://doi.org/10.1016/j.cej.2012.04.034.

[63] S. Khaisri, D. deMontigny, P. Tontiwachwuthikul, R. Jiraratananon, Comparing membrane resistance and absorption performance of three different membranes in a gas absorption membrane contactor, Separation and Purification Technology. 65 (n.d.) 290–297.

[64] J.D. Seader, E.J. Henley, Separation process principles, 2nd ed, Wiley, Hoboken, N.J, 2006.

[65] N. Boucif, P.T. Nguyen, D. Roizard, E. Favre, Theoretical Studies on Carbon Dioxide Removal from a Gas Stream in Hollow Fiber Membrane Contactors, Desalination and Water Treatment. 14 (2010) 146–157. https://doi.org/10.5004/dwt.2010.1020.

[66] W.J. DeCoursey, Absorption with chemical reaction: development of a new relation for the Danckwerts model, Chemical Engineering Science. 29 (1974) 1867–1872. https://doi.org/10.1016/0009-2509(74)85003-7.

[67] W.P.M. van Swaaij, G.F. Versteeg, Mass transfer accompanied with complex reversible chemical reactions in gas—liquid systems: an overview, Chemical Engineering Science. 47 (1992) 3181–3195. https://doi.org/10.1016/0009-2509(92)85028-A.

[68] G.F. Versteeg, W.P.M. Van Swaaij, Solubility and diffusivity of acid gases (carbon dioxide, nitrous oxide) in aqueous alkanolamine solutions, J. Chem. Eng. Data. 33 (1988) 29–34. https://doi.org/10.1021/je00051a011.

[69] S. Weisenberger, A. Schumpe, Estimation of gas solubilities in salt solutions at temperatures from 273 K to 363 K, AIChE Journal. 42 (1996) 298–300. https://doi.org/10.1002/aic.690420130.

[70] A. Schumpe, The estimation of gas solubilities in salt solutions, Chemical Engineering Science. 48 (1993) 153–158. https://doi.org/10.1016/0009-2509(93)80291-W.

[71] C.A. Scholes, S.E. Kentish, G.W. Stevens, J. Jin, D. deMontigny, Thin-film composite membrane contactors for desorption of $CO_2$ from Monoethanolamine at elevated temperatures, Separation and Purification Technology. 156 (2015) 841–847. https://doi.org/10.1016/j.seppur.2015.11.010.

[72] S. Shen, S.E. Kentish, G.W. Stevens, Shell-Side Mass-Transfer Performance in Hollow-Fiber Membrane Contactors, Solvent Extraction and Ion Exchange. 28 (2010) 817–844. https://doi.org/10.1080/07366299.2010.515176.

[73] C.Y. Wang, E. Mercer, F. Kamranvand, L. Williams, A. Kolios, A. Parker, S. Tyrrel, E. Cartmell, E.J. McAdam, Tube-side mass transfer for hollow fibre membrane contactors operated in the low Graetz range, Journal of Membrane Science. 523 (2017) 235–246. https://doi.org/10.1016/j.memsci.2016.09.049.

[74] S.R. Wickramasinghe, M.J. Semmens, E.L. Cussler, Mass transfer in various hollow fiber geometries, Journal of Membrane Science. 69 (1992) 235–250. https://doi.org/10.1016/0376-7388(92)80042-I.

[75] Li, L.-J., Liu, L.-Y., Ding, Z.-W., Effect of packing density on shell-side mass transfer performance of hollow fiber membrane module, Thesis, Beijing University of Chemical Technology, 2005.

[76] S. Kartohardjono, V. Chen, Mass Transfer and Fluid Hydrodynamics in Sealed End Hydrophobic Hollow Fiber Membrane Gas-liquid Contactors, Journal of Applied Membrane Science & Technology. 2 (2005). https://doi.org/10.11113/amst.v2i1.1.

[77] J.-M. Zheng, Z.-K. Xu, J.-M. Li, S.-Y. Wang, Y.-Y. Xu, Influence of random arrangement of hollow fiber membranes on shell side mass transfer performance: a novel model prediction, Journal of Membrane Science. 236 (2004) 145–151. https://doi.org/10.1016/j.memsci.2004.02.016.

[78] J.-M. Zheng, Y.-Y. Xu, Z.-K. Xu, Shell Side Mass Transfer Characteristics in a Parallel Flow Hollow Fiber Membrane Module, Separation Science and Technology. 38 (2003) 1247–1267. https://doi.org/10.1081/SS-120018808.

[79] J. Wu, V. Chen, Shell-side mass transfer performance of randomly packed hollow fiber modules, Journal of Membrane Science. 172 (2000) 59–74. https://doi.org/10.1016/S0376-7388(00)00318-5.

[80] D.W. Johnson, M.J. Semmens, J.S. Gulliver, Diffusive transport across unconfined hollow fiber membranes, Journal of Membrane Science. 128 (1997) 67–81. https://doi.org/10.1016/S0376-7388(96)00323-7.

[81] M.J. Costello, A.G. Fane, P.A. Hogan, R.W. Schofield, The effect of shell side hydrodynamics on the performance of axial flow hollow fibre modules, Journal of Membrane Science. 80 (1993) 1–11. https://doi.org/10.1016/0376-7388(93)85127-I.

[82] M.-C. Yang, E.L. Cussler, Designing hollow-fiber contactors, AIChE Journal. 32 (1986) 1910–1916. https://doi.org/10.1002/aic.690321117.

[83] A. McLeod, B. Jefferson, E.J. McAdam, Toward gas-phase controlled mass transfer in micro-porous membrane contactors for recovery and concentration of dissolved methane in the gas phase, Journal of Membrane Science. 510 (2016) 466–471. https://doi.org/10.1016/j.memsci.2016.03.030.

[84] X. Tan, G. Capar, K. Li, Analysis of dissolved oxygen removal in hollow fibre membrane modules: effect of water vapour, Journal of Membrane Science. 251 (2005) 111–119. https://doi.org/10.1016/j.memsci.2004.11.005.

[85] L. Dahuron, E.L. Cussler, Protein extractions with hollow fibers, AIChE Journal. 34 (1988) 130–136. https://doi.org/10.1002/aic.690340115.

[86] A.P. Korikov, K.K. Sirkar, Membrane gas permeance in gas–liquid membrane contactor systems for solutions containing a highly reactive absorbent, Journal of Membrane Science. 246 (2005) 27–37. https://doi.org/10.1016/j.memsci.2004.06.042.

[87] R.H. Keil, M.H.I. Baird, Enhancement of Heat Transfer by Flow Pulsation, Ind. Eng. Chem. Proc. Des. Dev. 10 (1971) 473–478. https://doi.org/10.1021/i260040a008.

[88] T.J. Kennedy, R.L. Merson, B.J. McCoy, Improving permeation flux by pulsed reverse osmosis, Chemical Engineering Science. 29 (1974) 1927–1931. https://doi.org/10.1016/0009-2509(74)85010-4.

[89] O.E. Karamercan, J.L. Gainer, The Effect of Pulsations on Heat Transfer, Ind. Eng. Chem. Fund. 18 (1979) 11–15. https://doi.org/10.1021/i160069a003.

[90] S. Najarian, B.J. Bellhouse, Effect of liquid pulsation on protein fractionation using ultrafiltration processes, Journal of Membrane Science. 114 (1996) 245–253. https://doi.org/10.1016/0376-7388(96)00004-X.

[91] P. Blanpain-Avet, N. Doubrovine, C. Lafforgue, M. Lalande, The effect of oscillatory flow on crossflow microfiltration of beer in a tubular mineral membrane system – Membrane fouling resistance decrease and energetic considerations, Journal of Membrane Science. 152 (1999) 151–174. https://doi.org/10.1016/S0376-7388(98)00214-2.

[92] P. Budzyński, A. Gwiazda, M. Dziubiński, Intensification of mass transfer in a pulsed bubble column, Chemical Engineering and Processing: Process Intensification. 112 (2017) 18–30. https://doi.org/10.1016/j.cep.2016.12.004.

[93] E. Piacentini, E. Drioli, L. Giorno, Pulsed back-and-forward cross-flow batch membrane emulsification with high productivity to obtain highly uniform and concentrate emulsions, Journal of Membrane Science. 453 (2014) 119–125. https://doi.org/10.1016/j.memsci.2013.10.063.

[94] T. Nishimura, S. Matsune, Mass transfer enhancement in a sinusoidal wavy channel for pulsatile flow, Heat and Mass Transfer. 32 (1996) 65–72. https://doi.org/10.1007/s002310050093.

[95] T. Luelf, M. Tepper, H. Breisig, M. Wessling, Sinusoidal shaped hollow fibers for enhanced mass transfer, Journal of Membrane Science. 533 (2017) 302–308. https://doi.org/10.1016/j.memsci.2017.03.030.

[96] A. Gabelman, S.-T. Hwang, Hollow fiber membrane contactors, Journal of Membrane Science. 159 (1999) 61–106. https://doi.org/10.1016/S0376-7388(99)00040-X.

[97] K.L. Wang, E.L. Cussler, Baffled membrane modules made with hollow fiber fabric, Journal of Membrane Science. 85 (1993) 265–278. https://doi.org/10.1016/0376-7388(93)85280-A.

[98] W.B. Krantz, R.R. Bilodeau, M.E. Voorhees, R.J. Elgas, Use of axial membrane vibrations to enhance mass transfer in a hollow tube oxygenator, Journal of Membrane Science. 124 (1997) 283–299. https://doi.org/10.1016/S0376-7388(96)00245-1.

[99] W. Zhang, Z. Hao, J. Li, J. Liu, Z. Wang, Z. Ren, Residence Time Distribution Analysis of a Hollow-Fiber Contactor for Membrane Gas Absorption and Vibration-Induced Mass Transfer Intensification, Ind. Eng. Chem. Res. 53 (2014) 8640–8650. https://doi.org/10.1021/ie500583v.

[100] M. Chai, Y. Ye, V. Chen, Application of rotational vibration in a submerged hollow fibre membrane system for bioseparation of high concentration yeast suspensions, Journal of Membrane Science. 573 (2019) 145–156. https://doi.org/10.1016/j.memsci.2018.11.069.

[101] M. Chai, Y. Ye, V. Chen, Separation and concentration of milk proteins with a submerged membrane vibrational system, Journal of Membrane Science. 524 (2017) 305–314. https://doi.org/10.1016/j.memsci.2016.11.043.

[102] W. Shi, M.M. Benjamin, Effect of shear rate on fouling in a Vibratory Shear Enhanced Processing (VSEP) RO system, Journal of Membrane Science. 366 (2011) 148–157. https://doi.org/10.1016/j.memsci.2010.09.051.

[103] M.D. Petala, A.I. Zouboulis, Vibratory shear enhanced processing membrane filtration applied for the removal of natural organic matter from surface waters, Journal of Membrane Science. 269 (2006) 1–14. https://doi.org/10.1016/j.memsci.2005.06.013.

[104] L. Wang, J.-P. Corriou, C. Castel, E. Favre, A critical review of cyclic transient membrane gas separation processes: State of the art, opportunities and limitations, Journal of Membrane Science. 383 (2011) 170–188. https://doi.org/10.1016/j.memsci.2011.08.052.

[105] D.R. Paul, Membrane Separation of Gases Using Steady Cyclic Operation, Ind. Eng. Chem. Proc. Des. Dev. 10 (1971) 375–379. https://doi.org/10.1021/i260039a016.

[106] M.M. Trubyanov, P.N. Drozdov, A.A. Atlaskin, S.V. Battalov, E.S. Puzanov, A.V. Vorotyntsev, A.N. Petukhov, V.M. Vorotyntsev, I.V. Vorotyntsev, Unsteady-state membrane gas separation by novel pulsed retentate mode for improved membrane module performance: Modelling and experimental verification, Journal of Membrane Science. 530 (2017) 53–64. https://doi.org/10.1016/j.memsci.2017.01.064.

[107] M. Albu, G.T. Heydt, On the use of RMS values in power quality assessment, IEEE Transactions on Power Delivery. 18 (2003) 1586–1587. https://doi.org/10.1109/TPWRD.2003.817518.

[108] M.R. Mackley, P. Stonestreet, Heat transfer and associated energy dissipation for oscillatory flow in baffled tubes, Chemical Engineering Science. 50 (1995) 2211–2224. https://doi.org/10.1016/0009-2509(95)00088-M.

[109] M. Hino, M. Sawamoto, S. Takasu, Experiments on transition to turbulence in an oscillatory pipe flow, Journal of Fluid Mechanics. 75 (1976) 193–207. https://doi.org/10.1017/S0022112076000177.

[110] E. Hosseini, E. Soroodan Miandoab, G.W. Stevens, C.A. Scholes, Absorption of $CO_2$ from flue gas under oscillating gas flow conditions in gas-solvent hollow fibre Membrane Contactors, Separation and Purification Technology. (2020) 117151. https://doi.org/10.1016/j.seppur.2020.117151.

[111] Bert Metz, O. Davison, H. De Coninck, M. Loos, L. Meyer, IPCC, Cambridge University Press, UK, 2005.

[112] S. Karoor, K.K. Sirkar, Gas absorption studies in microporous hollow fiber membrane modules, Ind. Eng. Chem. Res. 32 (1993) 674–684. https://doi.org/10.1021/ie00016a014.

[113] J.M. Coulson, J.F. Richardson, J.M. Coulson, Coulson & Richardson's chemical engineering. Volume 1: Fluid flow, heat transfer and mass transfer, Butterworth-Heinemann, Amsterdam ; Boston, 2009.

[114] A. Lee, M. Wolf, N. Kromer, K.A. Mumford, N.J. Nicholas, S.E. Kentish, G.W. Stevens, A study of the vapour–liquid equilibrium of $CO_2$ in mixed solutions of potassium carbonate and potassium glycinate, International Journal of Greenhouse Gas Control. 36 (2015) 27–33. https://doi.org/10.1016/j.ijggc.2015.02.007.

[115] F. Panahinia, J. Safdari, M. Ghannadi-Maragheh, P. Amani, M.H. Mallah, Modeling and simulation of a horizontal pulsed sieve-plate extraction column using axial dispersion model, Separation Science and Technology. 52 (2017) 1537–1552. https://doi.org/10.1080/01496395.2017.1293097.

[116] O.E. Karamercan, J.L. Gainer, The Effect of Pulsations on Heat Transfer, Ind. Eng. Chem. Fund. 18 (1979) 11–15. https://doi.org/10.1021/i160069a003.

[117] J. Franco, D. deMontigny, S. Kentish, J. Perera, G. Stevens, A Study of the Mass Transfer of $CO_2$ through Different Membrane Materials in the Membrane Gas Absorption Process, Separation Science and Technology. 43 (2008) 225–244. https://doi.org/10.1080/01496390701791554.

[118] E. Soroodan Miandoab, S.E. Kentish, C.A. Scholes, Non-ideal modelling of polymeric hollow-fibre membrane systems: Pre-combustion $CO_2$ capture case study, Journal of Membrane Science. 595 (2020) 117470. https://doi.org/10.1016/j.memsci.2019.117470.

[119] E. Favre, H.F. Svendsen, Membrane contactors for intensified post-combustion carbon dioxide capture by gas–liquid absorption processes, Journal of Membrane Science. 407–408 (2012) 1–7. https://doi.org/10.1016/j.memsci.2012.03.019.

[120] Q. He, G. Yu, S. Yan, L.F. Dumée, Y. Zhang, V. Strezov, S. Zhao, Renewable $CO_2$ absorbent for carbon capture and biogas upgrading by membrane contactor, Separation and Purification Technology. 194 (2018) 207–215. https://doi.org/10.1016/j.seppur.2017.11.043.

[121] M. Mavroudi, S.P. Kaldis, G.P. Sakellaropoulos, A study of mass transfer resistance in membrane gas–liquid contacting processes, Journal of Membrane Science. 272 (2006) 103–115. https://doi.org/10.1016/j.memsci.2005.07.025.

[122] A. Samanta, A. Zhao, G.K.H. Shimizu, P. Sarkar, R. Gupta, Post-Combustion $CO_2$ Capture Using Solid Sorbents: A Review, Ind. Eng. Chem. Res. 51 (2012) 1438–1463. https://doi.org/10.1021/ie200686q.

[123] M. Xiao, H. Liu, R. Idem, P. Tontiwachwuthikul, Z. Liang, A study of structure–activity relationships of commercial tertiary amines for post-combustion $CO_2$ capture, Applied Energy. 184 (2016) 219–229. https://doi.org/10.1016/j.apenergy.2016.10.006.

[124] H. Liu, H. Gao, R. Idem, P. Tontiwachwuthikul, Z. Liang, Analysis of $CO_2$ solubility and absorption heat into 1-dimethylamino-2-propanol solution, Chemical Engineering Science. 170 (2017) 3–15. https://doi.org/10.1016/j.ces.2017.02.032.

[125] H. Gao, N. Wang, J. Du, X. Luo, Z. Liang, Comparative kinetics of carbon dioxide (CO2) absorption into EAE, 1DMA2P and their blends in aqueous solution using the stopped-flow technique, International Journal of Greenhouse Gas Control. 94 (2020) 102948. https://doi.org/10.1016/j.ijggc.2019.102948.

[126] H. Ling, H. Gao, Z. Liang, Comprehensive solubility of $N_2O$ and mass transfer studies on an effective reactive N,N-dimethylethanolamine (DMEA) solvent for post-combustion CO2 capture, Chemical Engineering Journal. 355 (2019) 369–379. https://doi.org/10.1016/j.cej.2018.08.147.

[127] F.A. Hatab, N. Abdullatif, S.A.M. Marzouk, M.H. Al-Marzouqi, Experimental and modeling of CO2 removal from gas mixtures using membrane contactors packed with glass beads, Separation and Purification Technology. 217 (2019) 240–246. https://doi.org/10.1016/j.seppur.2019.01.081.

[128] G.B. Schubauer, H.K. Skramstad, Laminar boundary-layer oscillations and transition on a flat plate, Journal of Research of the National Bureau of Standards. 38 (1947) 251. https://doi.org/10.6028/jres.038.013.

[129] J. Ghobadi, D. Ramirez, S. Khoramfar, R. Jerman, M. Crane, K. Hobbs, Simultaneous absorption of carbon dioxide and nitrogen dioxide from simulated flue gas stream using

gas-liquid membrane contacting system, International Journal of Greenhouse Gas Control. 77 (2018) 37–45. https://doi.org/10.1016/j.ijggc.2018.07.026.

[130] R. Prasad, K.K. Sirkar, Dispersion-free solvent extraction with microporous hollow-fiber modules, AIChE Journal. 34 (1988) 177–188. https://doi.org/10.1002/aic.690340202.

[131] S. Qazi, L. Gómez-Coma, J. Albo, S. Druon-Bocquet, A. Irabien, J. Sanchez-Marcano, CO2 capture in a hollow fiber membrane contactor coupled with ionic liquid: Influence of membrane wetting and process parameters, Separation and Purification Technology. 233 (2020) 115986. https://doi.org/10.1016/j.seppur.2019.115986.

[132] Y. Ji, M. Zhang, K. Guan, J. Zhao, G. Liu, W. Jin, High-Performance $CO_2$ Capture through Polymer-Based Ultrathin Membranes, Advanced Functional Materials. 29 (2019) 1900735. https://doi.org/10.1002/adfm.201900735.

[133] A. Mourgues, J. Sanchez, Theoretical analysis of concentration polarization in membrane modules for gas separation with feed inside the hollow-fibers, Journal of Membrane Science. 252 (2005) 133–144. https://doi.org/10.1016/j.memsci.2004.11.024.